



**AN INVESTIGATION OF PVPOWERED  
ABSORPTION REFRIGERATION SYSTEMS**

**2024  
MASTER THESIS  
MECHANICAL ENGINEERING**

**Jawad Yahya Khudhur KHUDHUR**

**Thesis Advisors  
Assist.Prof. Dr.Abdulrazzak Ahmed Saleh  
AKROOT  
Prof. Dr. Ahmed AL-SAMARI**

**AN INVESTIGATION OF PV POWERED ABSORPTION REFRIGERATION  
SYSTEMS**

**Jawad Yahya Khudhur KHUDHUR**

**Thesis Advisors**

**Assist. Prof. Dr. Abdulrazzak A. S. AKROOT**

**Prof. Dr. Ahmed AL-SAMARI**

**T.C.**

**Karabük University**

**Institute of Graduate Programs**

**Department of Mechanical Engineering**

**Prepared as**

**Master Thesis**

**KARABÜK**

**January 2024**

I certify that in my opinion the thesis submitted by Jawad Yahya Khudhur KHUDHUR titled “AN INVESTIGATION OF PV POWERED ABSORPTION REFRIGERATION SYSTEMS” is fully adequate in scope and in quality as a thesis for the degree of Master of Science.

Assist. Prof. Dr. Abdulrazzak Ahmed Saleh AKROOT .....

Thesis Advisor, Department of Mechanical Engineering

Prof. Dr. Ahmed AL-SAMARI .....

Co-Supervisor, Department of Mechanical Engineering of Iraq University of Diyala

This thesis is accepted by the examining committee with a unanimous vote in the Department of Mechanical Engineering as a Master of Science thesis 25/01/2024

Examining Committee Members (Institutions)

Signature

Chairman: Assist. Prof. Dr. Erhan KAYABAŞI (KBÜ) .....

Member : Prof. Dr. Emrah DENİZ (KBU) .....

Member : Assist. Prof. Dr. Abdulrazzak AKROOT (KBU) .....

Member : Prof. Dr. Ahmed AL-SAMARI (University of Diyala) .....

Member : Assoc. Prof. Dr. Hasanain Adnan Abdul WAHHAB (UOT) .....

The degree of Master of Science by the thesis submitted is approved by the Administrative Board of the Institute of Graduate Programs, Karabük University.

Assoc. Prof. Dr. Zeynep ÖZCAN .....

Director of the Institute of Graduate Programs

*“I declare that all the information within this thesis has been gathered and presented in accordance with academic regulations and ethical principles and I have according to the requirements of these regulations and principles cited all those which do not originate in this work as well.”*

Jawad Yahya Khudhur KHUDHUR

## **ABSTRACT**

**M. Sc. Thesis**

### **AN INVESTIGATION OF PV POWERED ABSORPTION REFRIGERATION SYSTEMS**

**Jawad Yahya Khudhur KHUDHUR**

**Karabük University  
Institute of Graduate Programmes  
Department of Mechanical Engineering**

**Thesis Advisors:**

**Assist. Prof. Dr. Abdurazzak Ahmed Saleh AKROOT**

**Prof. Dr. Ahmed AL-SAMARI**

**January 2024, 105 pages**

This study aims to investigate the possibilities of using renewable and sustainable energy sources (solar photovoltaic energy) to drive a direct absorption cooling system. Four different scenarios are proposed to evaluate PV power for the operation of a direct DC absorption cooling system (ARS). The first scenario is that the weather will be mostly cloudy and slightly dusty for 4 hours in September 2022. The second scenario is that the weather be clear for two-and-a-half hours in September 2022. In the third scenario, clear weather is experienced continuously for three days, including the first day, with AC. In the fourth scenario, the experiment was conducted in December 2022, for approximately three days at an angle of 20°. Comparisons were made by changing the angle to 30° under the same operating conditions. The reason for selecting these four scenarios is to investigate and optimise the effect of the photovoltaic panel on operating an absorption cooling

system in different weather conditions. The results of using photovoltaic solar energy were examined according to weather conditions and different angles. According to the results, it was observed that the efficiency of the cooling cycle is not negatively affected by voltage fluctuations if the weather is mostly cloudy or dusty, unlike compression cooling systems that require a constant and stable current and voltage. Finally, out of these four scenarios, when looking at angle differences, the absorption cooling system gave the worst results at an angle of 30° and the best results at 20°.

**Key Words** : Absorption Refrigeration System, Renewable energy, Solar energy, Photovoltaic cells, Sustainable energy.

**Science Code:** 91413

## **ÖZET**

**Yüksek Lisans Tezi**

### **FOTOVOLTAİK ENERJİYLE ÇALIŞAN ABSORPSİYONLU SOĞUTMA SİSTEMİNİN İNCELENMESİ**

**Jawad Yahya KHUDHUR**

**Karabük, Üniversitesi**

**Lisansüstü Eğitim Enstitüsü**

**Makine Mühendisliği Anabilim Dalı**

**Tez Danışmanları:**

**Dr. Öğr. Üyesi Abdurazzak Ahmed Saleh AKROOT**

**Prof. Dr. Ahmed AL-SAMARI**

**January 2024, 105 sayfa**

Bu çalışma, yenilenebilir ve sürdürülebilir enerji kaynaklarının (güneş fotovoltaik enerjisi) doğrudan absorpsiyonlu bir soğutma sistemini çalıştırmak için kullanılma olanaklarını araştırmayı amaçlamaktadır. Bu çalışmada, doğrudan DC absorpsiyonlu soğutma sisteminin (ARS) çalışması için PV gücünü değerlendirmek üzere dört farklı senaryo önerilmektedir. İlk senaryo Eylül 2022'de 4 saat boyunca havanın çoğunlukla bulutlu ve hafif tozlu olması durumudur. İkinci senaryo ise yine Eylül 2022'de iki buçuk saat boyunca havanın açık olması durumudur. Üçüncü senaryoda ise AC akımıyla ilk gün de dahil olmak üzere 3 gün boyunca sürekli açık hava yaşanmaktadır. Dördüncü senaryo. Deney Aralık 2022'de, önceki deneylere ek olarak yaklaşık 3 gün 20 derecelik açıyla yapılmıştır. Aynı çalışma şartlarında açılış otuz dereceye değiştirilerek bir karşılaştırma yapılmıştır. Bu dört senaryonun seçilmesinin nedeni, fotovoltaik panelin farklı hava koşullarında absorpsiyonlu bir

soğutma sistemini çalıştırmaya olan etkisini arařtırmak ve bunu optimize etmektir. Fotovoltaik güneř enerjisi kullanımının sonuçları hava řartlarına ve farklı açılara göre incelenmiřtir. Sonuçlara göre, hava durumu ile ilgili olarak, sabit ve kararlı bir akım ve gerilime ihtiyaç duyan sıkıřtırmalı soğutma sistemlerinden farklı olarak havanın çoğunlukla bulutlu veya tozlu olması durumunda soğutma çevriminin veriminin voltaj dalgalanmasından olumsuz etkilenmediğı görölmüřtür. Son olarak, açı farkına bakıldığında, absorpsiyonlu bir soğutma sisteminin performansı bu dört senaryodan 30 derecelik açıda en kötü, 20 derecelik açıda ise en iyi sonuçları vermiřtir.

**Anahtar Kelimeler** : Absorpsiyonlu soğutma sistemi, Yenilenebilir enerji, Güneř enerjisi, Fotovoltaik hücreler, Sürdürülebilir enerji.

**Bilim Kodu** : 91413



## **ACKNOWLEDGMENT**

First of all, we thank God who enabled me to complete this scientific study. I am very grateful to the first supervisor of my thesis, Assistant Prof. Dr. Abdulrazzak AKROOT for his guidance and supervision. I also extend my thanks and gratitude to the second supervisor of my thesis, Assistant Prof. Dr. Ahmed Shihab AL-SAMARI for his guidance and continuous supervision, as well as for giving me a golden opportunity to complete this work, which also helped me in conducting a great amount of research, the most important of which is scientific research that has been published globally within Scopus containers. I would like to express my appreciation to the Department of Mechanical Engineering, Faculty of Engineering at Karabük University, Turkey. I would also like to express my appreciation to the Department of Mechanical Engineering, Faculty of Engineering at Diyala University in Iraq. Without it, all this would not have been possible. Finally, I would like to thank my parents (may God have mercy on them), who always urged us to continue climbing the academic ladder to the end, and my mother who did not skimp on us in prayer and supplication to reach this academic rank. I thank my wife who endured many hardships of travel and assumed the responsibility of taking care of our child, in addition to her studies for a master degree at the Department of Public Health, Karabük University, where we started our master studies at the same time.

## CONTENTS

	<b><u>Page</u></b>
APPROVAL.....	ii
ABSTRACT.....	iv
ÖZET.....	vi
ACKNOWLEDGMENT.....	viii
CONTENTS.....	ix
LIST OF FIGURES .....	xiii
LIST OF TABLES .....	xv
SYMBOLS AND ABBREVIATIONS .....	xvii
PART 1 .....	1
INTRODUCTION .....	1
1.1. ENERGY SUPPLY .....	4
1.1.1. Renewable Energy .....	5
1.1.2. Photovoltaic Development.....	6
1.2. ABSORPTION REFRIGERATOR.....	7
1.2.1. Principle of an Absorption Refrigerator .....	7
1.2.2. Improvement of the Absorption Process .....	9
1.3. EFFICIENCY LOSSES .....	10
1.4. OBJECTIVES .....	10
1.5. THE STUDY PROBLEM.....	10
1.6. THE IMPORTANCE OF THE STUDY .....	11
1.7. THESIS STRUCTURE .....	11
PART 2 .....	12
LITERATURE REVIEW.....	12
2.1. PREVIOUS LITERATURE.....	12
2.2. SUMMARY .....	36
PART 3 .....	37

THEORETICAL BACKGROUND .....	37
3.1. EQUATIONS OF A GENERAL THERMODYNAMIC NATURE .....	37
3.1.1. The First Law of Thermodynamics .....	37
3.2. GENERAL ABSORPTION REFRIGERATION CYCLE EQUATIONS ....	39
3.2.1. Generator and Bubble Pump .....	40
3.2.2. Rectifier .....	41
3.2.3. SHX .....	41
3.2.4. Condenser .....	42
3.2.5. Evaporator.....	43
3.2.6. Absorber .....	43
PART 4 .....	48
EXPERIMENTAL WORK.....	48
4.1. THE TRADITIONAL ABSORPTION REFRIGERATION SYSTEM (ARS)	48
4.1.1. THE TRADITIONAL ABSORPTION REFRIGERATION SYSTEM (ARS)	48
4.2. REFRIGERATOR INSTALLATION.....	48
4.3. SOLAR ABSORPTION REFRIGERATION SYSTEM .....	49
4.4. INSTALLATION STEPS OF THE REFRIGERATOR .....	50
4.4.1. Photovoltaic Panel .....	52
4.4.2. DC Heater .....	53
4.4.3. Ceramic Wool Thermal insulator .....	53
PART 5 .....	55
RESULTS AND DISCUSSION .....	55
5.1. THE FIRST EXPERIMENT .....	56
5.2. THE SECOND EXPERIMENT .....	62
5.3. THE THIRD EXPERIMENT.....	74
5.4. THE FOURTH EXPERIMENT .....	78
PART 6 .....	84
CONCLUSIONS AND RECOMMENDATIONS .....	84
6.1. CONCLUSIONS .....	84
6.2. RECOMMENDATIONS .....	84
REFERENCES.....	86

APPENDIX A.....	94
APPENDIX B.....	100
ABSORPTION REFRIGERATION SYSTEM CATALOG.....	100
RESUME .....	105

## LIST OF FIGURES

	<u>Page</u>
Figure 1.1. The solar thermochemical energy conversion process.....	3
Figure 1.2. Simple Carnot heat engine.....	4
Figure 1.3. The capacity for renewable energy increases by 10% from 2020 to 2021 ( <i>x</i> -axis represents the number of years and <i>y</i> -axis represents the amount of energy expected to increase over the years).....	6
Figure 1.4. Components of an absorption refrigeration system.....	9
Figure 2.1. Schematic diagram of the DAR cycle (adapted from Dometic, 2004)....	16
Figure 2.2. Experimental apparatus developed and adapted from. ....	22
Figure 2.3. Laboratory DAR system used in tests. ....	27
Figure 3.1. DAR cycle .....	40
Figure 3.2. Circuit of a photovoltaic cell .....	45
Figure 3.3. Maximum power on a characteristic of current and voltage .....	46
Figure 4.1. Solar absorption refrigeration system.....	49
Figure 4.2. The absorptive cryosection system (ARS) during the experiment. ....	51
Figure 4.3. The absorptive refrigeration system that was tested showing the rectifier and the condenser. ....	51
Figure 4.4. The absorption refrigeration system that was tested showing the absorber, receiver and generator. ....	52
Figure 4.5. Photovoltaic panel, nominal power 580 W.....	52
Figure 4.6. DC heater (48 V, 450 W).....	53
Figure 4.7. Ceramic wool thermal insulator.....	54
Figure 5.1. Temperature curve at the input of the generator over 232 minutes. ....	56
Figure 5.2. Rectifier temperature data for 232 minutes. ....	57
Figure 5.3. Data for condenser input temperature for 232 minutes. ....	57
Figure 5.4. Temperatures at the exit of the condenser over a 232-minute period.....	58
Figure 5.5. Evaporator temperature data over a 232-minute period. ....	59
Figure 5.6. Fridge temperatures of the system during the 232-minute period.....	59
Figure 5.7. Ambient temperatures of the system over a 232-minute period.....	60
Figure 5.8. Comparison between the generator temperature and evaporator temperature with room temperature around the refrigerator over the 232-minute period. ....	61

	<u>Page</u>
Figure 5.9. 3D model of a comparison between the generator temperature and evaporator temperature over a period of 232 minutes. ....	62
Figure 5.10. Generator temperature entry data during the 156-minute period of the second experiment. ....	63
Figure 5.11. Generator output temperature data curve during the 156-minute period. ....	64
Figure 5.12. Rectifier temperature data over the 156 minutes of the second experiment. ....	65
Figure 5.13. Inlet condenser temperature data over the 156 minutes of the second experiment. ....	66
Figure 5.14. Condenser temperature output data over the 156 minutes of the second experiment. ....	66
Figure 5.15. Evaporator temperature data during the 156 minutes of the second experiment. ....	67
Figure 5.16. Fridge temperature data during the 156 minutes of the second experiment. ....	68
Figure 5.17. Absorber temperature curve after 156 minutes of the second experiment. ....	69
Figure 5.18. Room temperature data over the 156 minutes of the second experiment. ....	69
Figure 5.19. Data of DC consumed by the refrigerator over the 156 minutes of the second experiment. ....	70
Figure 5.20. Data of the voltage consumed by the electric heater during the 156 minutes of the second experiment. ....	71
Figure 5.21. Comparison between the voltage and current of the DC heater during the operation of the ARS system. ....	72
Figure 5.22. 3D model of input temperature in the generator and temperatures in the evaporator of the SARS solar absorption refrigerator over 156 minutes. ....	72
Figure 5.23. Comparison of the temperatures of the generator, evaporator, condenser, and rectifier, as well as room temperature during the 156 minutes of the second experiment. ....	73
Figure 5.24. Comparison between the generator output temperature and the evaporator temperature as well as the refrigerator temperature and the amount of power in the generator. ....	74
Figure 5.25. Temperature data shown in the curves on the first day of the third experiment, during the first 24 hours. ....	75
Figure 5.26. Temperature data shown in the curves on the second day of the third experiment, during the second 24-hour period. ....	76

	<u>Page</u>
Figure 5.27. Temperature data for the parts of the system from the third day of the third experiment over a 24-hour period. ....	77
Figure 5.28. A three-dimensional model for the third experiment over three days... ..	77
Figure 5.30. Temperature data are shown in the curves for three consecutive days of the third experiment, over a 72-hour period .....	78
Figure 5.31. Temperature data for system components over a 2,246-minute period. ..	79
Figure 5.32. Comparison of the temperatures of the components of the system during 1,440 minutes.....	80
Figure 5.33. Temperature data over an 800-minute period for the second day within the last 13 hours. ....	81
Figure 5.34. Temperature data for system components in curves over 2,700 minutes within 45 hours. ....	82

## LIST OF TABLES

	<u>Page</u>
Table 1.1. Cost of home heating in South Africa delivered by electricity and bottled gas.....	2
Table 4.1. Specifications of the conventional and solar-assisted absorption refrigeration system. ARS & AC.ARS V170KE model. ....	48



## SYMBOLS AND ABBREVIATIONS

### SYMBOLS

ARS	: Absorption refrigeration system
SARS	: Solar absorption refrigeration system
T	: Temperature ( $^{\circ}\text{C}$ , K)
P	: pressure (bar)
h	: Specific enthalpy (J/kg)
$\dot{m}$	: Mass flow rate (kg/s)
cp	: Specific heat capacity at constant pressure (J/kg K)
$\dot{Q}$	: Heat transfer rate (W)
X	: Molar fraction of liquid solution [-]
Y	: Ammonia mole fraction of vapour mixture [-]

### ABBREVIATIONS

Amb.	: Ambient
Abs	: Absorber
Gen.	: Generator
Cond.	: Condenser
Evap.	: inert gas
IG	: inert gas
Rect.	: Rectifier
Loss	: Thermal losses in the bubble pump
LSHE	: Liquid solution heat exchanger
GHX	: Gas heat exchanger
DAR	: Diffusion absorption refrigeration
PIR	: Polyisocyanurate
COP	: Coefficient of performance

## **PART 1**

### **INTRODUCTION**

Since the beginning of time, the necessity of sheltering from the elements and preserving and preparing food has been helped by meeting our household energy needs. In addition to the passive insulation that homes can provide, heating has become vital throughout any winter. Prior to the invention of artificial refrigeration, ice cellars were utilised by aristocratic people in ancient Greece and Rome to keep and store perishable items. Moreover, ice was used to cool wine. Records even show the Caliph of Baghdad in the eighth century using packed ice between the walls of his summer villa for cooling [1].

Due to the exponential growth of these energy requirements, electricity presently meets the bulk of the heating and cooling needs of homes, businesses, and other facilities. This is especially true in South Africa, where a lack of infrastructure prevents the use of natural gas or industrial waste heat to cover a portion of the country's heating needs, as is commonplace in Europe. It is expected that all hot water geysers, heaters, and air conditioners be powered by readily available electricity. This may change in the future, as rising electricity prices [2] will drive savvy and energy-conscious consumers to examine alternative energy sources, when accessible.

Egoli Gas has been a local provider of natural gas to the greater Johannesburg metropolitan region since 2000, supplying various residential, commercial, and industrial clients [3]. Their natural gas consists of 92% methane and it is delivered independently of power failures or load shedding [3] at peak hours or times of heavy demand. For the purpose of brevity, from here on, all types of gas fuels shall be referred to as "gas." Gas-powered appliances, which may offer direct heating for

both hot water and for spaces, are more convenient than their electrical counterparts owing to the availability of a fuel supply.

Table 1.1. Cost of home heating in South Africa delivered by electricity and bottled gas.

<b>Source R/kW.h</b>	<b>Sources R/kW.h</b>
<b>Electricity 1.19</b>	Electricity 1.19
<b>LP Gas 1.42</b>	LP Gas 1.42

Gas appliances are more expensive than typical electric appliances. However, Egoli's natural gas heating costs are comparable to household electricity rates. Egoli Gas has not responded to a request for a price list as of the writing of this dissertation. According to Table 1.1, the cost of heating with bottled propane, butane, or similar mixtures is approximately 20% greater than the cost of heating with electricity.

The familiarity with typical gas-powered freezers (a type of absorption chiller) indicates that chilling may be achieved through the use of thermal energy. This dissertation will give a comprehensive analysis of the topic, since it serves as the foundation for the proposed diffusion absorption thermodynamic cycle. Using tri-generation, whereby an absorption unit is coupled to a steam generating cycle, Egoli Gas is also capable of concurrently delivering power, heating, and cooling to industrial customers, all of which is accomplished utilising natural gas as the source of energy [3].

Utilising gas, liquid, or solid fuels provides the advantage of on-site fuel conversion to heat energy. This conversion is based on an appliance or tool's combustion efficiency and heat transmission losses. Induction ovens and stoves reduce these losses; however, the heat source must be electricity, which is produced inefficiently from the chemical energy of coal.

According to Storm [4], using a simple coal burner for cooking is approximately 70% more effective in terms of energy conversion when using coal as the direct heat source.

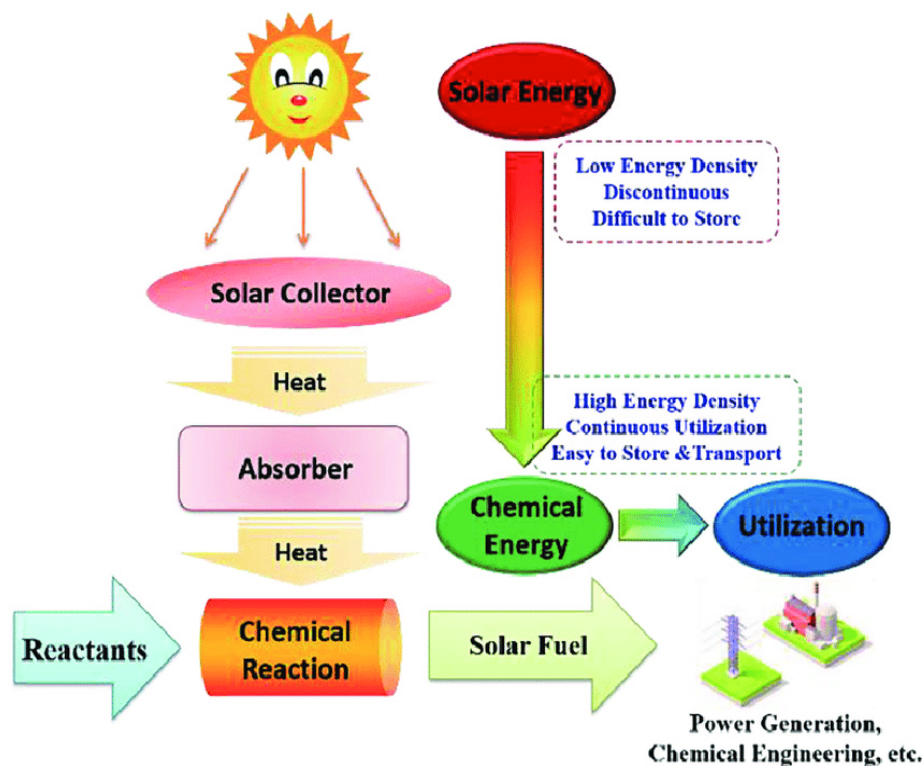


Figure 1.1. The solar thermochemical energy conversion process. Wang, H. S. (2020).

Organic plant matter is compressed under high pressures over millions of years (or thousands of years, depending on one's religious beliefs) while interacting with other substances and undergoing other processes. These secondary processes create natural gases, such as methane, propane, and butane in addition to crude oil. Coal, with varying amounts of energy content, comprises the bulk of the surviving fossilised materials. [5]. In the current period, these fossil fuels with their very high energy density are irreplaceable.

Numerous losses ensue from converting these fuels into electrical energy, which is subsequently transmitted (with further losses) to shaft power to drive household air conditioners and thermal power to provide warmth. When the aforementioned energy stream is finally traced back to its source, the sun, it is discovered that the consumption of its initial supply is highly inefficient.

When solar energy is directly used, the process of energy conversion is many orders of magnitude more effective and renewable. Figure 1.1 illustrates two ways. Due to

its essential reliance on the availability of sunshine throughout the year, the direct use of solar energy is impractical in a number of locations around the globe.

### 1.1. ENERGY SUPPLY

The bulk of South Africa's base-load energy needs are met by Eskom's thirteen coal-fired thermal power facilities, with two further comparable stations now under construction [6]. Due to South Africa's abundant coal supply, this is the most cost-effective method for generating energy. A variety of cutting-edge technologies have been used not to only allow the burning of up until now ineffective low-grade coals, but also to drastically decrease and even collect emissions of common SO<sub>x</sub> and NO<sub>x</sub> compounds and fly ash. In addition, the zero-effluent construction regulation that has been enforced on all new plants for the last three decades has eliminated the transport of toxins from these plants into groundwater and rivers. Despite the country's low pollution levels and massive coal reserves, coal is not a sustainable energy source. The question of whether these are the sole issues will be examined in further detail.

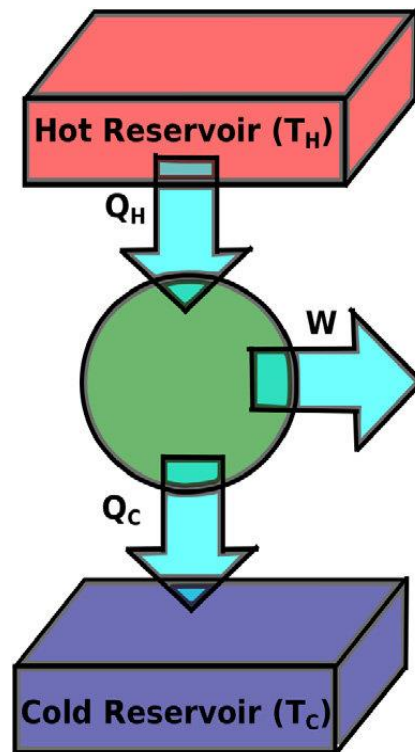


Figure 1.2. Simple Carnot heat engine. Rajani, K. V., et al.(2020)

Net work done by cycle. (1.1)

$$\Delta U_{\text{ws}} - Q_{\text{net}} - W_{\text{net}} = Q_H - Q_L - W = 0$$

$$Q_H - Q_L = W$$

Carnot cycle efficiency (1.2)

$$\eta = W / Q_H = (Q_H - Q_L) / Q_H = 1 - Q_L / Q_H$$

Carnot's Theorem is derived from the Second Law of Thermodynamics and asserts that even under ideal circumstances, a considerable fraction of the input energy must be rejected for a heat engine to create a significant amount of power. Eq. 1.1 shows the link between energy intake,  $Q_H$ , and energy rejected,  $Q_L$ , in terms of a thermodynamic cycle's work output (in  $W$ ). Figure 1.3 illustrates the inputs and outputs of this methodology. All thermodynamic cycles can be reduced to Carnot cycle elements; thus, Eq. 1.1 is true.

### 1.1.1. Renewable Energy

Renewable energy refers to energy sources that are naturally renewed during the lifespan of humans. These include the sun, the wind, the flow of water, and geothermal heat. Despite the fact that many renewable energy sources are sustainable, others, such as some biomass sources, may not be if present extraction rates continue. Renewable energy is used for a range of reasons, including the production of electricity, the heating and cooling of air and water, and the operation of independent power systems [7-9]. It may be applied in large-scale projects, rural and distant places, and emerging nations where energy is crucial to human growth. Integration of renewable energy with greater electrification offers various advantages, including enhanced efficiency in energy consumption and the capacity to transmit heat and items using clean energy in an effective manner. Consequently, the utilisation of renewable energy may result in substantial reductions in primary energy demands [10-14].

Between 2011 and 2021, the proportion of the global supply of renewable energy increased from 20% to 28%, whereas the share of fossil energy decreased from 68%

to 62% and for nuclear energy, it decreased from 12% to 10%. The amount of hydropower declined from 16% to 15%, while solar and wind generation increased from 2% to 10%. Additionally, biomass and geothermal energy usage increased from 2% to 3%. As of 2021, 3,146 GW of renewable energy facilities had been built in 135 nations, and 156 countries have legislation governing the renewable energy industry. China was responsible for over half of the global increase in renewable power in the same period [15, 16]. Figure 1.3 illustrates the evolution of energy usage in recent years.

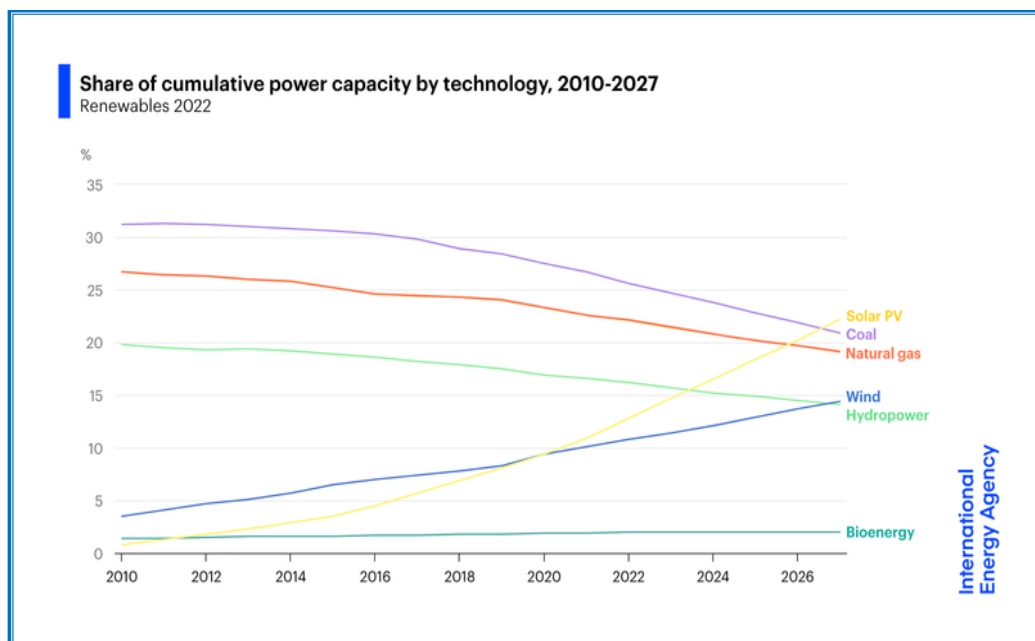


Figure 1.3. The capacity for renewable energy increases by 10% from 2020 to 2021 (x-axis represents the number of years and y-axis represents the amount of energy expected to increase over the years)

### 1.1.2. Photovoltaic Development

The photovoltaic (PV) technology converts sunlight into electrical energy using solar panels composed of linked solar cells. PV system deployment ranges from modest rooftop or building-integrated installations to large, utility-scale solar power facilities. Crystalline silicon is the main material used in photovoltaics, whereas thin-film solar cell technology accounts for a small percentage of worldwide photovoltaic deployment. In recent years, developments in PV technology have enhanced the efficiency of power generation, decreased the cost per watt, and shortened the energy

payback period. In at least thirty markets, grid parity had already been achieved by 2014. Building-integrated photovoltaics or onsite PV systems makes use of existing buildings and land to produce electricity close to the point of consumption [17]. China had considerable growth in photovoltaics between 2016 and 2021, adding 560 GW to the grid and exceeding the combined growth of all advanced economies. It is anticipated that by 2027, the installed capacity of solar PVs would exceed that of coal, giving it the greatest capacity in the world. This will demand an increase in installed PV capacity to 4,600 GW, with China and India deploying more than half of that amount [18].

## **1.2. ABSORPTION REFRIGERATOR**

The Absorption Refrigerator is a type of refrigeration system that uses heat as its energy source for chilling. The system employs two coolants, the first of which undergoes evaporative cooling and is then absorbed by the second. Heat is necessary to return the two coolants to their original condition. This approach may also be used for the air conditioning of buildings by using waste heat from a gas turbine or water heater. This method, known as tri-generation, is very efficient. Due to the variety of available heat sources to fuel them, absorption refrigerators are prevalent in recreational vehicles, campers, and caravans. A propane fuel burner, a low-voltage DC electric heater driven by a battery or vehicle electrical system, and a mains-powered electric heater are examples of these sources. Absorption refrigerators, unlike conventional vapour-compression refrigeration systems, have no moving components, making them a stable and lasting solution for cooling requirements [19].

### **1.2.1. Principle of an Absorption Refrigerator**

Solar energy, industrial waste heat, and district heating systems are examples of heat sources that may be used to power absorption refrigeration systems. In contrast to compression refrigeration systems, which use refrigerants such as HCFCs or HFCs, absorption refrigeration systems use coolants such as ammonia or water in conjunction with an absorbent, such as brine for water, to absorb the coolant. Both methods depend on evaporative cooling, in which the refrigerant evaporates and



absorbs heat from the environment. The primary difference between the two systems is how the refrigerant is transformed back into a liquid so that the cycle may be repeated. Absorption refrigeration systems use a heat-based process to convert the gas back into a liquid and have no moving components other than the fluids [20-22]. The three steps of the absorption cooling cycle are evaporation, absorption, and regeneration. The liquid refrigerant evaporates in a low partial pressure environment during the evaporation phase, extracting heat from its surroundings. When the second fluid in a depleted condition absorbs the gaseous refrigerant, a refrigerant-saturated liquid is produced. The regeneration phase occurs when a liquid saturated with refrigerant is heated, causing the refrigerant to evaporate. This evaporation occurs at the bottom end of a thin tube, and the refrigerant-depleted liquid is pushed into a higher chamber by refrigerant gas bubbles. The heated, gaseous refrigerant passes through a heat exchanger, where its heat is transferred outside of the system and condenses at a higher elevation. The condensed liquid refrigerant then returns to the phase of evaporation [23].

A compressor-based heat pump, on the other hand, operates by pushing refrigerant gas from an evaporator to a condenser using energy from an electric motor or internal combustion engine. The compressor decreases the evaporator's pressure and boiling temperature while raising the condenser's pressure and condensing temperature [24]. The heated, high-pressure gas reaches the condenser, where it undergoes a phase transition to a liquid and releases heat into the surrounding environment. Through an expansion valve, the heated liquid refrigerant flows from the high-pressure condenser to the low-pressure evaporator. The expansion valve partly vaporises the refrigerant, combining evaporative and expansive cooling to chill it. The cold, low-pressure liquid refrigerant absorbs heat from the evaporator's environment, vaporises, and enters the compressor to begin the cycle again [19, 25].

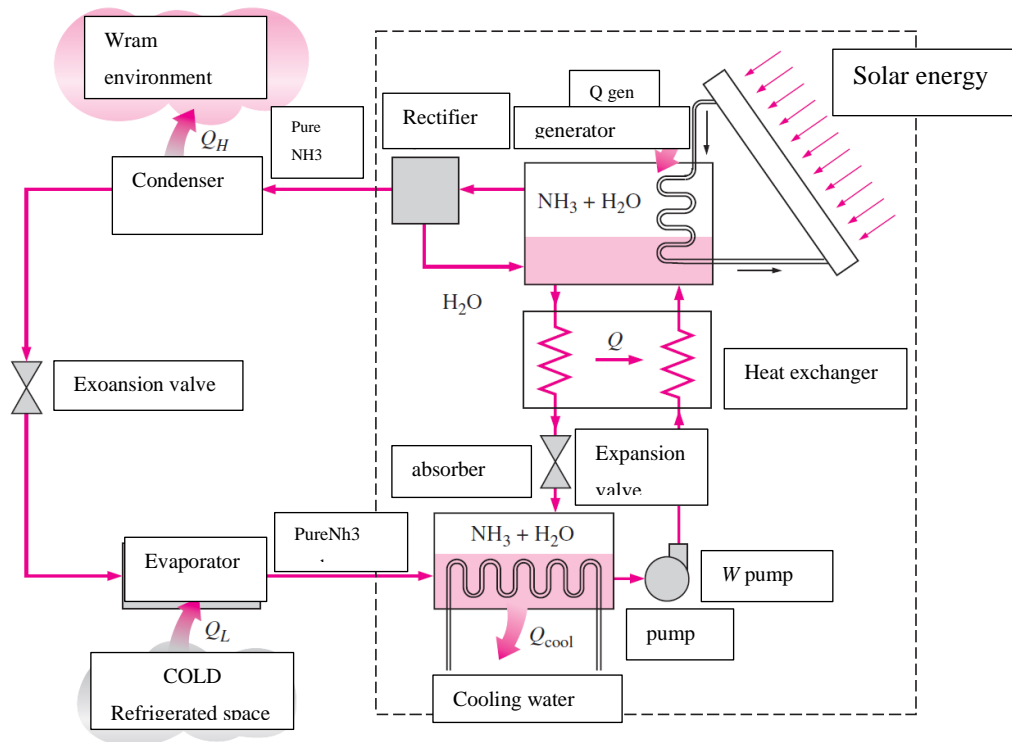


Figure 1.4. Components of an absorption refrigeration system. (derived from Kumar, Subhash, and Dr. RR Arakerimath)

### 1.2.2. Improvement of the Absorption Process

An absorber is an essential component of any absorption refrigeration system. Due to the non-equilibrium condition of the solution, research indicates that the solution circulation rate in the absorber is two to five times greater than the predicted value. This results in less refrigerant being absorbed than is theoretically achievable for a given temperature and pressure. Numerous investigations have been conducted to comprehend and enhance the absorption mechanism between refrigerant vapour and solution. [26, 27]. The most prevalent absorber design for the LiBr/water system is the falling film absorber, in which the vapour refrigerant is absorbed into a liquid film over cooled horizontal tubes. This design permits simultaneous heat removal from the liquid sheet, resulting in a higher absorption rate. Nonetheless, this design needs a high recirculation rate for optimum efficiency. Rotex proposes as an additional effective method the absorption of refrigerant vapour into a liquid coating on cooled revolving discs. Compared to traditional designs, the absorption rate on spinning discs is substantially greater for a given surface area, allowing for a lower

absorber size. Further examined is the absorption mechanism inside a revolving drum. For the water/NH<sub>3</sub> system, there is also a substantial amount of literature on absorber designs [28-34].

### **1.3. EFFICIENCY LOSSES**

Efficiency is a performance statistic for the conversion of energy into work, as shown by Eq. 1.2. All energy that is not converted into work is either accounted for as rejected energy or as losses since the cycle cannot be reversed. This means that, for coal-fired facilities using the Rankine thermodynamic cycle, the percentage of energy that is not converted into electrical power is lost as thermal energy. The design efficiency of the Lethabo Power Plant at maximum continuous turbine rating is 37.80%. This amounts to 62.2 MW of thermal losses for a 100 MW input at the design point. This amounts to 6,101 MW of thermal losses for a total installed capacity of 3,708 MW, which may be broken down into heat rejected by cooling systems and heat rejected by waste heat.

### **1.4. OBJECTIVES**

The main aim of this project is to integrate solar photovoltaic energy into the Absorption Refrigeration System (ARS) directly without the use of a power converter that provides alternating current, which leads to a significant reduction in costs and the elimination of maintenance costs as well and benefits from the lack of the effect of voltage fluctuations on the heater that was designed to operate the system. Other objectives include calculating and comparing COP for solar ARS cycles and conventional ARS, as well as analysing the temperature connection between the generator, evaporator, and other components.

### **1.5. THE STUDY PROBLEM**

Energy crises are increasing regularly due to limited energy resources that feed electrical energy consumption for air conditioning (heating and cooling), which represents approximately 70% of electrical energy consumption.

## **1.6. THE IMPORTANCE OF THE STUDY**

The importance of this study lies in establishing a solar-powered cooling system partially to replace the use of traditional energy. Thus, energy production and storage costs and harmful emissions can be reduced. This system can be used from sunrise until sunset in all health, commercial, and residential sectors and institutions, especially in remote and rural areas to which it is difficult to deliver electrical power and to store medicines, vaccines, food, etc.

## **1.7. THESIS STRUCTURE**

This study consists of five main parts. An introduction and general information about energy, renewable energy, and absorption icing systems are given in Part 1. The literature related to this study is presented in Part 2. The theoretical basic relationships of heat transfer between parts of an absorption icing system as well as the theoretical basic relationships related to solar PV are presented in Part 3. The practical method, materials used and the mechanism of action are presented in Part 4. The results and a discussion are presented in Part 5. Finally, conclusions are given in Part 6.

## **PART 2**

### **LITERATURE REVIEW**

Absorption cooling cycles are used by a variety of large industrial chillers and residential freezers. The majority of industrial units obtain mass flow by a pressure difference established by a pump, thus the phrase dual-pressure cycle. The pump may either be driven by an electric motor or a turbine. Flow in single-pressure or diffusion absorption cycles (such as freezers for camping) is powered by a bubble pump that functions on the principles of natural convective boiling and any resulting density changes in the working fluid. After a comprehensive analysis of absorption technology and its applications, the operation of single-pressure or diffusion cycles will be examined in detail. Various pairings and mixtures of working fluids are analysed in terms of their benefits and drawbacks. Studies completed previously on solar-powered applications will then be examined. In addition to practical trials that are used to verify the model covered in this study, a comprehensive analysis of competing models is presented.

This literature evaluation aims to assess whether absorption technology might cover residential energy requirements when powered only by solar energy at a cost equivalent to or lower than that of vapour compression systems. Few college textbooks and courses discuss diffusion absorption cycles as there is a paucity of literature in this topic. The many processes, interactions, and performance of absorption machine components are influenced by several variables. This chapter attempts to offer a complete review of the investigation's key components.

#### **2.1. PREVIOUS LITERATURE**

E. Ruiz, V. Ferro, J. De Riva, D. Moreno and J. Palomar [35] estimated the thermodynamic performance of ammonia absorption refrigeration cycles using ionic

liquids as absorbents by applying COSMO-based process simulations with Aspen Plus/Aspen HYSYS. This enabled them not only to select or design ionic liquids with optimal characteristics but also to analyse techniques for enhancing the performance of the cycle. The COSMO-RS approach supplied the essential data for the creation of the non-database ionic liquid components and the specification of the COSMOSAC property model for the Aspen Plus computations. The computational findings for numerous ionic liquid-based systems were found to be in good agreement with those previously published in the scientific literature. In addition, task-specific ionic liquids with enhanced ammonia absorption characteristics and binary ionic liquid mixes were analysed, and it was discovered that ionic liquids with a higher ammonia absorption capacity provided the best cycle performance, and that the cycle performance varied widely depending on the ammonia concentration in the refrigerant + absorbent solution, with this behaviour being strongly modulated by the ammonia absorption capacity of the absorbent. Ionic liquid mixes would not only permit the changing of the working concentration interval of the cycle but also enhanced its performance.

A. Najjaran and J. Freeman [36] conducted an experimental assessment of a 120-watt nominal cooling capacity ammonia-water ARS system. The system was heated by electrical cartridge heaters with variable thermal inputs of 300-700 W and variable generating temperatures, of 150-200°C, indirectly measuring the cooling output of the system by heating the air inside an insulated cold box around the evaporator to counteract its cooling impact. Tests were done using the DAR system's factory default settings (23.8 bar and an ammonia concentration of 30 wt.%). The cooling output achieved was between 79 W and 104 W, equivalent to a COP of between 0.11 and 0.26. The agreement between the findings and performance estimations using a steady-state system model was satisfactory. Temperature measurements at various points in the system were used to further validate the model assumptions, with a focus on the condenser temperatures to evaluate the degree of sub-cooling and the efficacy of the rectification process, as well as the effect of the air temperature and flow regime in contact with the evaporator on the predictions of the cooling output and the COP of the system.

S. Mazouz, R. Mansouri and A. Bellagi [37] performed experimental and thermodynamic research on a commercial absorption diffusion device taking two distinct experimental approaches, namely steady state and dynamic, to examine the machine's features and its cooling capability. The total heat transfer coefficients (UA ext and UA int) were calculated to be 0.43 W/K and 0.21 W/K, respectively. The experiments were performed under realistic circumstances of indoor air quality and varying heat loads. A COP of 0.12 was determined for a heat supply of 42 W and a generating temperature of 185°C.

A. Acuña, N. Velázquez and J. Cerezo [38] conducted a study using ammonia (NH<sub>3</sub>) as the refrigerant, comparing lithium nitrate (LiNO<sub>3</sub>), sodium thiocyanate (NaSCN), and water (H<sub>2</sub>O) as absorbent components in a diffusion absorption cooling system. They also investigated the impact of introducing gases such as helium (He) or hydrogen (H<sub>2</sub>) on the efficiency of the system. At a generator temperature of 120°C and absorber and condenser temperatures of 40°C, the NH<sub>3</sub>-LiNO<sub>3</sub>-He combination was found to have the highest COP of 0.48, followed by the NH<sub>3</sub>-NaSCN-He and NH<sub>3</sub>-LiNO<sub>3</sub>-He mixes at an evaporator temperature of 10°C. The NH<sub>3</sub>-NaSCN-He combination showed a greater COP at lower evaporator temperatures than the NH<sub>3</sub>-H<sub>2</sub>O-He mixture. In the generator, the NH<sub>3</sub>-LiNO<sub>3</sub> combination likewise crystallised at higher temperatures and had lower activation temperatures than the NH<sub>3</sub>-NaSCN mixture.

F. Assilzadeh, S.A. Kalogirou, Y. Ali and K. Sopian [39] conducted an study on evacuated tube solar collectors and a lithium bromide (LiBr) absorption unit, wherein they investigated a solar-powered air-conditioning system intended for use in Malaysia and comparable tropical locations. The system was modelled and simulated using TRNSYS and a file containing Malaysian weather data for a typical meteorological year. The findings indicated that the system was synchronised with the weather, with a strong need for cooling during times of intense solar radiation. A 0.80 m<sup>3</sup> hot water storage tank would be required to enable continuous operation and improve the system's dependability. The best solution for the climate of Malaysia for a 3.5 kW (1 refrigeration ton) system would be comprised of 35 m<sup>2</sup> evacuated tube solar collectors sloping at 20°C.

M. Herrando and A.M. Pantaleo [40] created and used a modelling approach to evaluate the techno-economic performance of solar combined cooling, heating, and power (S-CCHP) systems based on hybrid photovoltaic thermal (PVT) collectors. According to the research, a 1.68-megawatt S-CCHP system was able respectively to provide 20.9%, 55.1%, and 16.3% of the heating, cooling, and electricity needs of a university campus in Bari, Italy. It was discovered that the S-CCHP system has a payback period of 16.7 years, which is 2.7 times longer than a PV system. The S-CCHP system also had a longer [41] payback time than a system that does not produce energy based on evacuated tube collectors (ETC). It was determined that the S-CCHP system displaces 911 tons of CO<sub>2</sub> annually, which is 16% and 1.4 times greater than the PV system and the ETC-based system. The research also indicated that the sensitivity of the systems to utility costs was substantial.

A. Ramos, M.A. Chatzopoulou [42] conducted research on solar energy systems with hybrid photovoltaic-thermal (PV-T) collectors with overall efficiency of at least 70% and that are able to produce both electricity and heat. When appropriately constructed for combined heating and cooling services, PV-T systems may provide over 60% of families' heating needs and over 50% of their cooling needs in urban contexts. A study of ten European sites revealed that PV-T systems paired with water-to-water heat pumps were the most efficient configuration and had the ability to satisfy 60% of combined heating and almost 100% of cooling needs in houses in the most promising areas (Seville, Rome, Madrid, and Bucharest). It was discovered that the levelised cost of energy for these systems is 30-40% less than that of identical PV-only systems.

G. Starace and L. De Pascalis [43] compared the performance of a novel thermodynamic model for a direct-absorption refrigeration (DAR) system to the predictions of an earlier investigation. In the latest research, which used pure ammonia, the modelling of the refrigerant composition was more accurate than in the previous investigation. As the generator temperature and absorption temperature rise, the new research revealed that the mass flow rate of the rich solution falls more than that of the refrigerant, and the coefficient of performance (COP) also declines. The COP was observed to rise when the ammonia concentration dropped. The study also



found that at lower heat fluxes supplied to the generator, heat dissipation toward the ambient dominates and the COP decreases. However, when the heat flux exceeds a certain threshold, the evaporator reaches its maximum heat transfer, which remains constant for any further increase in heat supplied. The COP attained its peak values within a narrow range of operating circumstances for the generator.

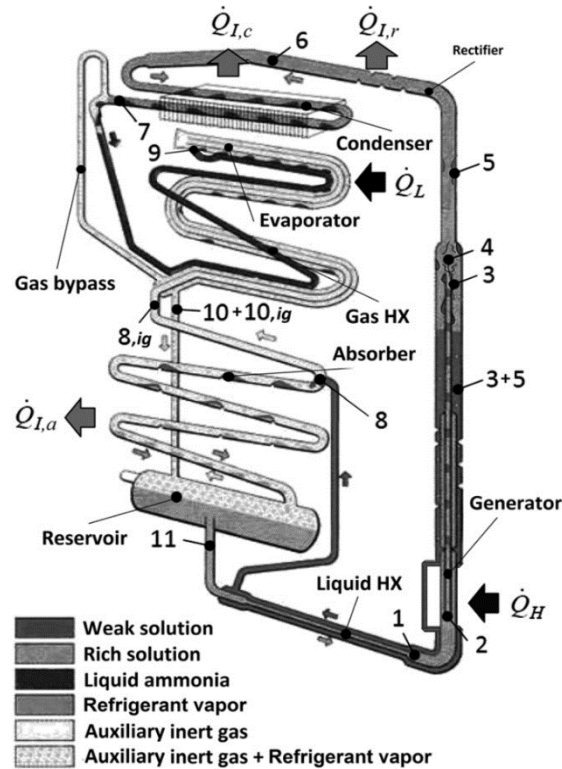


Figure 2.1. Schematic diagram of the DAR cycle [16].

A. Zohar, M. Jelinek [44] studied the effectiveness of three distinct configurations of diffusion absorption refrigeration (DAR) systems powered by heat and did not have any moving components. These systems are well-known for their dependability and their ability to operate quietly despite their rather poor COP. The configurations that were investigated included (a) heat being introduced into the rich solution, but without any heat transfer to the poor solution, (b) heat being introduced into the rich solution with heat transfer to the poor solution in the annular region, and (c) heat being introduced into the rich solution through the poor solution, and there being heat transfer to the poor solution in the annular region (a configuration used in commercial systems). According to the findings of the study, the second

configuration desorbed the greatest quantity of refrigerant and had the highest COP, while the third configuration was less efficient than the second. The first configuration had the poorest performance. All three configurations had received the same amount of heat input.

G. Vicatos and A. Bennett [45] assessed the performance of a diffusion absorption refrigerator equipped with a multiple lift-tube bubble pump. This kind of pump is intended to boost the volume flow rates of fluids and the refrigeration capacity of a refrigerator. During tests conducted on the plant, it was discovered that the refrigeration cooling capacity had been increased without a significant drop in the COP. Furthermore, it was determined that the multiple lift-tube bubble pumps have no limitation on the fluid flow rate and are solely dependent on the amount of heat input. Instead of being constrained by the capacity of the pump, as is the situation in the industry at the present time, it enables more design versatility and a capability to satisfy the refrigeration requirement of the unit.

U. Jakob, U. Eicker, D. Schneider, A. Taki and M. Cook [46], in the course of their research project, the created and tested a solar-powered cooling machine utilising ammonia and water as refrigerants. The developed piece of equipment, which had a cooling capacity of 2.5 kW and known as a Diffusion-Absorption Cooling Machine (DACM), was developed specifically for use in air conditioning applications. The DACM has a bubble pump and an indirectly heated generator, both of which had shown promising performance in prototypes. However, the DACM had difficulties in maintaining consistent pressure and spreading liquid condensate in the evaporator, which resulted in the cooling capacity of the second prototype being restricted to 1.6 kW. In the third iteration of the prototype, the evaporator was improved so that it could achieve a maximum COP of 0.38. Additionally, the cooling capacity was raised to 3 kW. An enlarged characteristic equation of sorption chillers was used to simulate the DACM, and the results showed good agreement with the experimental data.

Ö. Kaynaklı and M. Kılıç (2007) [47] performed an extensive thermodynamic analysis of the water/lithium bromide absorption refrigeration cycle in order to investigate the impact that operating temperature and efficiency of the heat

exchanger have on the thermal loads of the components, as well as on the coefficients of performance (COP<sub>c</sub> and COP), and the efficiency ratio. According to the findings, raising the temperatures of the generator and the evaporator would lead to an increase in the COP<sub>c</sub> and COP values, whereas increasing the temperatures of the condenser and the absorber would lead to a fall in these values. In addition, it was discovered that the value varies with various temperatures. The effects of the solution heat exchanger and the refrigerant heat exchanger on the performance, efficiency ratio, and fluid temperatures were compared, and the results indicated that the solution heat exchanger (SHE) had a more significant impact on these parameters compared to the refrigerant heat exchanger (RHE) [Citation needed].

A. Dalkılıç and S. Wongwises [49] present the findings of a theoretical study on the performance of a conventional vapour-compression refrigeration system, a system employing refrigerant mixtures based on HFC134a, HFC152a, HFC32, HC290, HC1270, HC600, and HC600a. The researchers then compare these findings to those obtained using CFC12, CFC22, and HFC134a as alternative refrigerants. We note that HC refrigerants are still employed in a variety of applications despite their high risk of ignition, which is due to the fact that there is no evidence that HC refrigerants contribute to the depletion of the ozone layer or to the acceleration of global warming. According to the findings of Dalkılıç and Wongwises, every alternative refrigerant had a performance coefficient (COP) that was somewhat lower than those of CFC12, CFC22, and HFC134a at a condensation temperature of 50°C and an evaporation temperature ranging between -30°C and 10°C. According to the findings of the research, the most effective alternatives to CFC12 and CFC22 as refrigerants would be the blends of HC290 and HC600a, which have weight percentages of 40 wt.% and 60 wt.%, respectively, and HC290 and HC1270, which have weight percentages of 20 wt.% and 80 wt.%, respectively. The effect that the primary performance parameters would have on the refrigerating effect, coefficient of performance, and volumetric refrigeration capacity was also investigated for a range of evaporating temperatures. These primary performance parameters included the type of refrigerant, the degree of sub-cooling, and the degree of superheating. Previously, it had been discovered that the SHE may boost the COP value by as much as 44%, whereas the RHE had a far less significant impact of only 2.8%.

A. Arora and S. Kaushik [48]. conducted an exhaustive investigation of the exergy characteristics of a vapour compression refrigeration (VCR) cycle. In order to compute the COP, exergy destruction, exergetic efficiency, and efficiency faults for R502, R404A, and R507A, a computer model was constructed. The study was carried out with the evaporator temperature ranging from  $-50^{\circ}\text{C}$  to  $0^{\circ}\text{C}$  and the condenser temperature ranging from  $40^{\circ}\text{C}$  to  $55^{\circ}\text{C}$ . Based on the findings, it appeared that R507A would be a more suitable alternative to R502 than R404A. For all of the refrigerants that were taken into account, the efficiency flaw that was found to be the worst was concentrated in the condenser, while it was found to be the least severe in the liquid-vapour heat exchanger.

A. Dalkılıç and S. Wongwises [49], in their paper, present the findings of a theoretical study on the performance of a conventional vapour-compression refrigeration system. The system employed refrigerant mixtures based on HFC134a, HFC152a, HFC32, HC290, HC1270, HC600, and HC600a. The researchers then compare these findings to those obtained using CFC12, CFC22, and HFC134a as alternative refrigerants. HC refrigerants are still employed in a variety of applications despite their high risk of ignition. This is due to the fact that there is no evidence that HC refrigerants contribute to the depletion of the ozone layer or to the acceleration of global warming. According to the findings, every alternative refrigerant has a performance coefficient (COP) that is somewhat lower than that of CFC12, CFC22, and HFC134a at a condensation temperature of  $50^{\circ}\text{C}$  and an evaporation temperature that ranges from  $-30^{\circ}\text{C}$  to  $10^{\circ}\text{C}$ . According to the findings of the research, the most effective alternatives to CFC12 and CFC22 as refrigerants are the blends of HC290 and HC600a that have weight percentages of 40 wt.% and 60 wt.%, respectively, and HC290 and HC1270 that have weight percentages of 20 wt.% and 80 wt.%, respectively. The effect that the primary performance parameters have on the refrigerating effect, coefficient of performance, and volumetric refrigeration capacity was also investigated for a range of evaporating temperatures. These primary performance parameters include the type of refrigerant, the degree of sub-cooling, and the degree of superheating.

Z. Sun, C. Wang et al. (2020) [50] evaluated the feasibility of a CO<sub>2</sub> two-stage compression refrigeration system combined with parallel compression and a solar absorption partial cascade refrigeration system (CTRS + PC + PCRS) in commercial supermarket applications. A comparison was made between the CO<sub>2</sub> two-stage compression refrigeration system, a basic CO<sub>2</sub> two-stage refrigeration system (BCTRS), and a CO<sub>2</sub> two-stage compression refrigeration system with parallel compression (CTRS + PC), making use of important parameters such as the COP, the energy saving share (ESS), and the partial seasonal energy efficiency ratio (PSEER) as objective functions. According to the findings of the study, which took into account five representative cities in China (Beijing, Harbin, Wuhan, Guangzhou, and Chengdu), the COP of the CTRS + PC + PCRS increased by 47.28% in the Harbin area in comparison to the BCTRS, and by 14.28% in comparison to the CTRS + PC, respectively. When compared to the CTRS + PC, the maximum COP of the CTRS + PC + PCRS increased by 31.71% under subcritical conditions, and by 47.28% under transcritical conditions. Comparatively, the maximum COP of the CTRS + PC + PCRS increased by 12.27% under subcritical conditions, and by 7.78% under transcritical conditions. The greatest ESS that could be achieved in Beijing was 0.19, with the PSEER having grown by 22.54% and 2.81%, respectively, when compared to the BCTRS and CTRS + PC. These findings provide a conceptual justification for the use of CO<sub>2</sub> two-stage compression refrigeration systems in institutional grocery stores and other retail food establishments.

H. Wijaksana et al. (2019) [51] carried out an experimental examination of the effects of altering ammonia concentrations in the operation of a pumpless ammonia-aqua absorption refrigeration system that utilises an evaporator flooded with water. The purpose of this research was to explore the features and effects of the concentration of ammonia on the performance of the system while it was subjected to a refrigeration load. The study comprised maintaining the temperature of the generator at a constant 80°C using an electric heater while altering the amount of ammonia in a 500 mL solution from 18% to 59%. According to the findings, raising the ammonia concentration led to a drop in the amount of heat created in the generator and a reduction in the cooling effect produced in the evaporator. However, it also led to an improvement in cooling capacity and performance coefficients

(COP). According to the data, there was a correlation between the level of ammonia concentration and the level of cooling capacity and COP, with the maximum values being recorded at 59% ammonia concentration. The greatest possible cooling capacity and coefficient of performance, respectively, were 0.7180 kW and 0.829.

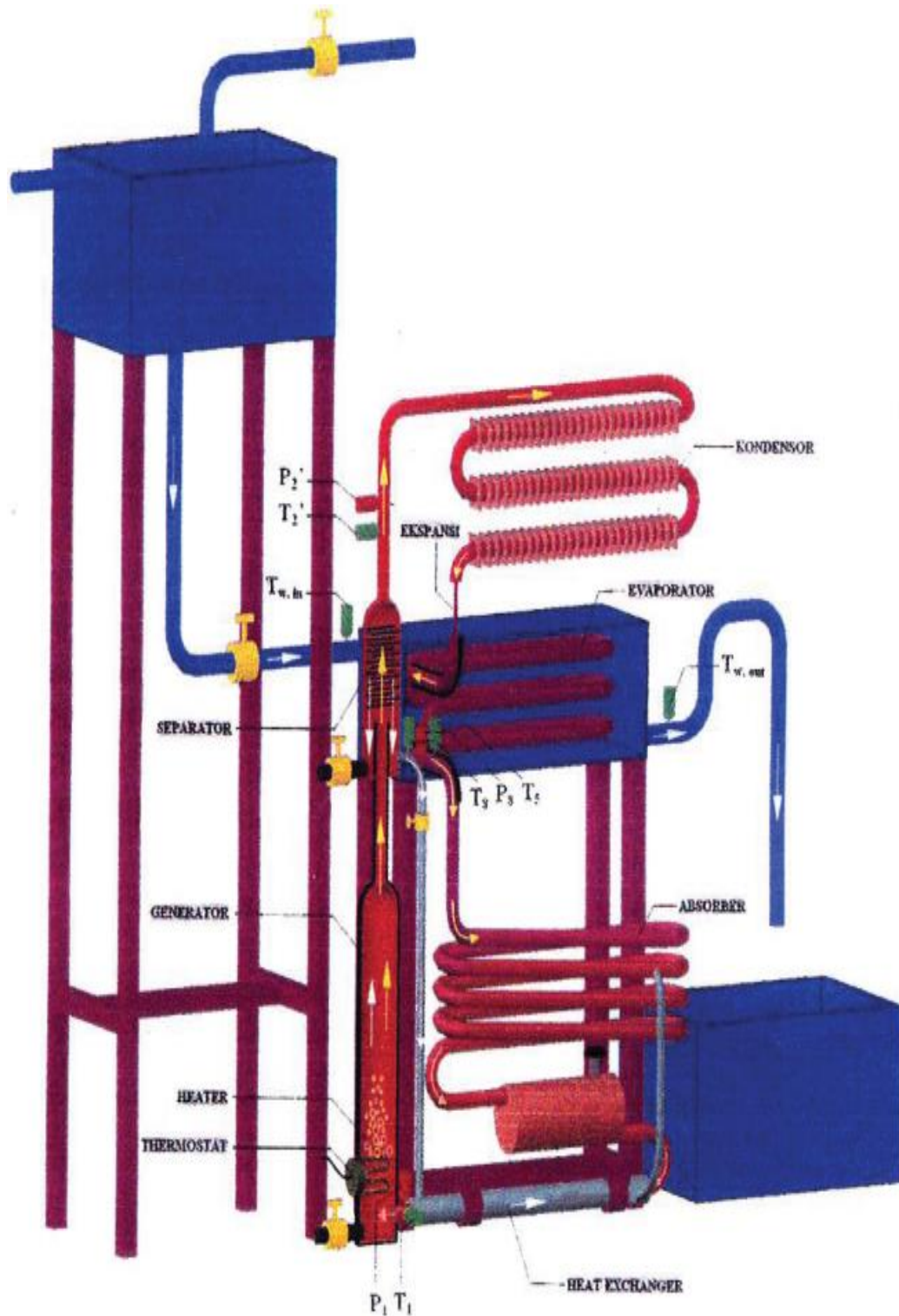


Figure 2.2. Experimental apparatus developed and adapted from Wijaksana, H., et al. [1].

M. Karamangil, et al. (2010) [52] focused on current improvements, including refrigerant-absorbent couples presently in use and future alternatives, in a literature

research on absorption refrigeration systems (ARSs). In addition, the study includes a thermodynamic analysis of the ARS utilising commonly occurring solution pairs and the development of a user-friendly software tool with visual components. Using the developed package, the effects of operating temperatures and the effectiveness of the solution, refrigerant, and solution-refrigerant heat exchangers were examined. The performance of the cycle was improved by raising the temperatures of the generator and evaporator; however, increasing the temperatures of the condenser and absorber had the opposite effect. Compared to the refrigerant and solution-refrigerant heat exchangers, the solution heat exchanger contributed 66% to the system's performance, while the refrigerant and solution-refrigerant heat exchangers provided only 14% and 6%, respectively. The investigation revealed that viable solutions for generator and evaporator temperatures varied according to operating conditions. The findings provide essential information for improving the performance of absorption refrigeration systems.

J. Aman, P. Henshaw and D.K. Ting [53] studied a thermally powered bubble pump in a water-based vapour absorption refrigeration (VAR) system. Since the 1920s, bubble pumps have been used in ammonia-water VAR systems; however, their employment in water-based refrigerant VAR systems has not been documented. The performance of a VAR system driven by a bubble pump is highly impacted by the characteristics of the refrigerant-absorbent solution and the settings of the bubble pump. However, there are only a few analytical models available for the performance study of a refrigeration cycle using a bubble pump, and there is no analytical model for the bubble pump itself. To address this deficiency, the research performed a dimensional analysis and produced a mathematical model that can be applied to any bubble pump-driven absorption refrigeration system. The investigation revealed that the bubble pump functions in a turbulent environment with a Reynolds number above 104 and a Morton number between 10-11 and 10-10. At the beginning of the slug flow phase, when the non-dimensional pressure was low, the bubble pump would reach its best efficiency (79%) with a high liquid Froude number and a high liquid Froude number. The suggested analytical model was confirmed by experimental findings using pure water and a LiCl-H<sub>2</sub>O solution, with results agreeing within 12%. This research gives insights into the performance of bubble



pump-driven absorption refrigeration systems and proposes an analytical model for the bubble pump's performance that can be used across diverse systems. This study's conclusions may also be used for constructing and improving VAR systems.

H. Al-Tahaineh et al. (2020) [54] investigated a hybrid system that combines a single-stage ammonia-water absorption refrigeration cycle with thermoelectric power generators powered by evacuated tube solar collectors. The goal of this inquiry was to better understand how such a system may be used. The EES modelling and analysis program was used to simulate and evaluate the system, which used a solution of ammonia and water as the working fluid. According to the findings, the COP of the system would rise as the temperature of the generator rose. When the system was run with an ammonia mass fraction of 0.99, it was discovered that the rectifier, located between the generator and the condenser, is the optimal placement for the thermoelectric generators. The COP was greater than 0.82 when there was a temperature differential of 60°C throughout the TEG. Performance was comparable at the other places, including between the condenser and the evaporator and between the evaporator and the absorber.

E.Y. Gürbüz et al. (2022) [55] examined the effects on the thermal performance of the Diffusion Absorption Refrigeration (DAR) system caused by varying amounts of zinc oxide aluminate spinel ( $\text{ZnOAl}_2\text{O}_3$ ) and titanium oxide ( $\text{TiO}_2$ ) nanoparticles. The purpose of the research was to find ways to improve the thermal performance of DAR systems so that they operate more efficiently. The first part of the research consisted of conducting experimental tests of the system using a variety of nanofluids, such as an ammonia/water solution containing 1 wt.% and 2 wt.% of  $\text{ZnOAl}_2\text{O}_3$  and  $\text{TiO}_2$  particles, respectively. The purpose of these tests was to develop passive heat transfer under the same ambient conditions. The second phase of the research consisted of designing the tested system in the MATLAB/Simulink toolbox environment so that the experimental findings may be compared to the numerical results. Because the use of nanofluids results in an increase in both the surface area expansion and the heat capacity of the fluid, it leads to a considerable improvement in the rate of heat transfer. The findings demonstrated that using nanofluid as the working fluid in the DAR system results in increased rates of evaporation, which in

turn would decrease the amount of time spent running the system and would boost the rate of heat transfer inside the generator. When compared to a base DAR system, the nanofluid solution with a concentration of 2 wt.% ZnOAl<sub>2</sub>O<sub>3</sub> nanoparticles causes a 57% increase in the coefficient of performance (COP) of the DAR system. As a result, this nanofluid concentration is the most effective of those that had been tested among the various nanofluid concentrations.

D. Martínez-Maradiaga et al. (2013) [56] focused on the steady-state operational data of a single-effect ammonia/water absorption chiller by applying data reconciliation to that data. The approach entailed locating the steady state, using systematic degrees of freedom analysis to establish a suitable set of measured input variables for the absorption chiller model, and reconciling the data, which would include the handling of large errors. The issue of reconciliation was overcome by employing a two-stage sequential technique in which MATLAB was used to minimise the objective function, and the Engineering Equation Solver was used to simulate an absorption chiller (EES). In order to identify significant mistakes in the measurements, the Modified Iterative Measurement Test was performed. Calculations of performance may also be made using this approach, which would permit calculations that are in compliance with the Laws of Conservation and enable the identification and eradication of the causes of large errors.

The study of A. Sözen, T. Menlik and E. Özbaş (2013) [57] provides the results of an experimental investigation into a diffusion absorption refrigeration system (DARS), with the goal of improving the system's overall performance. Three different DARS cycles were created and investigated. The first cycle, known as DARS-1, is the model that is used in the industry the most often. The second cycle, known as DARS-2, suggests detaching the gas heat exchanger from the evaporator. The third cycle, referred to as DARS-1WE, is a unique system that was suggested in this research. In this system, an ejector is inserted at the absorber intake of DARS-1. The DARS-1WE cycle performed far better than the DARS-1 and DARS-2 cycles, according to the findings of the experiments. The decrease in energy usage at relatively low temperatures in the cooling area, of 6°C, is on the order of 40%. When temperatures were increased by 10°C, the equivalent amount of energy savings

would drop to 20%. In the DARS-1WE, the time it took to reach the preset temperature of the cooling area reduced even more. In addition, the temperature within the cooling region of DARS-1WE dropped to 3.2°C as it cooled.

A. Najjaran et al. (2019) [58]. conducted an experimental investigation of the performance of a diffusion absorption refrigeration (DAR) unit with a notional cooling capacity of 100 W, designed for use in solar-powered cooling systems in hot climates. DAR is a cooling technique that is suitable for use on a small scale and uses only thermal energy; electrical and mechanical inputs are not necessary for its operation. Electrical cartridge heaters were responsible for providing the DAR unit with its thermal input. In the study, the heat source temperatures could be adjusted over a range of 175-215°C by adjusting the thermal input power over a range of 150-700 W. According to the findings, the DAR unit was able to keep a cooling temperature of 7°C constant across the entire range of thermal input, which is indicative of a dependable and consistent performance. The results of the experiments showed that solar thermal energy has the ability to be utilised to power the DAR unit, which makes it a viable technology for small-scale, low-cost cooling applications in warm areas.

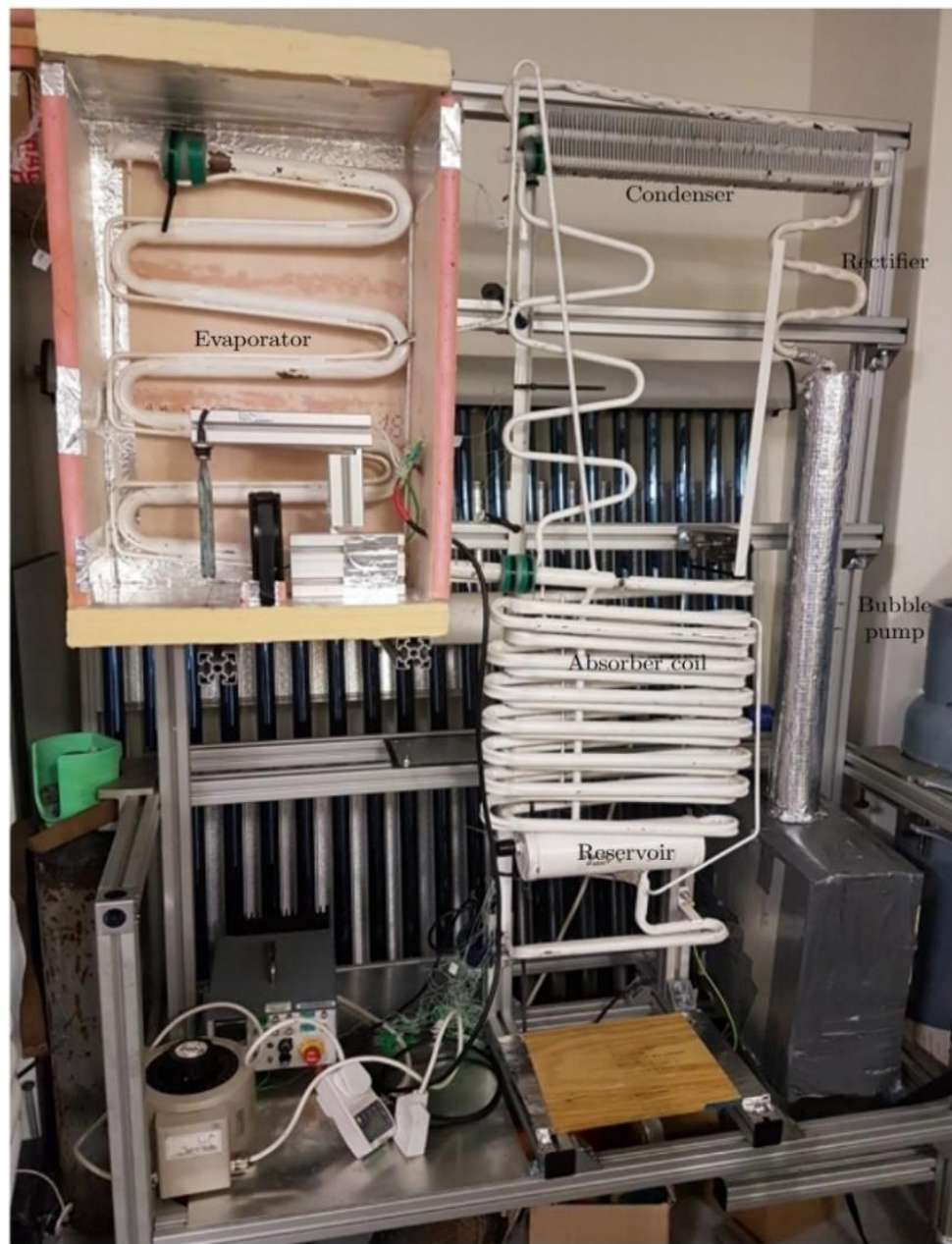


Figure 2.3. Laboratory DAR system used in tests (adapted from Najjaran, A., et al.) [58].

R. Farzadi and M. Bazargan (2020) [59] performed experimental research on the use of absorption refrigeration cycles powered by the waste heat from an automobile exhaust. The research was carried out with the assistance of a commercial diffusion absorption refrigerator and the exhaust flow from a small vehicle engine. Engine speeds varied from 1,000 rpm to 2,500 rpm during the course of the investigation. According to the findings, the amount of heat that was transmitted to the generator while the engine was operating at low speeds was insufficient to reach the low

temperatures that were necessary for the refrigerated compartment. In order to solve this problem, a new generator was planned and constructed, which ultimately led to an increase in heat transmission to the generator that was 19% more efficient. The redesigned generator was able to attain ideal temperatures of 5.7°C in the evaporator and 4.2°C in the refrigerated compartment while the engine was operating at 2,000 rpm. A further improvement was found when the engine speed was increased to 1,000 rpm, with temperatures in the evaporator and refrigerated compartment falling by around 4°C. The research revealed that it is possible to utilise absorption refrigeration cycles in automobiles, even at low engine speeds, by using adapted generators.

T.T.G. de Rezende, et al. (2020) [60] studied a technique that does not need any intrusion in order to compute the ammonia mass flow rate at the entrance of the expansion device in refrigerators that use the diffusion-absorption cooling system (DAR). A calculation of the air-side convection heat transfer coefficient using six empirical correlations was carried out by making use of geometric data and the temperature of the condenser. This was followed by a calculation for the condenser's energy balance to establish the mass flow rate. It was possible to estimate the ammonia mass flow by using only geometric data and condenser temperatures due to the similarity of the heat transfer coefficients that were supplied by four different correlations. This strategy, which may enhance the coefficient of performance and boost energy efficiency in cogeneration systems, was effective owing to the lack of sub-cooling in the condenser in the DAR cycle.

The study of E. Bellos et al. (2020) [61] is an inquiry into a solar-powered refrigeration system that made use of solar collectors shaped as parabolic troughs as the primary emphasis of the study. The refrigeration system was a one-stage absorption machine that employed NH<sub>3</sub> and water as the working pair and produced refrigeration temperatures ranging from -35°C to 5°C. The investigation of the system had been carried out from three distinct points of view, namely energetically, exergetically, and financially. The basis for this investigation was meteorological data gathered in Athens, Greece. Matlab was used to build the code for the dynamic model, while Engineering Equation Solver was used to produce the model and check

the thermodynamic model. The data from the published research was utilised to validate the model. The energy and mass flow rates balances had been used in the system devices in order to conduct a thermodynamic analysis of the system. An application of the energy balance was made in the solar field storage tank whenever one was undertaking a dynamic study. According to the results, the performance of the system was at its best when the generator temperature was at its ideal level, as defined by the operating conditions. The optimal level of the generator temperature was determined by the findings. With regard to refrigeration at  $-20^{\circ}\text{C}$  and heat rejection at  $40^{\circ}\text{C}$ , the system had a coefficient of performance of 0.255, which equates to a monthly exergy efficiency of 4.86% and a simple payback time of almost 10 years.

L. He, L. Tang and G. Chen (2009) [62] conducted a theoretical examination of the coefficient of performance for three working fluid pairs in a single-stage and intermittent absorption refrigerator, namely R22 + DMF, R134a + DMF, and R32 + DMF. The refrigerator utilised heat pipe evacuated tubular collectors, and the modelling and simulation of the performance took into account both the solar collector system and the absorption cooling system. During the simulation of the system, the usual meteorological year file for Hangzhou was used. The research concluded that a hot water storage tank is necessary for the dependability of the system. The findings also suggested that the combination of R134a and DMF had fascinating qualities for solar absorption cycles at moderate condensation and absorption temperatures. These properties are especially useful for the preservation of food and in the air conditioning of rural regions. According to the findings of the research, the optimal ratio of storage tank to solar collector area for a 1.0 kW system in the environment of Hangzhou would be between 0.035 and 0.043 litres.

P. Bermejo, F.J. Pino and F. Rosa (2010) [63], at the Engineering School of Seville, evaluated a solar- and gas-powered cooling system and provided recommendations for its further development. The system was a double-effect LiBr + water absorption chiller with a nominal cooling capacity of 174 kW, comprising a water absorption chiller powered by a mixture of a pressured hot water flow that was transported via a solar field  $352\text{ m}^2$  in size and a direct-fired natural gas burner. The size and

cleanliness of the solar collector, as well as climate, pipe heat losses, operational management, and the connection between the solar collector and the chiller were the primary focuses of the study. The daily average efficiency of the Fresnel collector was 0.35, with a maximum of 0.4, while the daily average COP of the absorption chiller ranged 1.1-1.25. The amount of solar energy that was injected into the generator accounted for 75% of the total heat input with solar cooling ratio of 0.44. The findings of the research provided valuable insights that may be used to enhance the design of solar- and gas-powered cooling systems in the future.

C. Fu, Q. Shen and T. Wu (2022) [64], at the Engineering School of Seville, evaluated a solar/gas cooling system and suggested design improvements for use in future plants. The system under investigation was a double-effect LiBr + water absorption chiller with a nominal cooling capacity of 174 kW, and comprised a water absorption chiller. The chiller was powered by a mixture of a pressured hot water that was transported via a solar field 352 m<sup>2</sup> in size and a direct-fired natural gas burner. The size and cleanliness of the solar collector, as well as the climate, pipe heat losses, operational management, and connections between the solar collector and the chiller were the primary focuses of the study. The daily average efficiency of the Fresnel collector was 0.35, with a high of 0.4, while the daily average coefficient of performance of the absorption chiller was 1.1-1.25. The amount of solar energy that was injected into the generator accounted for 75% of the total heat input, and the solar cooling ratio was 0.44. The findings of the research provide valuable insights that may be used to enhance the design of solar and gas-powered cooling systems in the future.

A.M. Abed et al. (2022) [65], in their study *A Techno-Economic Analysis of a Dual Ejectors-Flash Tank Absorption Cooling Cycle Assisted by Solar Energy*, included both a simulation of the solar system and a modelling of a one-dimensional ejector. The working fluids for the ejector were composed of NH<sub>3</sub> and H<sub>2</sub>O. The thermal solar system had been optimised in order to select the optimal size for a cooling capacity of 5 kW under the climatic conditions of Malaysia. This was accomplished through the optimisation process. According to the findings, the combined dual ejectors and flash tank cycle should be considered the best choice owing to the

economic feasibility of such a configuration. Both the repayment time and the profit gain for this cycle were determined to be 11 years, with the payback being \$3,192. The solar percentage varied from 53.6% in March to up to 68.6% in February. The findings also indicate that the combined cycle of dual ejectors and flash tanks cost 27% less than the absorption combined ejector system and 10% less than the combined system of combined ejectors and flash tanks.

J. Wang and Y. Yang (2016) [66] conducted a study on a combined cooling, heating, and power (CCHP) system. To improve the system's energy efficiency, they used solar energy and biomass. A biomass gasification sub-system, a solar evacuated collector, an internal combustion engine, and a dual-source mixed-effect absorption chiller were the components that would come together to form the CCHP system. The gas that was created by the gasifier was used to power the internal combustion engine, which in turn generated electricity. Meanwhile, the waste heat would be combined with the heat that collected from solar collectors to provide cooling and heating. The performance of the system was examined under a variety of external circumstances and energy ratios. The main energy ratio and exergy efficiency were found to be 57.9% and 16.1%, respectively, and the carbon emission reduction ratio was 95.7%. According to the findings of the research, the biomass subsystem had a far greater influence on the primary energy ratio and exergy efficiency of the system, while the solar subsystem contributed to the reduction of emissions.

M. Mehrpooya, B. Ghorbani and S.S. Hosseini (2018) [67] describe the development and exergetic assessment of an innovative concentrated solar power plant integrated with a desalination process and absorption refrigeration cycle, aimed at supplying power, fresh water, and refrigeration. The system consists of a concentrated solar thermal power plant with parabolic dish collectors and a steam turbine, a multi-effect desalination process with parallel seawater feed, and a single-stage ammonia-water absorption refrigeration system. The parabolic dish collectors provide 21,030 kW of thermal power to the steam power plant, with 4,632 kW converted to electrical power. The absorption refrigeration cycle produces 820.8 kW of refrigeration, and the desalination cycle provides fresh water at a rate of 22.79 kg/s. The integrated system was simulated using Aspen Hysys, and the components were individually



analysed based on the Second Law of Thermodynamics, with the exergy destruction rate and efficiency of each component obtained and discussed. The distillation column and heat exchangers accounted for 86% of the total exergy destruction rate of the system. The overall exergy efficiency of the cycle was 66.05%, and the net overall thermal efficiency was 80.70%. The economic analysis shows that the proposed integrated structure would have an investment return period of 5.738 years and a net annual profit of US\$6.828 million per year. Additionally, sensitivity analysis investigated the impact of various factors on the system's performance.

M.S. Khan et al. (2022) [68] presented a novel correlation that may be used to estimate the coefficient of performance (COP) of single-effect vapour absorption refrigeration (VAR) systems. The correlation takes into account fluid characteristics such the boiling points of absorbents and refrigerants, the latent heat of the vaporisation of refrigerants, and the specific heat of absorbents in addition to the temperatures of the generator, condenser, absorber and evaporator. The proposed correlation was verified using a total of 1,568 data points taken from the relevant body of literature, and it was considered appropriate for both small-scale and large-scale VAR systems. For the 100 TR H<sub>2</sub>O-LiBr system, the maximum mean absolute percentage error (MAPE) was determined to be 13.51%. The created model is capable of being utilised for forecasting the COP of various fluids in single-effect VAR cycles. This opens the field to researching the implementation of VAR in large-scale district cooling systems. According to the findings of the research, vapour absorption refrigeration has the potential to provide greener cooling by making use of waste heat or heat from renewable sources, thereby lowering the dependency on fossil-based power that is required by traditional chillers.

C. Monné, S. Alonso, F. Palacín and L. Serra (2011) [69] conducted a study in 2007 and 2008 to investigate the effectiveness of a solar-powered absorption cooling system. Flat plate collectors, a LiBr-H<sub>2</sub>O rotating absorption chiller, and a dry cooler tower were the components of the system. According to the findings of the study, the system had a COP close to 0.6 in 2007 and between 0.46 and 0.56 in 2008, with average values for cooling power ranging from 4.0 kW to 5.6 kW in 2007 and 3.6 kW to 5.3 kW in 2008. In addition, the system had a COP close to 0.6 in 2007.

TRNSYS was used to create a thorough model of the system, and then the findings of that model were confirmed using data from actual experiments. According to the findings of the research, the coefficient of performance (COP) was significantly influenced by both the temperature of the cooling water and the temperature at which the generator was operating. An alternate heat rejection sink was devised in order to increase the coefficient of performance (COP), and finally, a geothermal sink was selected since there was a water well in the surrounding area. According to the findings of the research, the geothermal sink increased the COP by as much as 42%.

F.A. Al-Sulaiman, F. Hamdullahpur and I. Dinçer [70] conducted in their study an analysis of the efficiency of a unique combined cooling, heating, and power (CCHP) system that made use of parabolic trough solar collectors and an organic Rankine cycle. Through the use of a single-effect absorption chiller, the system would make use of waste heat for both heating and cooling purposes. Three possible modes of operation were being explored here: the solar mode, the solar mode combined with storage, and the storage mode. The system was intended to generate 500 kW of electrical power, and its efficiency, net electrical power, and ratio of electrical to heating and cooling were analysed. According to the findings of the research, the greatest possible electrical efficiency may be achieved in the solar mode at a rate of 15%, in the solar and storage mode at a rate of 7%, and in the storage mode at a rate of 6.5%. The use of CCHP, on the other hand, resulted in a considerable improvement in efficiency. The highest CCHP efficiency for the solar mode was found to be 94%, while the greatest efficiency for the solar plus storage mode was found to be 47%, and the maximum efficiency for the storage mode was found to be 42%. The research also demonstrated that the temperature at the entrance of the ORC pump has an effect on the electrical-to-cooling ratio, and that the ability of this temperature to be adjusted might be utilised to regulate the amount of cooling power that is necessary.

I. Atmaca and A. Yiğit (2003) [71] conducted a study on the amount of energy required for new, developing technologies as a continually expanding global population, the needs of which cannot be satisfied using traditional forms of energy, which in turn brings into focus the significance of switching to renewable forms of

energy. Because of its many benefits, solar energy is a particularly important source of energy. One possible application of solar energy would be in the use of absorption cooling systems, which employ renewable and waste heat energy in place of electricity. The city of Antalya in Turkey served as the setting for this research, which focused on a simulated solar-powered, single-stage, water-lithium bromide absorption cooling system. The effects of hot water inlet temperatures on the COP and surface area of absorption cooling components, as well as the impact of minimum allowable hot water inlet temperatures on the fraction of non-purchased energy (FNP), were investigated with the help of a modular computer program developed for this purpose. In addition, the research explores how the system's performance was affected by the collector type and the storage tank mass.

A. Elsafty and A. Al-Daini (2002) [72] examined the costs, both upfront and ongoing, associated with single- and double-effect vapour absorption and vapour compression air-conditioning systems. The primary emphasis of this investigation was on startup expenses. The objective of the study was to identify which cooling system would be most suitable for a student hospital in Alexandria, Egypt, that has five floors with a cooling load of 250 TOR. On the basis of data from a normal climatic year in Alexandria, a modular computer program was used to make an estimate of the cooling load that the building would need. The costs of each system were compared, and the technique with the lowest total cost during its lifetime was determined by using both the present worth value approach and the equivalent yearly cost method. In addition to this, both the economic and thermodynamic variables, such as the influence that the climate of the area has on the operational expenses, were taken into account. According to the findings, the hospital would benefit most from using the double-effect vapour absorption system, resulting in the lowest overall cost. Regarding the choice of an HVAC system, the findings of this study provide researchers and decision-makers with knowledge that is quite helpful.

J. Wang, Y. Lu, Y. Yang and T. Mao (2016) [73] performed a thermodynamic analysis on a CCHP system by utilising both natural gas and solar energy as its primary power sources. The system consisted of a storage tank, a heat recovery system, an absorption cooling system, and a power production unit. In this research,

thermodynamic modelling was used to explore how well the system would function when subjected to a variety of different working situations. These variables would include the electric load factor, solar irradiance, and the installation ratio. According to the findings, including solar photovoltaics (PV) into a CCHP system would enhance its exergy efficiency, while incorporating a solar heat collector would improve the energy efficiency of the system. When matching the building loads, the optimisation approach was used to optimise the combined advantages of energy and economic expenses. This would be accomplished via maximisation. According to the findings of the optimisation, the incorporation of a solar heat collector produces superior results in terms of functionality when compared to the incorporation of solar photovoltaic cells in the particular case study. In general, this study provides academics and others who make decisions with significant information that may be used when constructing and improving CCHP systems.

J. Wang, S. Li, G. Zhang and Y. Yang (2019) [74] conducted a study on a solar-assisted hybrid combined cooling, heating, and power (CCHP) system. The thermodynamic modelling and validation process was used to examine and evaluate the performance of the system in terms of energy, exergy, exergy-economics, and energy-environmental impacts. The effects of thermal storage and supplementation on the efficiency of the system as well as the unit cost of the products were explored, and Sankey diagrams were used to show the findings of the energy and exergy analyses. According to the findings of the study, the hybrid system would achieve an annual energy efficiency of 76.3% and an exergy efficiency of 22.4%, resulting in savings of 11.3% of natural gas and a reduction in the amount of time required to recoup the initial investment in capital by one year in comparison to a conventional CCHP system that does not utilise solar energy. The exergo-economic analysis, which was based on energy levels, was also used to establish the unit costs of items and to compare the costs of products both including and excluding the cost of carbon dioxide emissions.

## **2.2. SUMMARY**

This chapter overview of absorption cooling technology and its applications, with emphasis on the operation of single-pressure and diffusion cycles, analyses the merits and disadvantages of various working fluid combinations, as well as prior research on solar-powered applications. Due to a dearth of research in this topic, this chapter also addresses the difficulties posed by diffusion absorption cycles. A rigorous analysis of competing models is presented with the objective of determining whether absorption technology can meet residential energy needs when powered solely by solar energy at a cost comparable to, or lower than, that of vapour compression systems, including process simulations based on COSMO, EES, etc., a thermodynamic model for a direct-absorption refrigeration system, and a complete experimental evaluation of a recently suggested diffusion absorption refrigeration unit.

## **PART 3**

### **THEORETICAL BACKGROUND**

In this chapter, the general theoretical equations describing the working principle of an ammonia-water-hydrogen diffusion adsorption refrigerator are discussed [75] in the first part. The equations are derived from the basic laws of thermodynamics and are used to explain the thermodynamic processes that occur in an absorption refrigeration cycle.

The third section delves into the aspects of the absorption refrigeration cycle that include the use of a working fluid in order to promote the transfer of heat from a source that is at a lower temperature to a sink that is at a higher temperature. The evaporator, absorber, generator, and condenser are the four basic components that make up the cycle. The condenser is the last stage of the cycle [52], making use of a fluid that is a combination of ammonia, water, and hydrogen as its working fluid. The governing equations for solar cells are covered in the final part. This model is frequently cited in the contemporary literature on DAR systems and has the potential to be adapted to a variety of DAR system settings due to the raw nature of its constituent sub-models and the manageable implementation process. In addition, this model is frequently cited in the contemporary literature on DAR systems.

### **3.1. EQUATIONS OF A GENERAL THERMODYNAMIC NATURE**

#### **3.1.1. The First Law of Thermodynamics**

The first law of thermodynamics states that the total energy of a system is conserved. In other words, energy cannot be created or destroyed, but it can be transformed from one form to another [76]. The following equation describes the First Law of Thermodynamics, thus [77-78].

$$U = Q - W \quad (3.1)$$

Where  $U$  is the change in the system's internal energy,  $Q$  the heat that was contributed to a system, and  $W$  the work that was done by a system.

The Fundamental Precept of the Second Law of Thermodynamics [79] is that the total entropy of an isolated system will always rise as time passes, according to the Second Rule of Thermodynamics, which asserts that this will always be the case. The following equation describes the Second Law of Thermodynamics.

$$\Delta S \geq Q/T \quad (3.2)$$

Where  $S$  denotes the shift in the entropy of a system,  $Q$  the heat that is contributed to the system, and  $T$  the temperature of the system.

Refrigeration Capacity [80]. The following equation may be used to determine the refrigeration capacity of the absorption refrigeration cycle.

$$Q_e = m_a \cdot (h_1 - h_4) \quad (3.3)$$

Where refrigeration capacity is denoted by  $Q_e$ , the mass flow rate of the working fluid by  $m_a$ , the enthalpy of the working fluid at the evaporator intake by  $h_1$ , and the enthalpy of the working fluid at the absorber outlet by  $h_4$ .

Where  $Q_e$  is the capacity of the refrigeration system and  $Q_g$  is the amount of heat that is sent into the generator.

LiBr-H<sub>2</sub>O Pair, Position [81]. The following equations may be used to compute the thermodynamic characteristics of the LiBr-H<sub>2</sub>O pair, which is used in the absorption refrigeration cycle.

The formula for calculating the vapour pressure of a solution of LiBr in H<sub>2</sub>O is as follows.

$$\ln(P/P_o) = -A/T + B - C.\ln T - D/T^2 \quad (3.4)$$

where  $P$  is the vapour pressure of the solution,  $P_o$  the vapour pressure of pure water,  $T$  the temperature in Kelvin, and  $A$ ,  $B$ ,  $C$  and  $D$  are constants.

The following equation may be used to find the enthalpy of the LiBr-H<sub>2</sub>O solution.

$$h = a + b + c + d + e/T + f \quad (3.5)$$

where  $h$  is the enthalpy,  $T$  the temperature in Kelvin, and  $a$ ,  $b$ ,  $c$ ,  $d$ ,  $e$  and  $f$  are constants.

### **3.2. GENERAL ABSORPTION REFRIGERATION CYCLE EQUATIONS**

This section presents a thermodynamic model for analysis of the recently introduced DAR system detailed in Section 2. Adapted from Zohar et al. [82], the thermodynamic analysis entails using the First Law of Thermodynamics to regulate volumes associated with each step of the DAR cycle. Figure 3.1 shows the respective control volumes. Presented here are the equations for achieving a mass and energy balance that account for heat losses, heat gains, and heat capacities of the main DAR system components. In addition, the state numbers shown in Figure 3.1 correspond to the critical points utilised in the theoretical study.



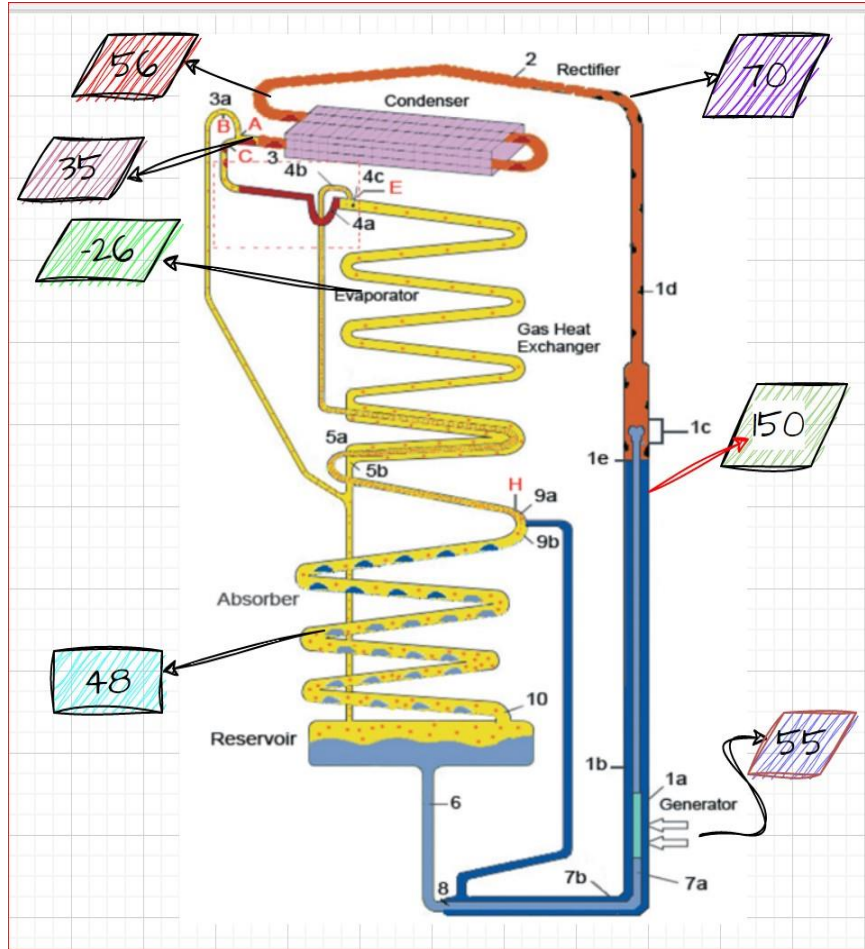


Figure 3.1. DAR cycle (derived from the work of Zohar et al.) [82].

### 3.2.1. Generator and Bubble Pump

As depicted in Figure 3.1, the system's boiler part consists of the generator and bubble pump. The nutrient-rich solution enters the boiler and absorbs heat from the generator, resulting in the production of ammonia vapour. The ammonia vapour ascends until it reaches the top of the bubble pump. Thus, the weak ammonia solution goes from the bubble pump to the generator, and then to the SHX. The mass and energy balances of the boiler section subsystem can be expressed as follows.

$$\dot{m}_{7a} = \dot{m}_{1c} + \dot{m}_{1e} \quad (3.6)$$

$$\dot{m}_{7a} \cdot x_{7a} = \dot{m}_{1c} \cdot x_{1c} + \dot{m}_{1e} \cdot x_{1e} \quad (3.7)$$

$$\dot{m}_{7a} \cdot h_{7a} + \dot{w}_{gen} = \dot{m}_{1c} \cdot h_{1c} + \dot{m}_{1e} \cdot h_{1e} \quad (3.8)$$

where  $h$  and  $\dot{w}_{gen}$ , respectively,  $\dot{m}$  the mass flow rate of the working fluid in  $\text{kg} \cdot \text{s}^{-1}$ , the specific enthalpy in  $\text{kJ} \cdot \text{kg}^{-1}$ , and the power output of the generator in kW. The mass fraction  $x$ .

### 3.2.2. Rectifier

Since there are still absorbent vapours and ammonia vapours present in the vapour, the vapour that is going to proceed through the rectifier is not totally pure. In order to achieve the extraction of the absorbent vapour from the ammonia vapour in the most efficient way possible, a rectifier is used in front of the condenser (see Figure 3.1). The rectifier was the location of the separation process, which saw the liquid water make its way back to the generator at various points. By using equations, one is able to determine the mass and energy balances of the rectifier. (Eq. 9-11).

$$\dot{m}_{1c} = \dot{m}_{1d} + \dot{m}_2 \quad (3.9)$$

$$x_{1c} \cdot \dot{m}_{1c} = x_{1d} \cdot \dot{m}_{1d} + x_2 \cdot \dot{m}_2 \quad (3.10)$$

$$h_{1c} \cdot \dot{m}_{1c} = h_{1d} \cdot \dot{m}_{1d} + h_2 \cdot \dot{m}_2 + \dot{Q}_{rf} \quad (3.11)$$

The heat rate of the rectifier is denoted by  $\dot{Q}_{rect}$  and expressed in kW.

### 3.2.3. SHX

The rich solution that was collected from the cooler absorber is the one that receives energy from the SHX, while the weak solution that was discharged from the generator is the one that transfers energy to the rich solution [83-84]. The following are expressions that may be used for the equations that describe the mass and energy balances, as well as the analysis of heat transfer, for the SHX. This expression is shown in Figure 3.1.

$$\dot{m}_6 = \dot{m}_{7a} \quad (3.12)$$

$$\dot{m}_8 = \dot{m}_{7b} \quad (3.13)$$

$$\dot{m}_{7b} = \dot{m}_{1e} + \dot{m}_{1d} \quad (3.14)$$

$$\dot{m}_{7b} \cdot x_{7b} = \dot{m}_{1e} \cdot x_{1e} + \dot{m}_{1d} \cdot x_{1d} \quad (3.15)$$

$$\dot{m}_{7b} \cdot h_{7b} = \dot{m}_{1e} \cdot h_{1e} + \dot{m}_{1d} \cdot h_{1d} \quad (3.16)$$

$$\dot{m}_{7b} \cdot h_{7b} + \dot{m}_6 \cdot h_6 = \dot{m}_8 \cdot h_8 + \dot{m}_{7a} \cdot h_{7a} + \dot{Q}_{shx} \quad (3.17)$$

where  $\dot{Q}_{shx}$  is the thermal rate of SHX, which is given in kW.

#### 3.2.4. Condenser

The pure ammonia vapours pass through a phase change at the condenser, transitioning from a gas state at a pressure that is the same as that of the system. The equations for the condenser's energy and mass conservation, which are governed by equations, may be expressed with reference to Figure 5 by using Equations 18 and 19 [85-86] .

$$\dot{m}_2 = \dot{m}_3 \quad (3.18)$$

$$\dot{m}_2 \cdot h_2 = \dot{m}_3 \cdot h_3 + \dot{Q}_{cond} \quad (3.19)$$

Inside the condenser unit is a horizontal tube that has forty rectangular fins. This is where the pure ammonia vapour condenses. The cooling process is helped by natural convection, which travels from the horizontal tube to the fins. As a direct result of this, the condenser heat transfer rate, which is denoted by  $\dot{Q}_{cond}$ , is calculated.

$$\dot{m}_2 \cdot (h_2 - h_3) = \dot{Q}_{cond} \quad (3.20)$$

$$\dot{Q}_{cond} = N\eta \lambda_{cond} A_{cond} (T_{cond} - T_{amb}) \quad (3.21)$$

### 3.2.5. Evaporator

The input of the evaporator receives the liquid ammonia that has been released from the condenser when the system is operating at its working pressure. At this moment, it comes into contact with the cold helium and ammonia vapour that is produced by the absorber. When cold helium is combined with ammonia vapour, the partial pressure of liquid ammonia drops by a large amount as a consequence of the reaction. Within the evaporator, liquid ammonia eventually turns into a gas that is a combination of helium and vapour. With reference to Figure 5, Equations 22 and 23 may be used to obtain the mass and energy balances of the evaporator [87-88].

$$\dot{m}_{Ac} + \dot{m}_{He} = \dot{m}_5 \quad (3.22)$$

$$\dot{m}_{Ac}h_{Ac} + \dot{m}_{He}h_{He} + \dot{Q}_{evap} = \dot{m}_5h_5 \quad (3.23)$$

where  $\dot{Q}_{evap}$  is the heat rate of the evaporator in kW.

### 3.2.6. Absorber

The weak solution that is released by the generator is responsible for absorbing the vaporised ammonia. The helium and ammonia that are still present make their way toward the evaporator. The equations for the mass and energy balances of the absorber that are shown below may be obtained from the state numbers that are displayed in Figure 3.1.

$$\dot{m}_{10} + \dot{m}_{He} = \dot{m}_{5b} + \dot{m}_{9b} \quad (3.24)$$

$$\dot{m}_{10}h_{10} + \dot{m}_{He}h_{He} + \dot{Q}_{abs} = \dot{m}_{5b}h_{5b} + \dot{m}_{9b}h_{9b} \quad (3.25)$$

where  $\dot{Q}_{abs}$  is the heat rate of the absorber measured in kW.

### The performance coefficient (COP)

The coefficient of performance (COP) of the ARS system can be expressed using Eq. 26 according to the First Law of Thermodynamics.

$$COP = \frac{Q_{-evap}}{W_{gen}} \quad (3.26)$$

### 3.3. GOVERNING EQUATIONS FOR PHOTOVOLTAIC CELLS

It is necessary to build an electrical circuit that is equal to a solar cell in order for a mathematical model to depict the behaviour of a solar cell correctly. Many models exist, but the model utilised the most often for better accuracy is this sophisticated circuit model (Figure 3.2). This model consists of a current source  $I_{ph}$  which is sensitive to the amount of solar radiation and the temperature, a parallel diode that has a temperature-dependent reverse saturation current, and a series resistor  $R_s$  that takes into account the internal resistance as well as the cell contacts. To take the model one step further, an additional resistor, denoted by  $R_p$ , may be connected in series with the diode to depict the passage of current through the crystal. The I-V characteristic curve of a genuine solar cell may be explained using the equations below [89].

$$I = I_{ph} - I_{sat} \times \left( \exp \left( q \times \frac{(V + R_s \times I)}{A \times k \times T_c} \right) - 1 \right) - \frac{(V + R_s \times I)}{R_p} \quad (3.27)$$

$$T_c - T_a = \frac{NOCT - 20}{800} \times E_c \quad (3.28)$$

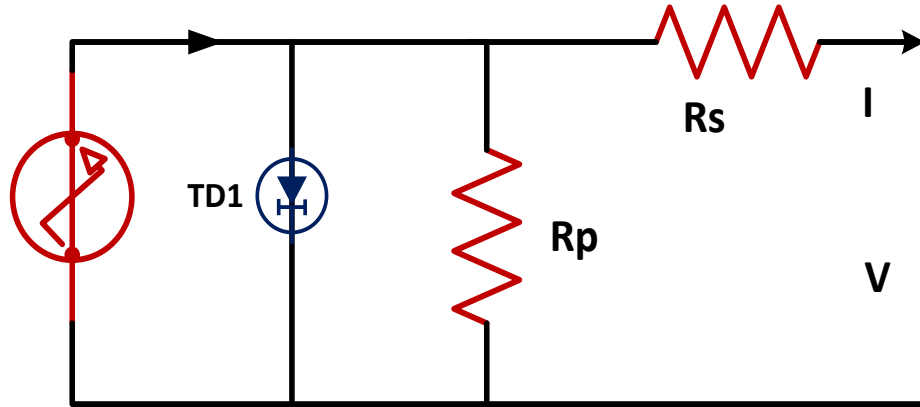


Figure 3.2. Circuit of a photovoltaic cell (derived from Chouder, A., et al.) [89].

### 3.3.1. Short-Circuit Current

At this current, denoted by  $I_{sc}$ , the voltage produced by the solar cell is equal to zero. In the case of the ideal scenario, this current,  $I_{sc}$ , combines with the photocurrent,  $I_{ph}$ . (where there is no  $R_s$  and  $R_p$  is infinite). The following equation (Eq. 28) is derived when  $V$  is set equal to 0.

$$I_{sc} = I_{ph} - I_{sat} \times \left( \exp \left( q \times \frac{R_s \times I_{sc}}{A \times k \times T_c} \right) - 1 \right) - \frac{R_s \times I_{sc}}{R_p} \quad (3.29)$$

### 3.3.2. Open-Circuit Voltage

This is the voltage,  $V_{oc}$ , at which the photovoltaic cell does not provide any current (the maximum voltage of a solar cell or a PV generator). For the expression  $I = 0$ , the following equation can be derived.

$$0 = I_{ph} - I_{sat} \times \left( \exp \left( q \times \frac{V_{oc}}{A \times k \times T_c} \right) - 1 \right) - \frac{V_{oc}}{R_p} \quad (3.30)$$

### The effectiveness, fill factor, and output power of a solar cell

The component of the current-voltage characteristic that is responsible for the generation of energy is the part in which the user is most interested. Because the product of current and voltage does not supply any power, this point will not be at

the point of open-circuit voltage, nor will it be at the point of the short-circuit current. Figure 3.3 shows the typical values under solar light as well as the constant power curves (with dots) [82].

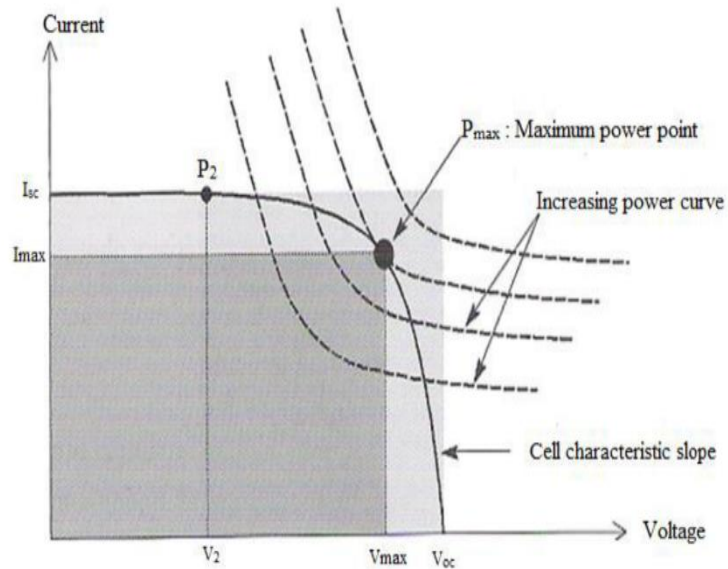


Figure 3.3. Maximum power on a characteristic of current and voltage (derived from Maammeur, H., Hamidat, A., & Loukarfi, L., 2013) [90].

At the point denoted by the notation  $P_{max}$ , which is located at the point of inflexion on the characteristic curve, the power output of the solar cell is at its utmost for the amount of irradiance that is being considered. The point of greatest power corresponds to the voltage and current that are at their highest. It is important to bear in mind, however, that the solar cell may also be needed to generate less power, such as at a voltage that is lower than its  $V_{max}$  rating (point,  $P_2$  in Figure 3.3). It is obvious that the maximum power, denoted by  $P_{max}$ , would increase as the curve becomes squarer. Using Eq. 36, we compute the value of this characteristic based on the fill factor [90].

$$ff = \frac{P_{max}}{V_{oc} \times I_{sc}} \quad (3.31)$$

The term “energy efficiency” refers to the ratio of the maximum power generated to the power of the solar radiation that is received by the photovoltaic cell. If  $S$

represents the surface of the cell and  $E_c$  the irradiance in  $\text{W/m}^{-2}$ , then Eq. 31 from [82] may be used to calculate the energy efficiency of the cell.

At the point denoted as  $P_{\max}$ , which is located at the point of inflexion on the characteristic curve, the power output of the solar cell is at its highest for the amount of irradiance that is being considered. The point of maximum power is synonymous with the maximum voltage, often known as  $V_{\max}$ .

$$NC = \frac{P_{\max}}{E_c \times S} \quad (3.32)$$



## PART 4

### EXPERIMENTAL WORK

#### 4.1. THE TRADITIONAL ABSORPTION REFRIGERATION SYSTEM (ARS)

As depicted in the ARS block diagram and the various components therein, the H<sub>2</sub>O-NH<sub>3</sub> mixture will function as the system's working fluid. In addition, unlike LiBr-H<sub>2</sub>O, H<sub>2</sub>O-NH<sub>3</sub> does not crystallise at temperatures below 0°C and it does not have the same negative impact on the environment as other commercial refrigerants. Elements that are part of the system include the heater, which is a resistance load that can function in both alternating current (AC) and direct current (DC) without any alterations to the design, and a 450-watt solar photovoltaic panel that will be the source of electrical power for the system. In a nation such as Iraq, where solar energy is consistently available throughout the year, there is not a great deal of demand for other forms of energy.

Table 4.1. Specifications of the conventional and solar-assisted absorption refrigeration system. ARS & AC.ARS V170KE model.

Name	AC, ARS	DC, ARS	Unit
Power	450	450	
Voltage	220-240	20-48	V
Current	1.4	8	A
Capacity	70	70	L
Condenser Type	Finned type	Finned type	-
Dimension (l × b × h)	-	-	-
Insulation	-	-	-
Working Fluid	H <sub>2</sub> O-NH <sub>3</sub>	H <sub>2</sub> O-NH <sub>3</sub>	-

#### 4.2. REFRIGERATOR INSTALLATION

The steps involved in installing the refrigerator are as follows.

- Place the refrigerator in a location that is as far away from any sources of heat as is reasonably possible. (It has been shown that the refrigerator can continue to perform reliably even when exposed to temperatures as high as 43°C.)
- There should be enough ventilation in the region, and the space immediately around the refrigerator should have open air circulation.
- Move the refrigerator away from any sources of heat and keep it out of the direct sunshine.
- Refrain from completely shutting windows and doors.
- There must be a clearance of at least 30 millimetres between the object and the wall and at least 400 millimetres between the object and the ceiling.
- Check that the door fits snugly against the cabinet and creates a good seal.
- If there is any usage of power, ensure sure the voltage is checked and adjusted appropriately.

#### 4.3. SOLAR ABSORPTION REFRIGERATION SYSTEM

The experiment was prepared in two stages according to the source of their operation in each stage. the first stage with DC, and the second stage with AC. Refrigeration was based on aqueous ammonia absorption technology with the help of photovoltaics, as seen in the Figure 4.5.

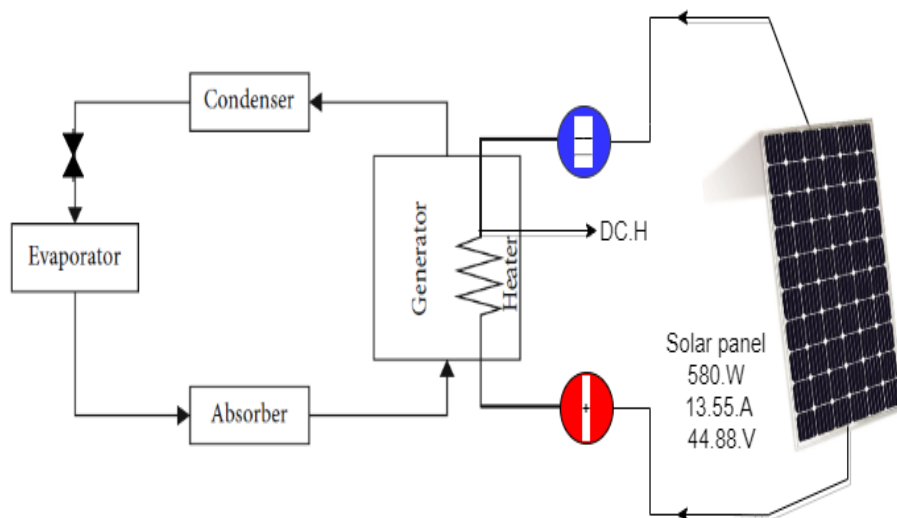


Figure 4.1. Solar absorption refrigeration system.

Figure 4.5 shows the V170 KE absorption refrigeration system during scientific experiments. Equipped with all the necessary thermal sensors, this refrigerator includes the main parts of the system. As shown in Figure 4.8 it includes the components of the upper part of the refrigerator and, as illustrated in Figure 4.9, the components of the lower part of the refrigerator in addition to a diagram of the components of the refrigerator, such as the generator, rectifier, condenser, evaporator, receiver and absorber. The diagram also shows the cycle of the refrigeration system with an aqueous ammonia solution. It shows the stage of separation of ammonia from water, and the stages of evaporation and condensation, as well as an indication of the stages of the cycle in numbers (see also Figure 4.6). Note that the refrigerator is charged with an aqueous ammonia solution with a total mass concentration of 30% and hydrogen pressure at 22 bar, according to the default specifications provided by the manufacturer.

#### **4.4. INSTALLATION STEPS OF THE REFRIGERATOR**

- Place the refrigerator in the coolest feasible location within a structure. The refrigerator has been tested to work reliably at temperatures as high as 43°C.
- The space must be aired, and open-air circulation surrounding the refrigerator is required.
- Keep the refrigerator in the shade and away from any sources of heat.
- Avoid closing door and window apertures.
- Clearances to the wall must be at least 30 mm and to the roof at least 400 mm.
- Ensure that the door seals correctly against the cabinet.
- If electricity is utilised, ensure that the voltage is correct.



Figure 4.2. The absorptive cryosection system (ARS) during the experiment.

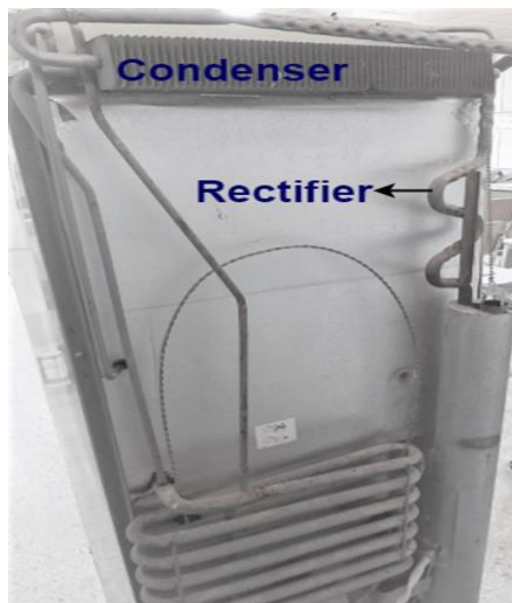


Figure 4.3. The absorptive refrigeration system that was tested showing the rectifier and the condenser.

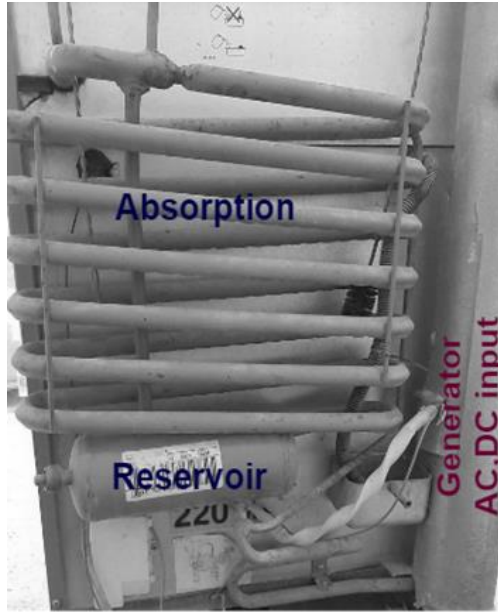


Figure 4.4. The absorption refrigeration system that was tested showing the absorber, receiver and generator.

#### 4.4.1. Photovoltaic Panel

Shows the olfactory PV panel (+5W/-0W) Pmpp 580 W and short circuit current  $I_{sc}$  13.55 A with open circuit voltage VOC, 53.56 V and current at max power,  $I_{mpp}$ , 12.92 A and voltage at max power,  $V_{mpp}$ , 44.88V Done Use it to directly drive the 70L absorption refrigeration system (ARS). as shown in the Figure 4.10.



Figure 4.5. Photovoltaic panel, nominal power 580 W.

#### 4.4.2. DC Heater

Figure 4.11 shows a DC heater of our design manufactured in the laboratory, with a length of 20 cm and a diameter of 12 mm. The outer cover of the heater is made of stainless steel with a resistance wire of 1.5 mm diameter. The resistance of the wire is  $1 \Omega$  per meter with a capacity of 48 V and 450 W. The total resistance of the heater is  $5 \Omega$ . It is placed inside the generator next to the AC heater. Thus, the process of converting photovoltaic energy into heat energy is done directly to drive the absorption refrigeration system.

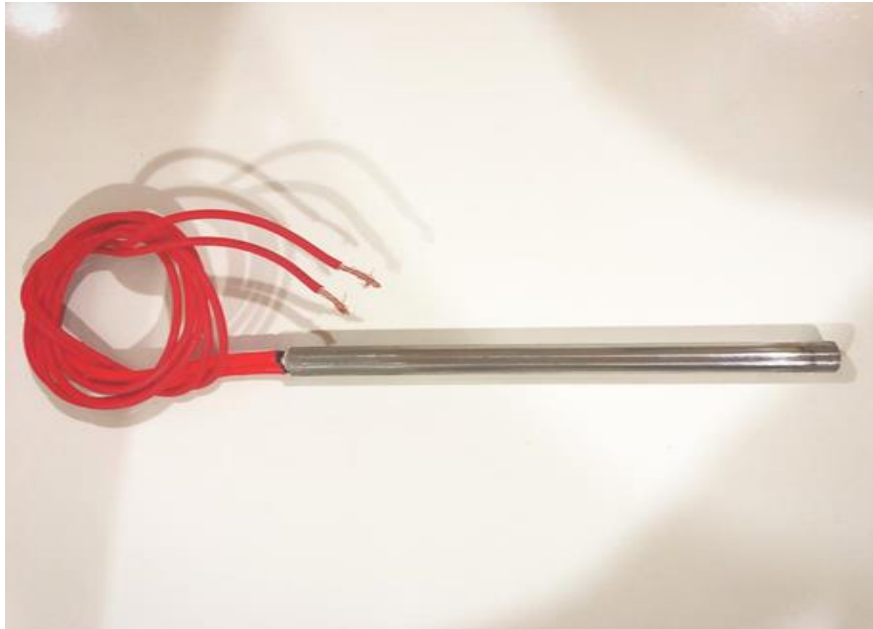


Figure 4.6. DC heater (48 V, 450 W).

#### 4.4.3. Ceramic Wool Thermal insulator

An inorganic thermal insulator of ceramic wool was used to isolate the generator from the inside in order to isolate it from the ambient temperature and not be affected by it according to HP 1260 specifications. The material has a density of  $128 \text{ kg/m}^3$  and a thickness of 50 mm. Raftherm ceramic fibres are used at temperatures between  $750^\circ\text{C}$  and  $1,430^\circ\text{C}$ . Textile technology produces ceramic fibres consisting of three basic elements, namely silica, alumina and zirconium, which are heat insulating materials for high tempera

tures. Some typical applications include industrial furnaces, boilers, stacks, places encountering high temperatures, kilns, reusable insulation for steam and gas turbines, lining for field steam generators, thermal reactor insulation, pressure and fire protection in cryogenic vessels, which reflects positively on the speed of the system's response to work in less than 30 minutes, as shown in Figure 4.12.

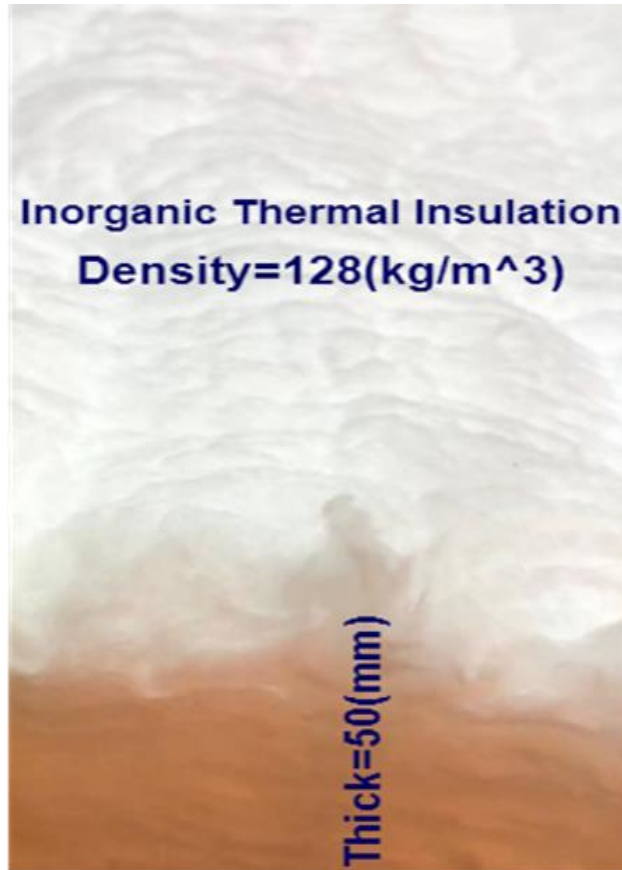


Figure 4.7. Ceramic wool thermal insulator.

Electrical connections of 2 mm × 6 mm thickness were used for the direct connection of the limiter. PV was the power source for DC heater. The cycle separator was used to separate the PV power from the refrigerator as needed or when converting from a DC system to an AC system to operate the refrigerator.

## **PART 5**

### **RESULTS AND DISCUSSION**

Failures occurred in the first two experiments with DC heaters, the first being a glass heater (20 V, 450 W) that was 60 cm long and 25 mm in diameter, and the second being a glass heater (40 V and 450 W) 70 cm in length and with a diameter of 25 mm placed inside the generator chimney during the two failed experiments. We succeeded in the third experiment by designing a completely new DC heater (48 V and 450 W) made of stainless steel 20 cm in length and a diameter of 12 mm. It was also relocated next to the chimney inside the generator. Ceramic wool was used to insulate the generator and a 580-watt photovoltaic panel was used.

The experimental results were used in this chapter to analyse the performance of the absorption refrigeration system (refrigerator) in two main cases. The first case included three experiments on a photovoltaic solar energy source directly with direct electric current. The first experiment occurred in cloudy and dusty weather, and the second was performed on a direct current source in clear weather. The first and second experiments occurred in September of 2022, and the parameter that was taken into account was the temperature, which was recorded every 4 minutes.

Third experiment took place in November 2022 over three consecutive days, the first day of which was on the AC power source only in order to compare and evaluate the performance of the refrigerator while working with the AC system and the DC system. The temperature was the parameter that was taken into account and measured every 2 minutes. As for the second case, through which the fourth experiment was carried out, it includes a comparison between 20° and 30° to determine the appropriate angle for the direction of the PV panel. Ensuing from the first experiment, something new was discovered.



Measurements from four different experiments to operate an ARS solar absorption cooling system directly using a PV panel and a DC heater were plotted over the studied range of temperature input rates in various parts of the system.

### 5.1. THE FIRST EXPERIMENT

This experiment occurred on 21 September 2022 in partly cloudy weather with a little dust, for 232 minutes between 9.15 a.m. and 1.10 p.m. (approximately 4 hours). The parameter taken into account was the temperature of the various devices. The refrigerator was solar PV powered directly using a photovoltaic panel, and a 450-watt DC heater.

Graph 5.3 shows the generator temperature inlet data, starting at 30°C. We notice the rise and fall of the temperatures as a result of voltage fluctuations due to the draw to reach 55°C. Therefore, we also notice the same effect on the rate, but slightly lower compared to the fluctuation in the temperature of the generator input, as these fluctuations in temperatures range between 55°C and 70°C, as shown in Figure 5.4.

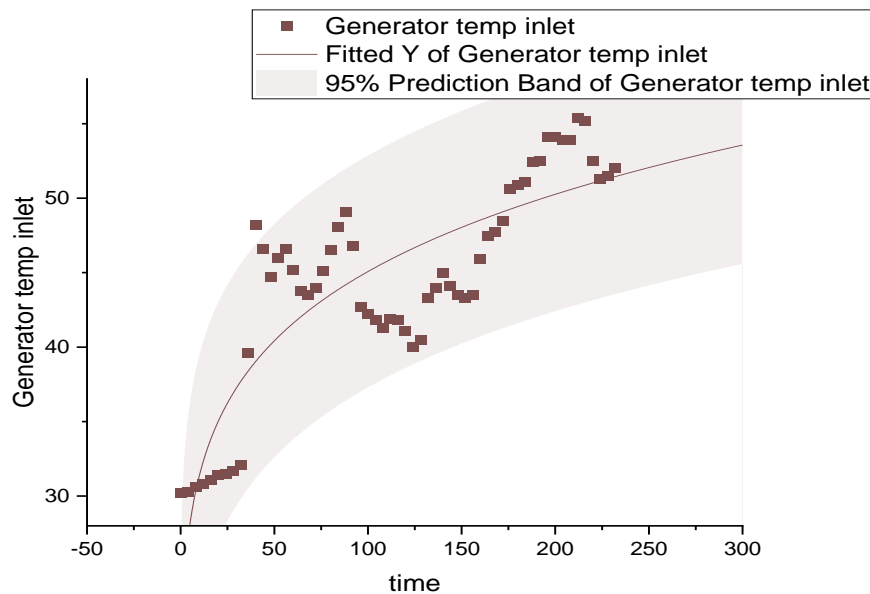


Figure 5.1. Temperature curve at the input of the generator over 232 minutes.

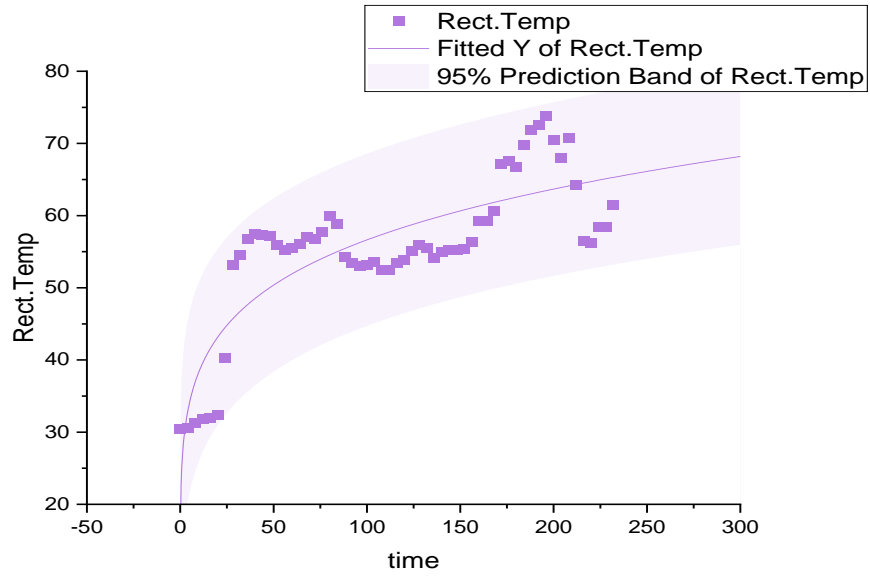


Figure 5.2. Rectifier temperature data for 232 minutes.

It is possible to observe from the input temperatures of the condenser, as shown in Figure 5.5, that the temperatures rise to a maximum of 60°C. The output temperatures of the condenser can also be seen in Figure 5.6, with a difference of approximately 25°C to that the work and efficiency of the condenser, which can be understood in operating conditions with such weather.

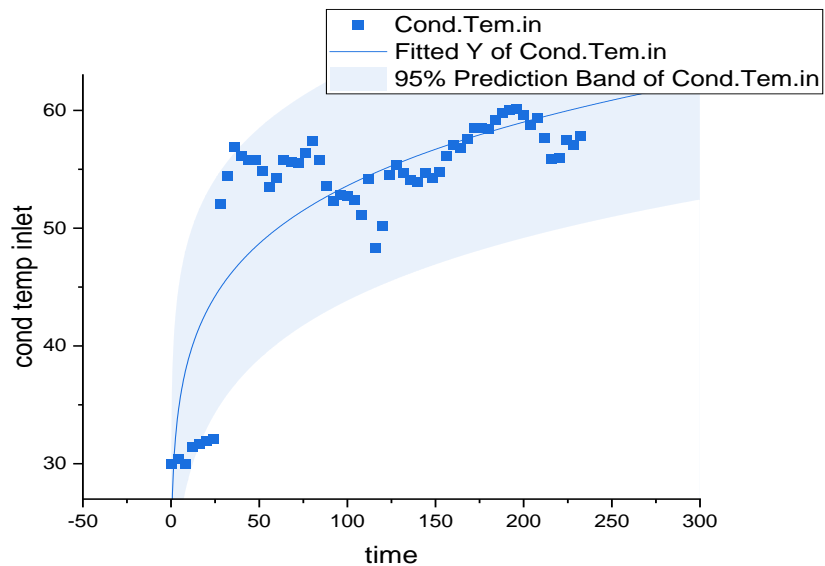


Figure 5.3. Data for condenser input temperature for 232 minutes.

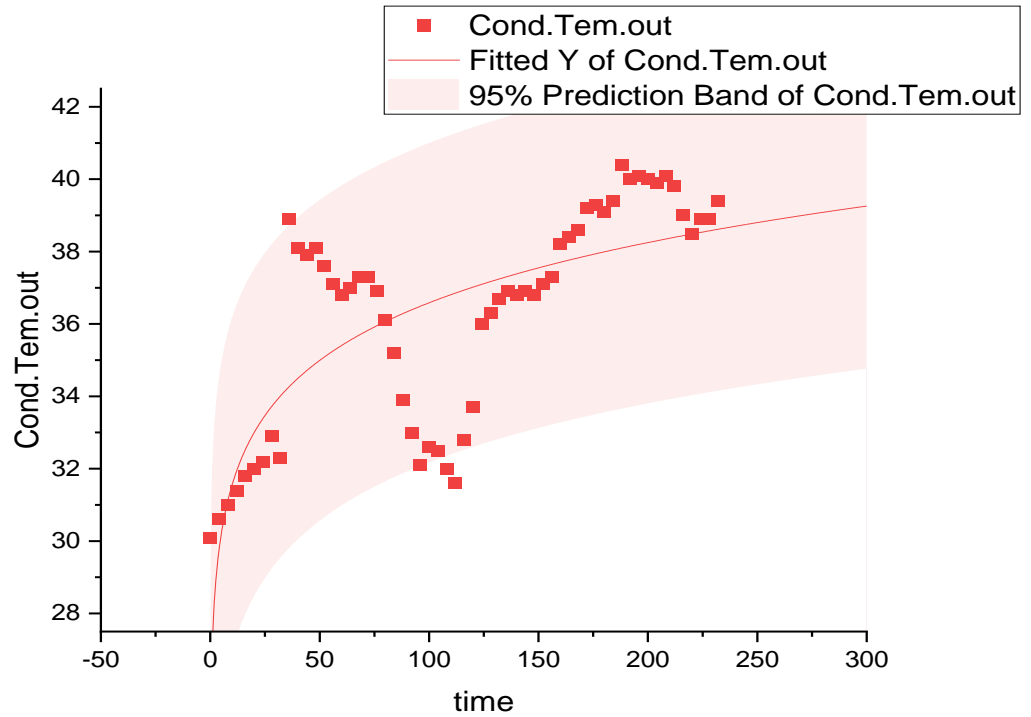


Figure 5.4. Temperatures at the exit of the condenser over a 232-minute period

Now, from the data illustrated in Figures 7.5 and 5.8, it is possible to observe how the temperature of the parts of the refrigerator under discussion affect the temperature of the evaporator and the refrigerator. We notice a gradual decrease in the temperature in the evaporator starting from 31°C to -17°C as the system responded to work in a short time, as well as a gradual decrease of temperatures in the refrigerator without fluctuations in temperature. This indicates the high efficiency of the work of the ARS system led by a solar PV in cloudy weather and not in ideal weather. Moreover, the temperature of the refrigerated space was maintained at 32°C ± 1°C, as shown in Figure 5.9.

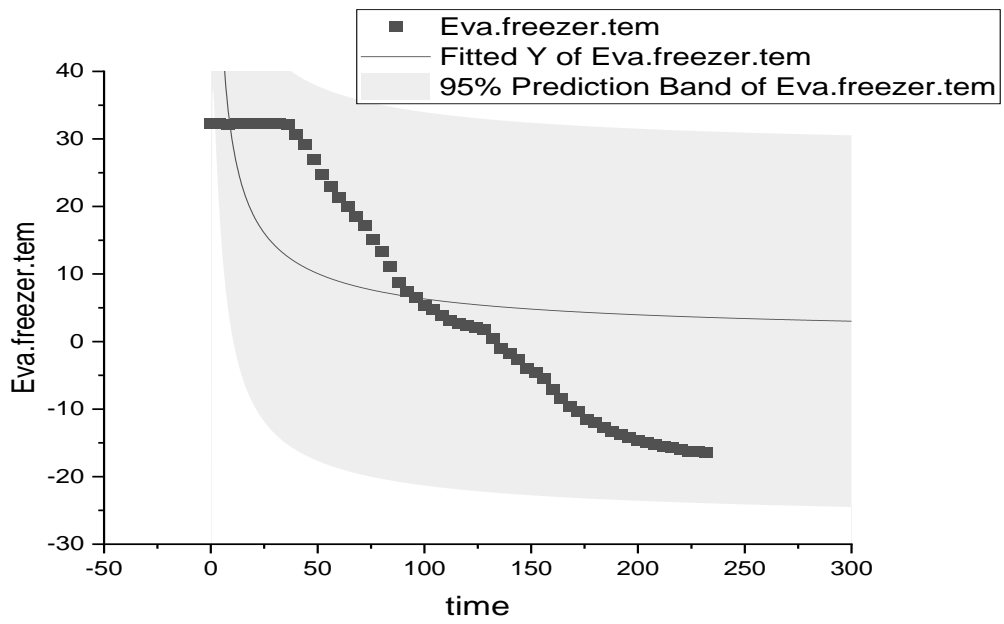


Figure 5.5. Evaporator temperature data over a 232-minute period.

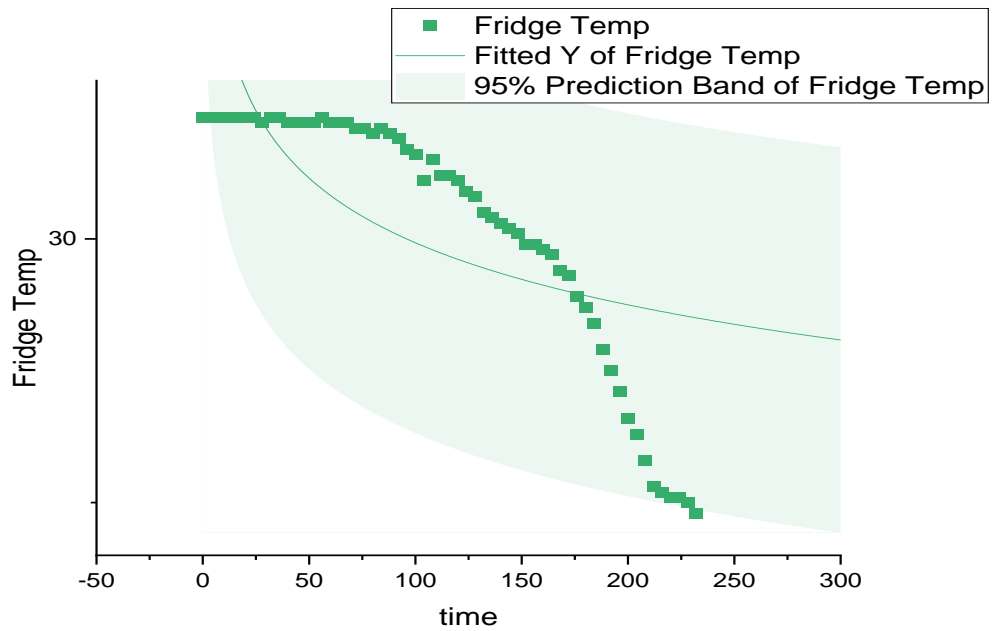


Figure 5.6. Fridge temperatures of the system during the 232-minute period.

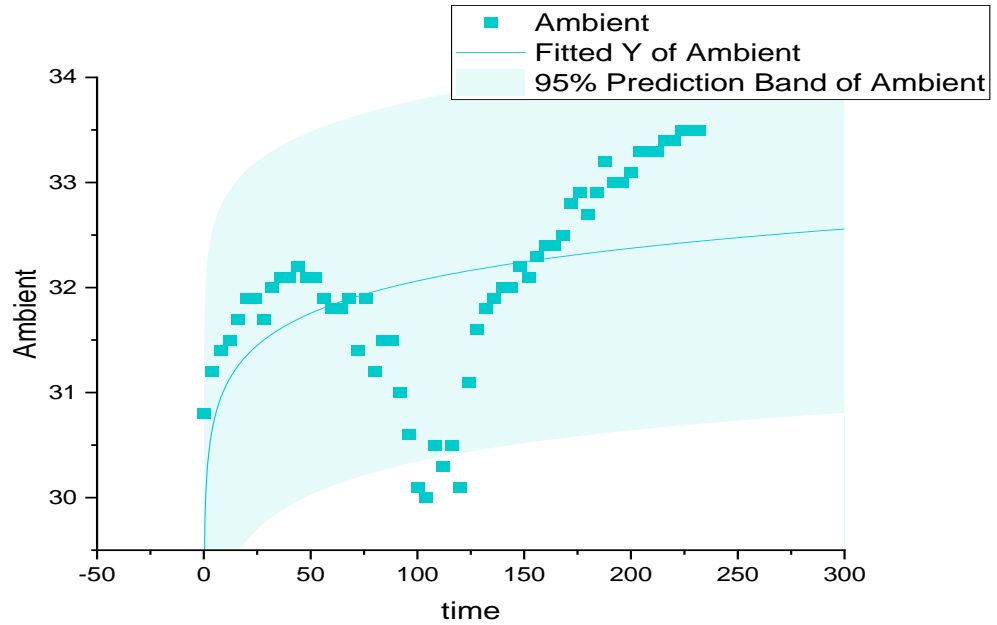


Figure 5.7. Ambient temperatures of the system over a 232-minute period.

Comparisons were made between the evaporator temperature, generator temperature and environment temperature over time. We can understand that as the temperature rises in the generator, the temperature in the evaporator gradually decreases, starting from 31°C with the refrigerator starting to work and reaching  $-17^{\circ}\text{C}$  in 232 minutes in not ideal and cloudy weather. In this experiment, we were able to discover something new, which was that the voltage fluctuation in the direct current caused by bad weather conditions, such as clouds, dust, or scattered solar light, does not significantly affect the efficiency of the solar system (ARS) or the work of the direct current heater that supplies the generator with thermal energy. As a result, the solar ARS can be operated in different weather conditions, as shown in Figure 5.10.

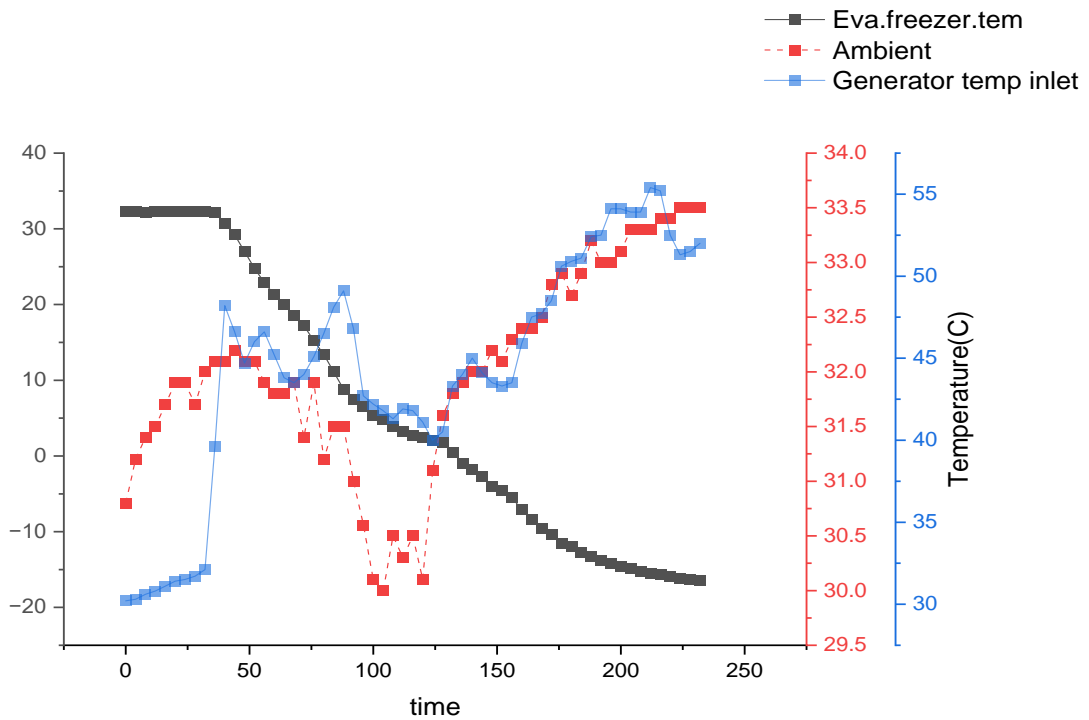


Figure 5.8. Comparison between the generator temperature and evaporator temperature with room temperature around the refrigerator over the 232-minute period.

It can be observed three-dimensionally that the temperature decreases and increases as a result of the fluctuation of the voltage difference and as a result of clouds and dust at higher temperatures in the generator. This corresponds to operating conditions in which the generator is connected to the maximum flow rate of ammonia gas vapour from the rectifier to the condenser, with values higher than  $Q_{gen}$ . This does not limit the specific cooling outputs that can be achieved at low values of  $Q_{ge}$ , as shown in Figure 5.11

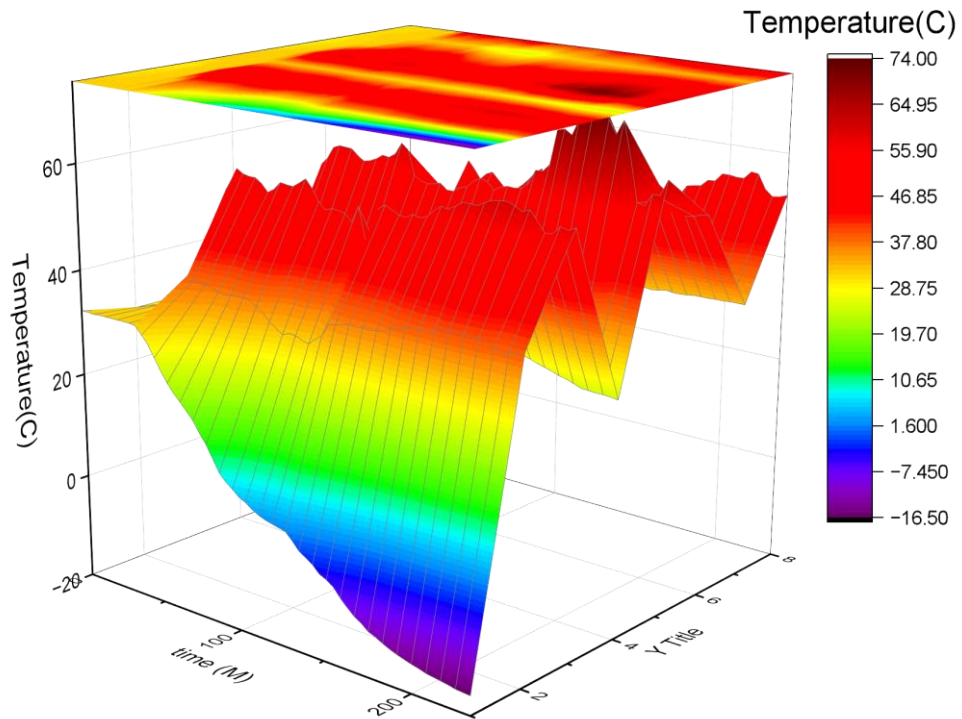


Figure 5.9. 3D model of a comparison between the generator temperature and evaporator temperature over a period of 232 minutes.

## 5.2. THE SECOND EXPERIMENT

This experiment was conducted on September 26, 2022 for a period of 156 minutes between 10.00 am and 12.30 pm. The parameter considered was the temperature of portions of the adsorption freeze system (ARS) taken every 4 minutes. DC voltage and current data were recorded, in addition to the ambient temperature data of the refrigerator, all in clear weather, so the refrigerator was powered by solar photovoltaic energy using a 580-watt photovoltaic cell and a 450-watt heater directly through direct current (DC). The temperature data for each part of the refrigerator was recorded independently so that the ambient temperature of the absorption cooling system was clearly visible. Weather quality had been compared to the first experiment, showing that the results were not much different, which once again proves that voltage fluctuations due to clouds or dust will not significantly affect the performance of the ARS absorption ice system directly driven by solar PV. We can notice a gradual increase in the temperature of the generator input from 25°C to 52°C, as shown in Figure 5.12. Furthermore, it is possible to read the output

temperatures of the generator, which reached 130°C within 25 minutes, after which time the temperature rose to 155°C in less than 60 minutes gradually. This experiment took 156 minutes, as shown in Figure 5.13.

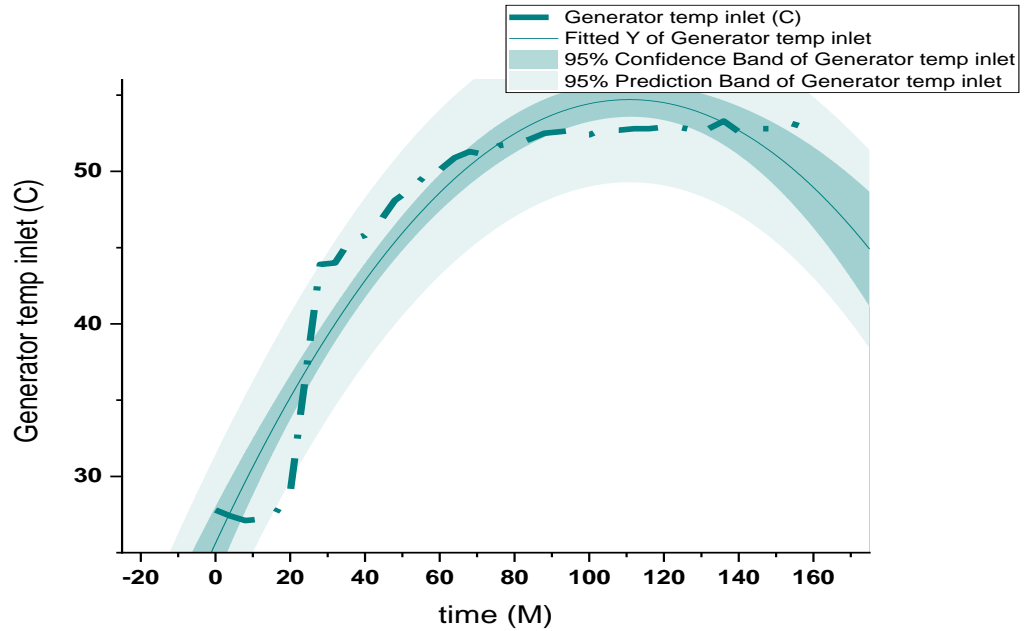


Figure 5.10. Generator temperature entry data during the 156-minute period of the second experiment.



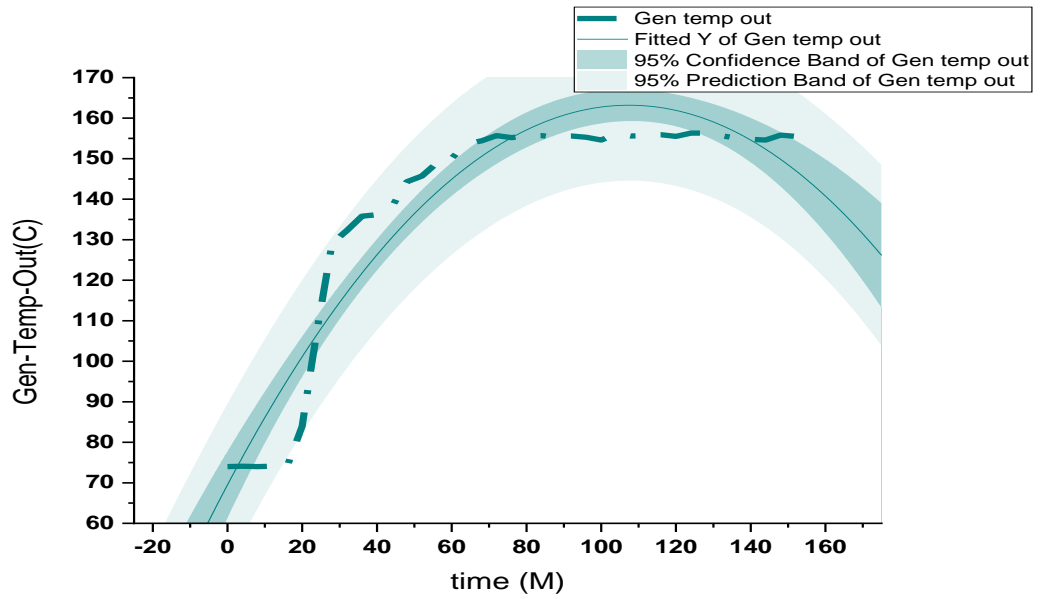


Figure 5.11. Generator output temperature data curve during the 156-minute period.

The rectifier data was analysed for the part that is important by isolating the amount of water associated with the ammonia vapour coming from the generator and reducing its temperature significantly. In our experiment, we noticed that the output temperature of the generator was 160°C, as shown in Figure 5.14.

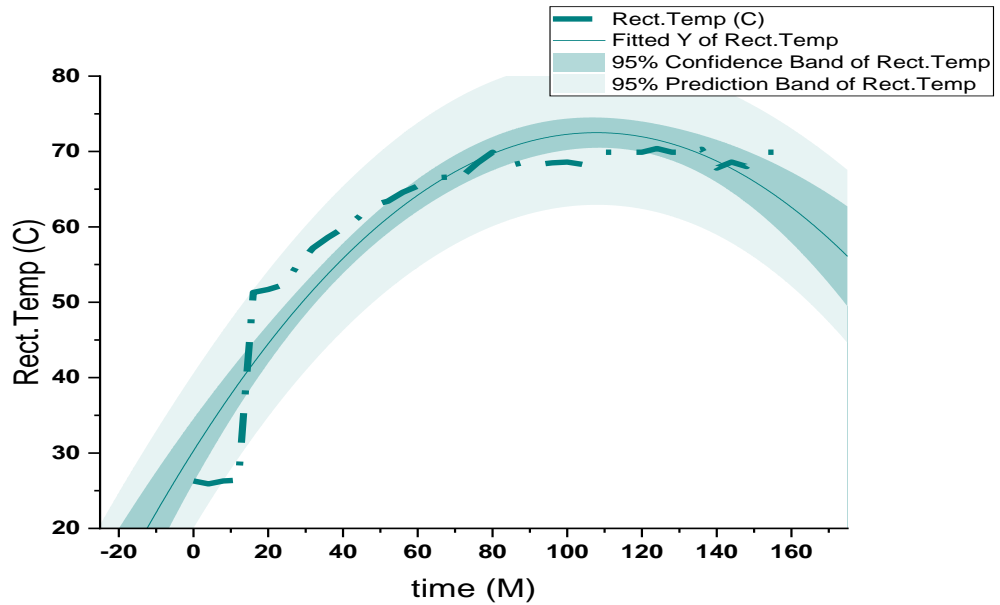


Figure 5.12. Rectifier temperature data over the 156 minutes of the second experiment.

Temperature data were also recorded at the entrance to the condenser, which in turn lowers the temperature coming from the rectifier, as the condenser is a heat exchanger that condenses ammonia vapour and converts it into a liquid state, which we noticed in this experiment as a gradual decrease. Approximately 15% from 70°C to 55°C under high pressure at the inlet of the condenser is shown in Figure 5.15, and after the gas enters the condenser, the condenser lowers the temperature so as to be able to condense ammonia vapour into ammonia liquid also at high pressure at the output of the capacitor, as shown in Figure 5.16.

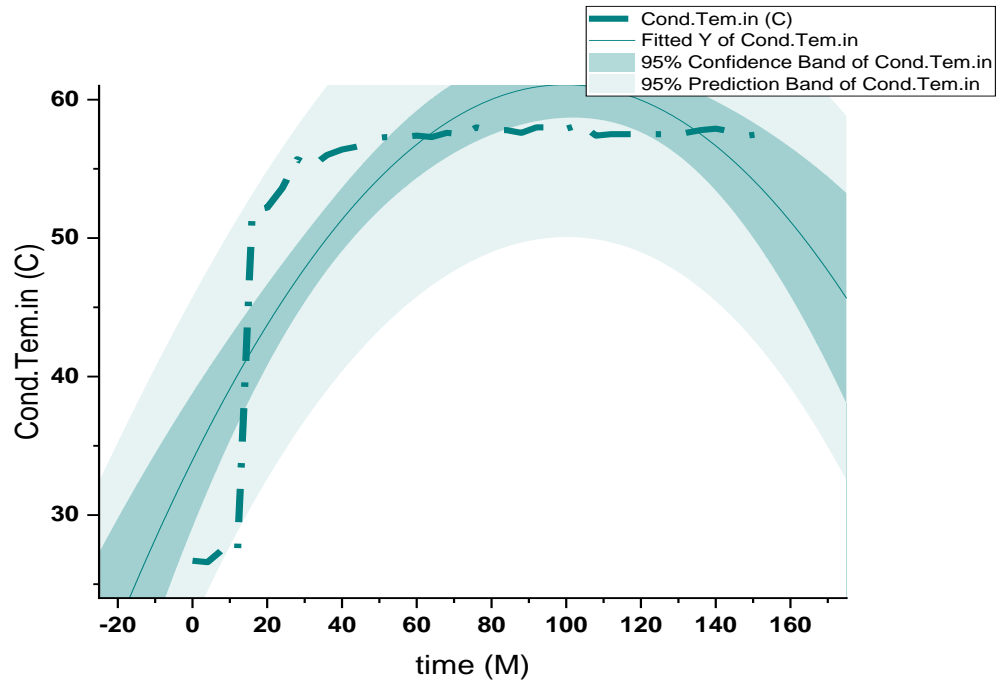


Figure 5.13. Inlet condenser temperature data over the 156 minutes of the second experiment.

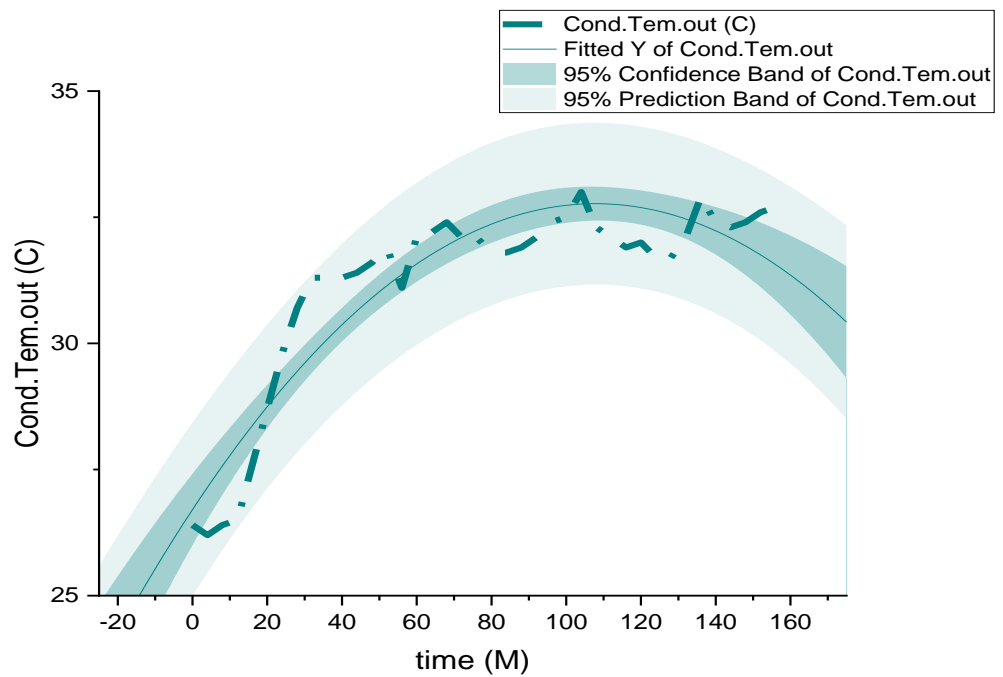


Figure 5.14. Condenser temperature output data over the 156 minutes of the second experiment.

After reducing the pressure and preparing the ammonia liquid by means of the expansion valve, it enters the evaporator, where it touches the hydrogen gas in order to obtain the evaporator refrigeration process (freezer). We notice a gradual decrease in the temperature of the evaporator during this experiment, down to  $-19^{\circ}\text{C}$  within 156 minutes. The response of the ARS system to work led by solar photovoltaic energy can be observed directly, as it was shown to work in less than 30 minutes, as shown in Figure 5.17. In addition, we notice a gradual decrease in the temperatures in Alfredj, A, starting from  $31^{\circ}\text{C}$  with the ARS starting to work, reaching  $17^{\circ}\text{C}$  in Alfredj, A, as shown in Figure 5.18. Several experiments were carried out, and it was discovered that if the experiment continued for a longer time, we would have a greater decrease in temperature in the evaporator and the fridge. This is what will be proved in the third and fourth experiments.

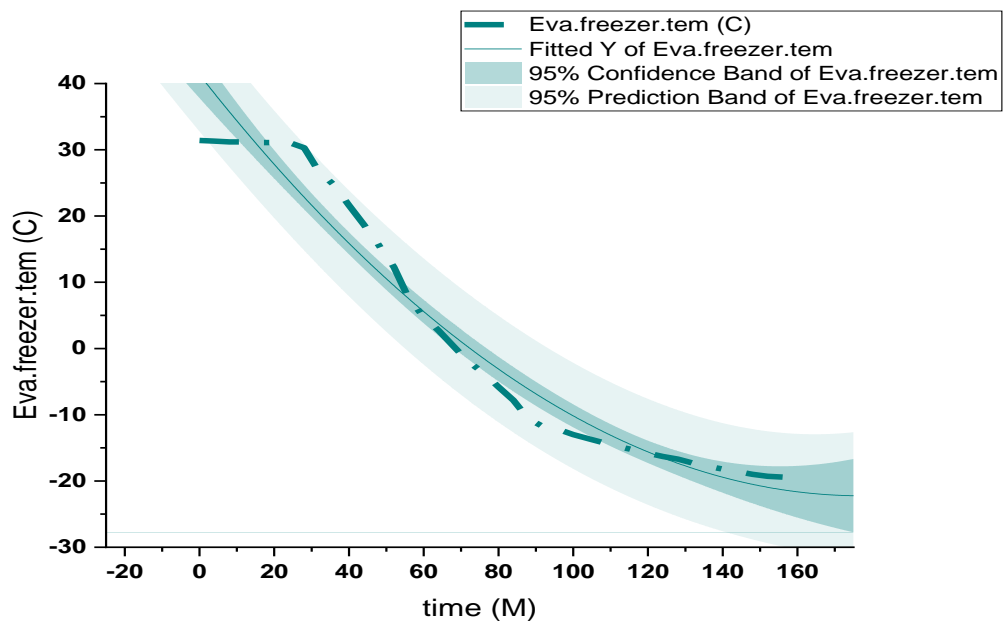


Figure 5.15. Evaporator temperature data during the 156 minutes of the second experiment.

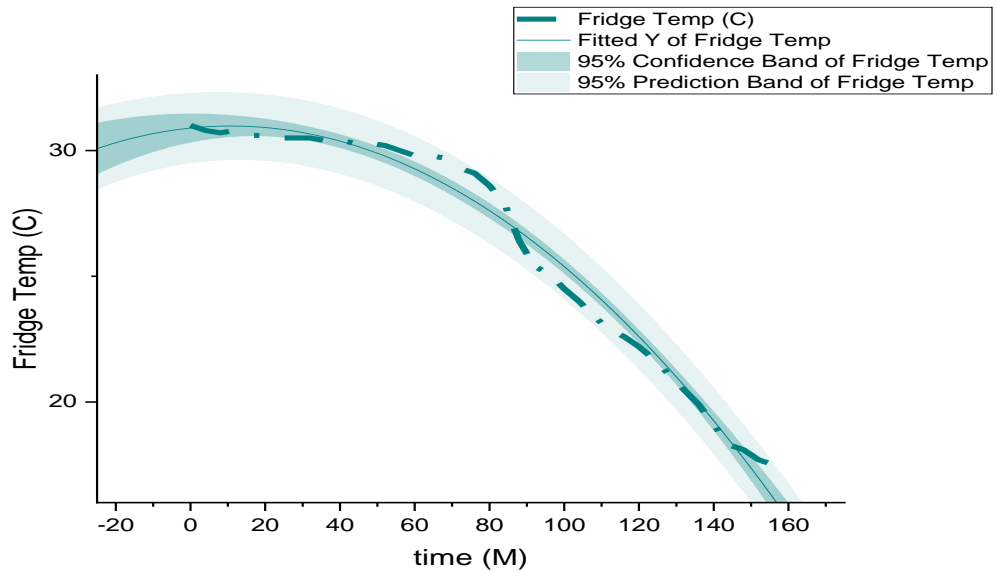


Figure 5.16. Fridge temperature data during the 156 minutes of the second experiment.

To complete the cycle, the refrigerant (ammonia liquid) must be transferred from the evaporator to the absorption vessel so that the process of mixing or dissolving the absorbent material (water) takes place inside the absorption vessel. The temperature of the absorption vessel, which was recorded from this experiment, reaches the average temperature of 47°C during the 156 minutes, which is the temperature of the absorbent material and the refrigerant, from which the cycle begins again, as shown in Figure 5.19.

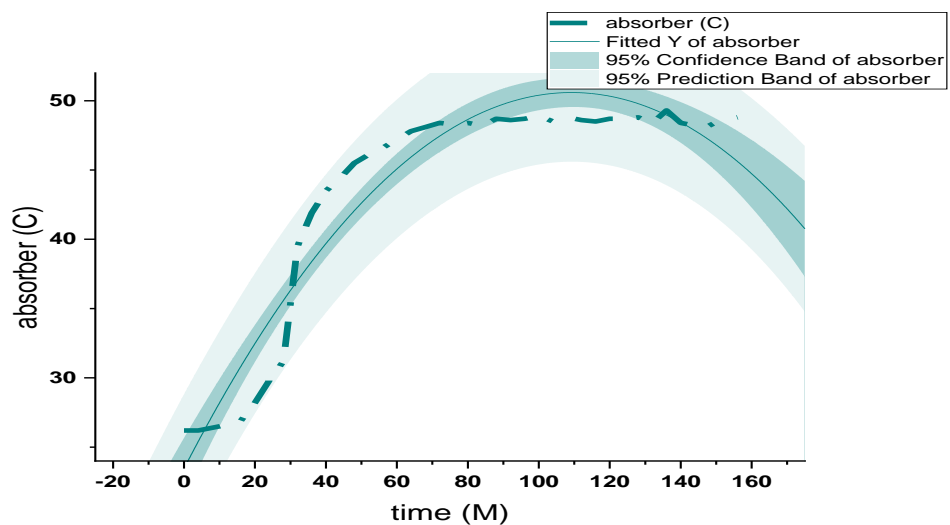


Figure 5.17. Absorber temperature curve after 156 minutes of the second experiment

The room temperature was set at  $25.6 \pm 1^\circ\text{C}$  for 156 minutes, noting that this temperature fluctuation does not affect the performance of the refrigerator directly driven by PV energy (Figure 5.20).

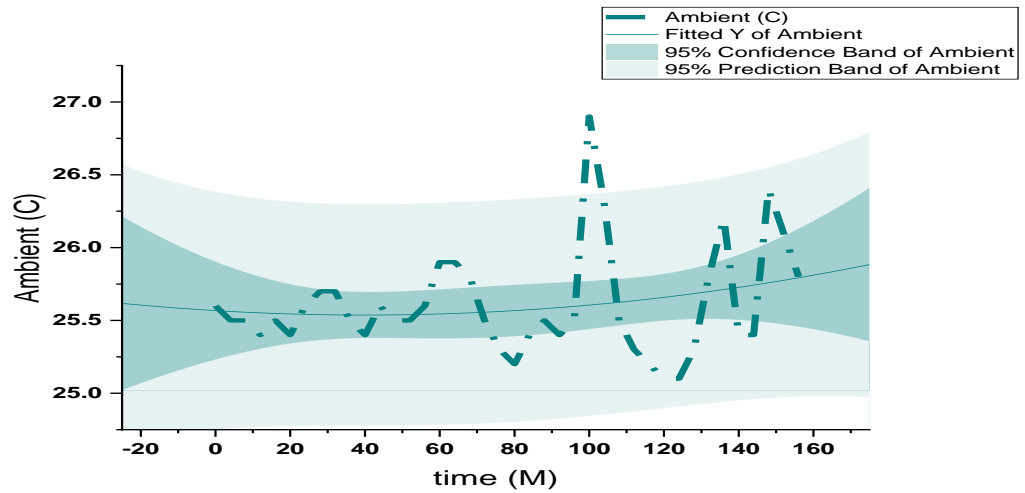


Figure 5.18. Room temperature data over the 156 minutes of the second experiment

The electrical current data was recorded by a continuous ammeter with the operation of the absorptive freezing system. It was recorded as 8.8 A, and after 20 minutes the continuous current decreased gradually, which means that the ARS system began to work, and then continued to decrease gradually to reach 8 A after 120 minutes, until the end of the experiment for a period of 156 minutes (Figure 5.21).

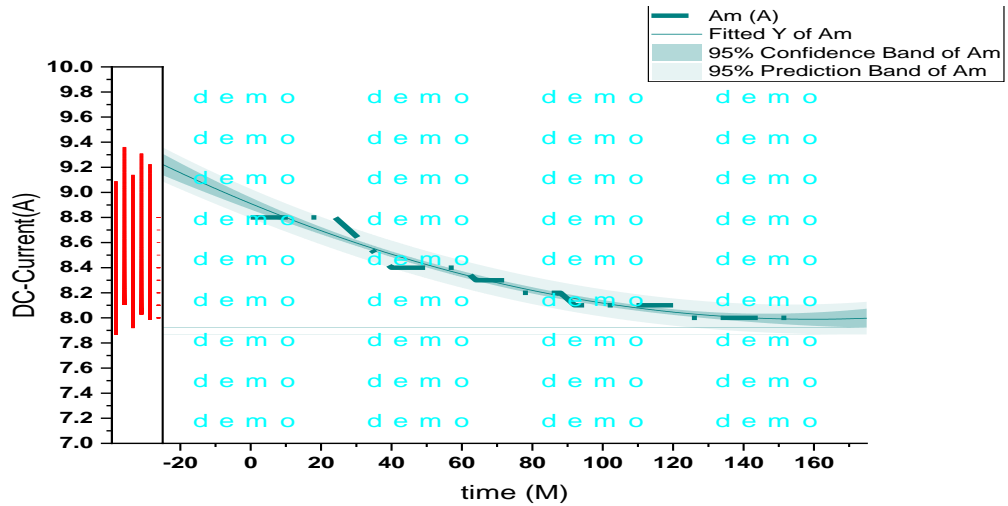


Figure 5.19. Data of DC consumed by the refrigerator over the 156 minutes of the second experiment.

The voltage data was recorded with a potentiometer, and with the operation of the absorption freezing system, 46 V was recorded. After 10 minutes, the voltage rose slightly to 46.8 V. Moreover, after approximately 20 minutes, it decreased gradually and fluctuated, which means that the ARS system began to work, and then continued to decrease gradually to reach 45.8 V after 120 minutes, until the end of the experiment for a period of 156 minutes (Figure 5.22).

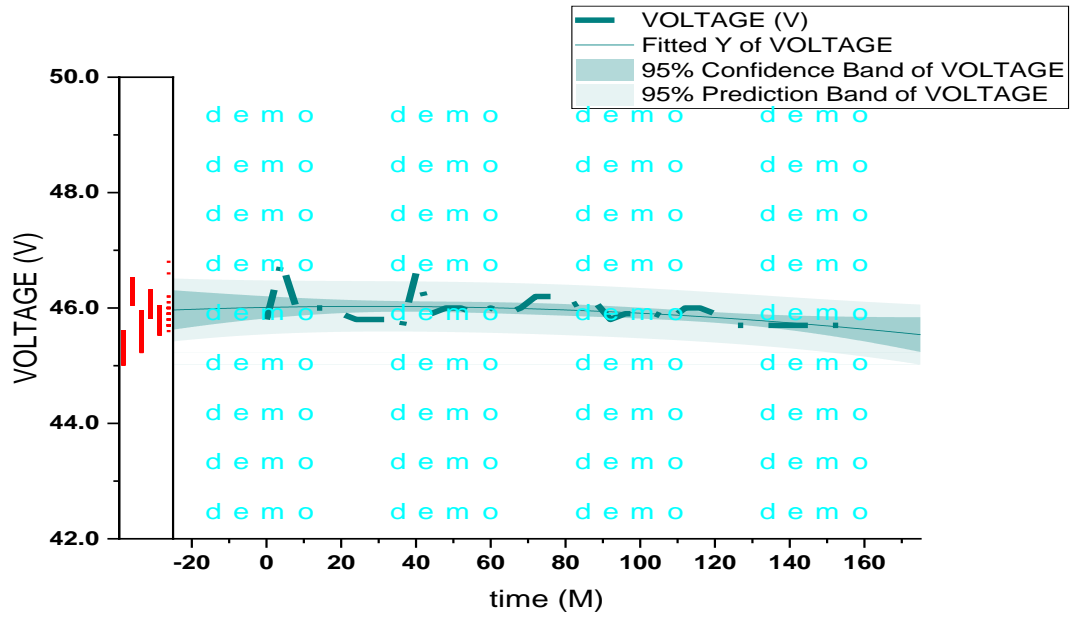


Figure 5.20. Data of the voltage consumed by the electric heater during the 156 minutes of the second experiment.

The voltage and current data are shown in Figure 5.23, which shows the normal operation of the refrigerator through a slight gradual decrease in the current as a result of the high temperatures in the generator. The refrigerator responded in less than half an hour until it was stabilised at  $-19.4^{\circ}\text{C}$  within 120 minutes.



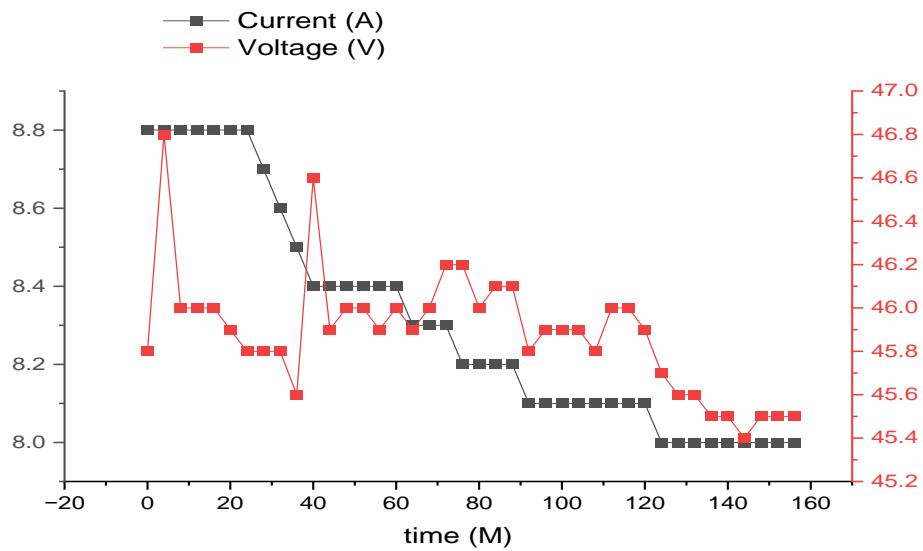


Figure 5.21. Comparison between the voltage and current of the DC heater during the operation of the ARS system.

A comparison was made between the generator input temperatures and the lower temperatures. In the evaporator in a three-dimensional form over 156 minutes in clear weather, we notice the generator output temperature is 157°C, and note the low temperature in the evaporator of -19°C, as shown in Figure 5.24.

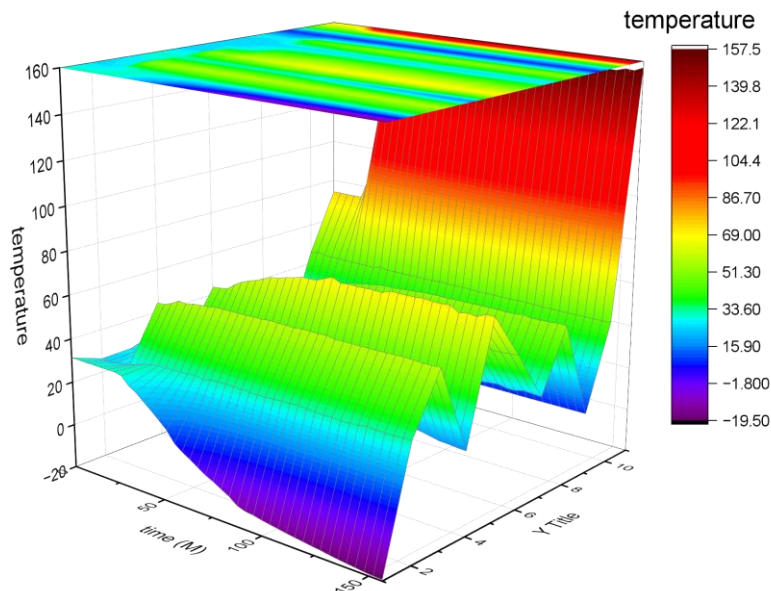


Figure 5.22. 3D model of input temperature in the generator and temperatures in the evaporator of the SARS solar absorption refrigerator over 156 minutes.

From Figure 5.25 and Figure 5.26, a comparison between the output temperature of the generator, the output temperature of the condenser, the temperature of the evaporator, rectifier, the fridge, in addition to the room temperature for 156 minutes. degrees Celsius to 157°C, and the temperature in the evaporator decreased from 31°C to -19.4°C and in the refrigerator from 31°C to 17°C, which is what will be proved in subsequent experiments.

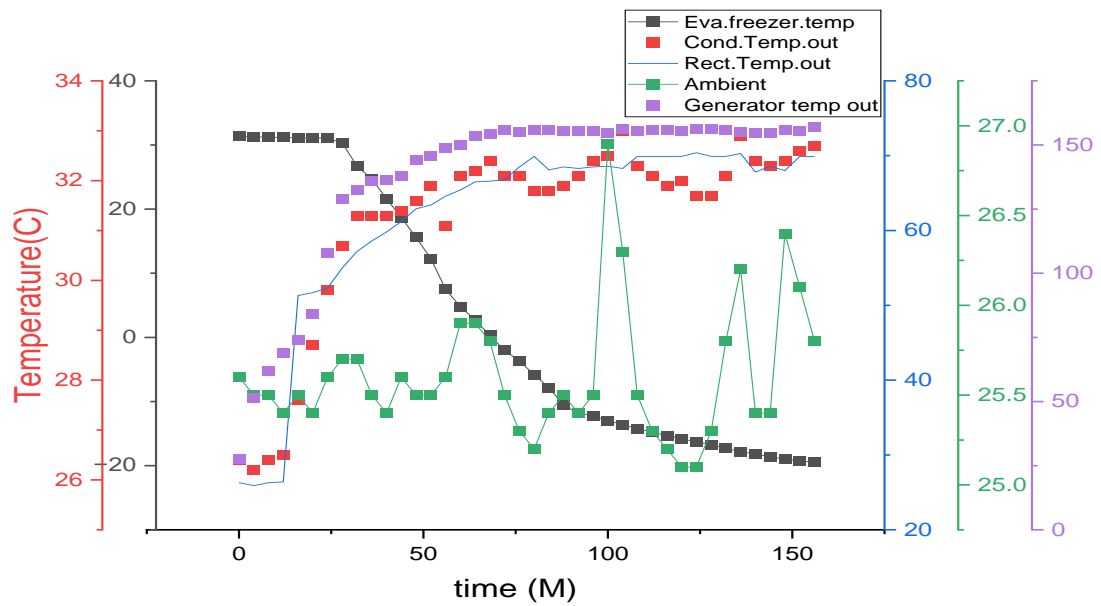


Figure 5.23. Comparison of the temperatures of the generator, evaporator, condenser, and rectifier, as well as room temperature during the 156 minutes of the second experiment.

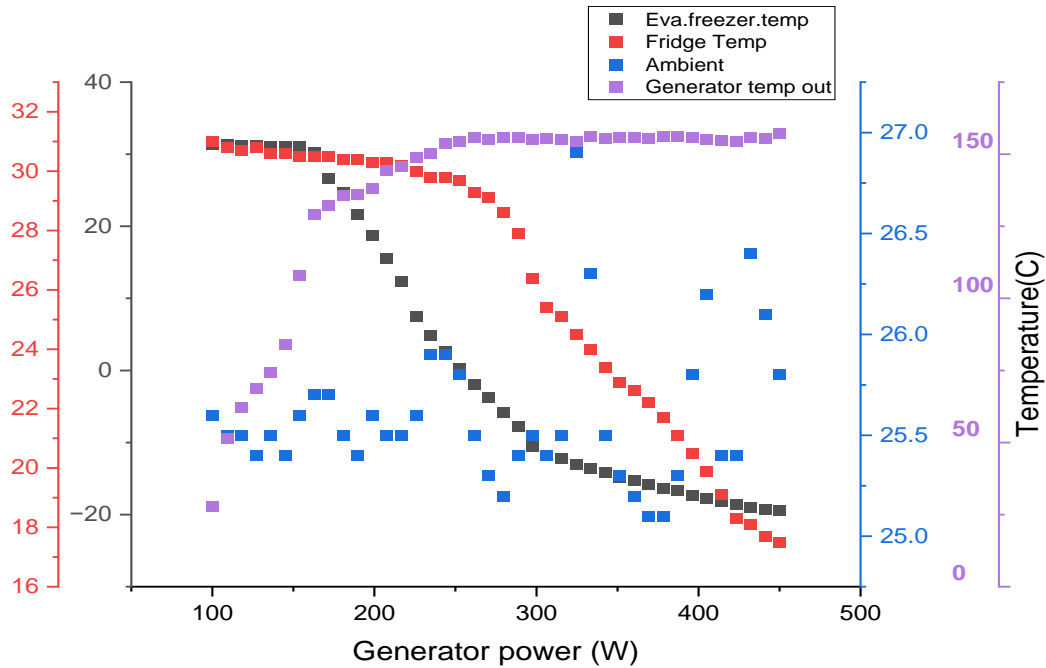


Figure 5.24. Comparison between the generator output temperature and the evaporator temperature as well as the refrigerator temperature and the amount of power in the generator.

In addition to the practical experiments, a simple simulation was performed using the EES program based on the temperature data of the refrigerator parts obtained from the practical experiment in the laboratory. The average concentration of ammonia in the water was estimated at 30%, according to the refrigerator manufacturer's specifications. This value was used during the simulation process and we were able to calculate the COP value, which is equal to 0.302. These results are similar to those of Starace, G., & De Pascalis, L. (2012) [43] and Gürbüz, E.Y., et al 2022 [55] .and Gürbüz, E.Y., et al

### 5.3. THE THIRD EXPERIMENT

This experiment was conducted continuously on December 17, 2022 from 8.38 am to 10.00 pm the next day. The photovoltaic panel was adjusted at an angle of 30 degrees in terms of the intensity of solar radiation using an S 220-T 8 portable thermocouple temperature data recorder. Digital temperature sensors (TPM-10) were also used, and then the data were recorded every two minutes to ensure the accuracy of the recorded data. In this experiment, the solar ARS was powered on November 19 from 8.30 am to November 20 at 8.30 am with an electric source (AC) as shown in Figure 5.27.

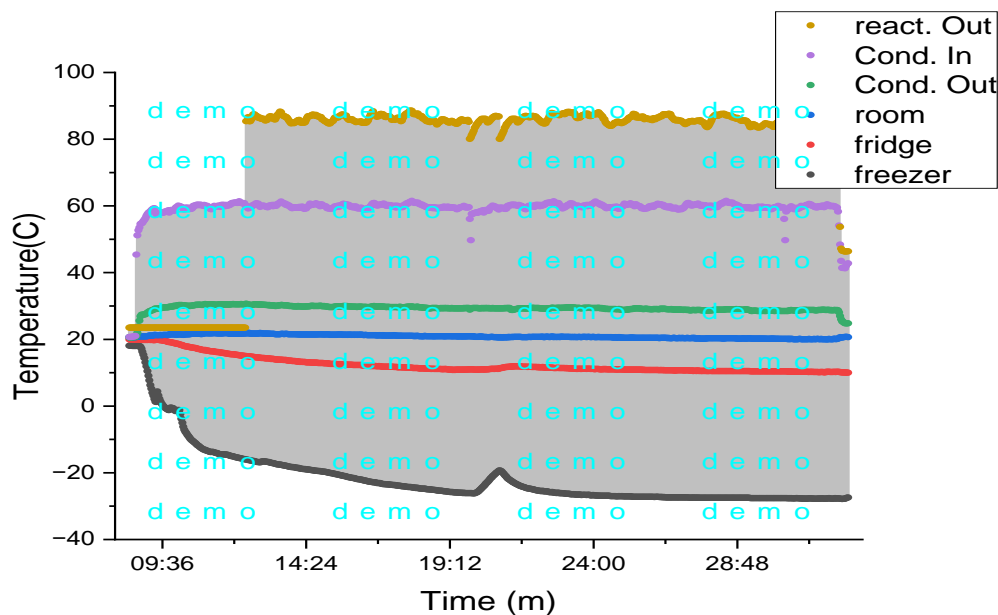


Figure 5.25. Temperature data shown in the curves on the first day of the third experiment, during the first 24 hours

The drive system was switched to DC from 8.30 a.m. on November 20, 2022, as shown in Figure 5.28 and Figure 5.29. On the first day of this experiment, after 178 minutes of work, we reached  $-19^{\circ}\text{C}$  inside the evaporator compared to the previous (second) experiment. This result was reached within 152 minutes using photovoltaic energy directly. Moreover, on the first day of this experiment, a temperature of  $-27^{\circ}\text{C}$  was observed in the evaporator. After converting the operating system to a direct solar light source (DC), it was observed that the refrigerator would continue to operate at the same efficiency, and  $-27^{\circ}\text{C}$  was observed in the evaporator for more than seven consecutive hours.

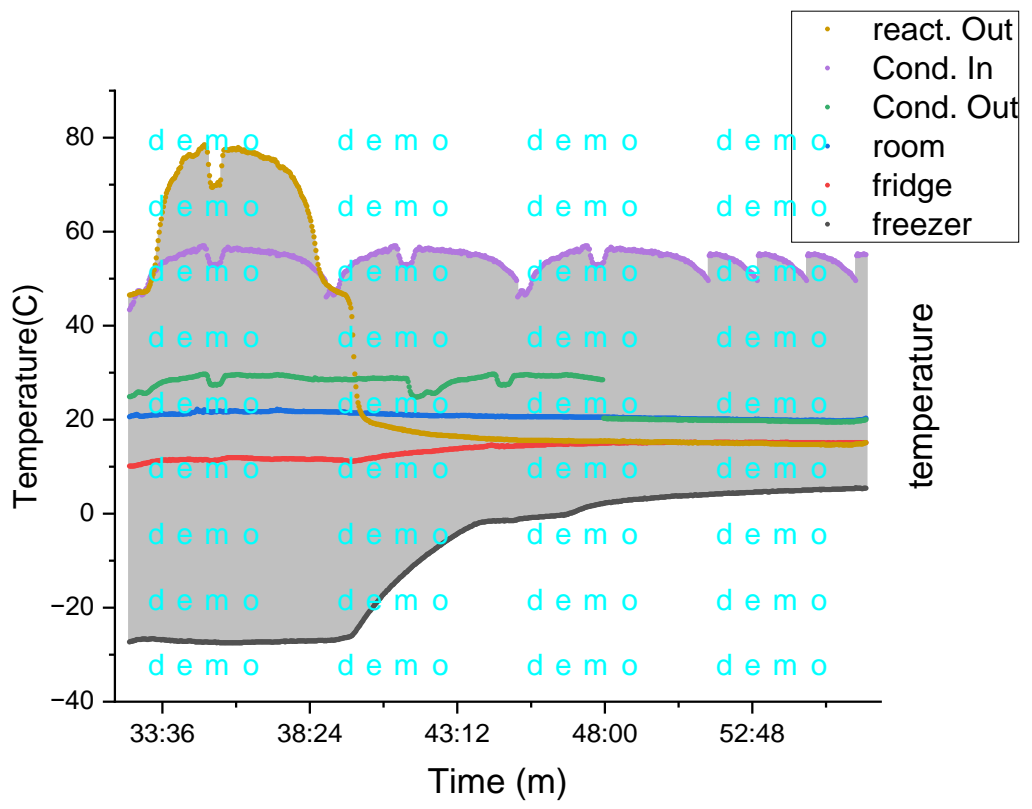


Figure 5.26. Temperature data shown in the curves on the second day of the third experiment, during the second 24-hour period.

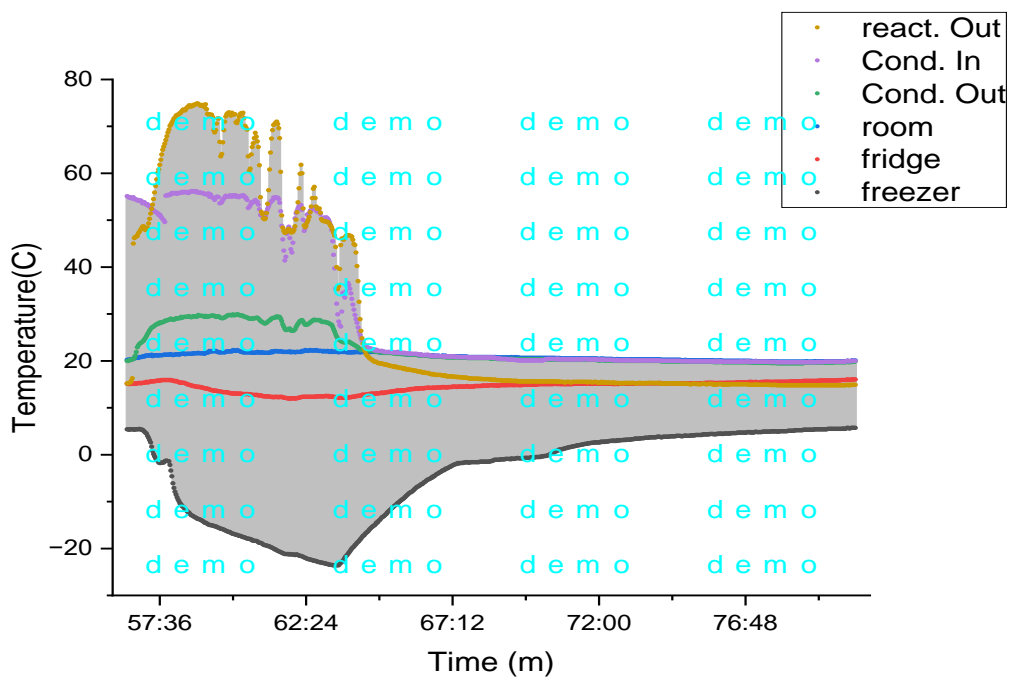


Figure 5.27. Temperature data for the parts of the system from the third day of the third experiment over a 24-hour period.

Figure 5.30 shows a 3D model of the third experiment for three days. It simulates a complete picture of the high and low temperatures of the two operating systems, DC and AC, as well as showing the high temperatures in the evaporator with a decrease in the intensity of solar radiation and stabilisation of 5°C in the DC operating system as the highest temperature recorded and -27°C as the lowest temperature recorded in both systems.

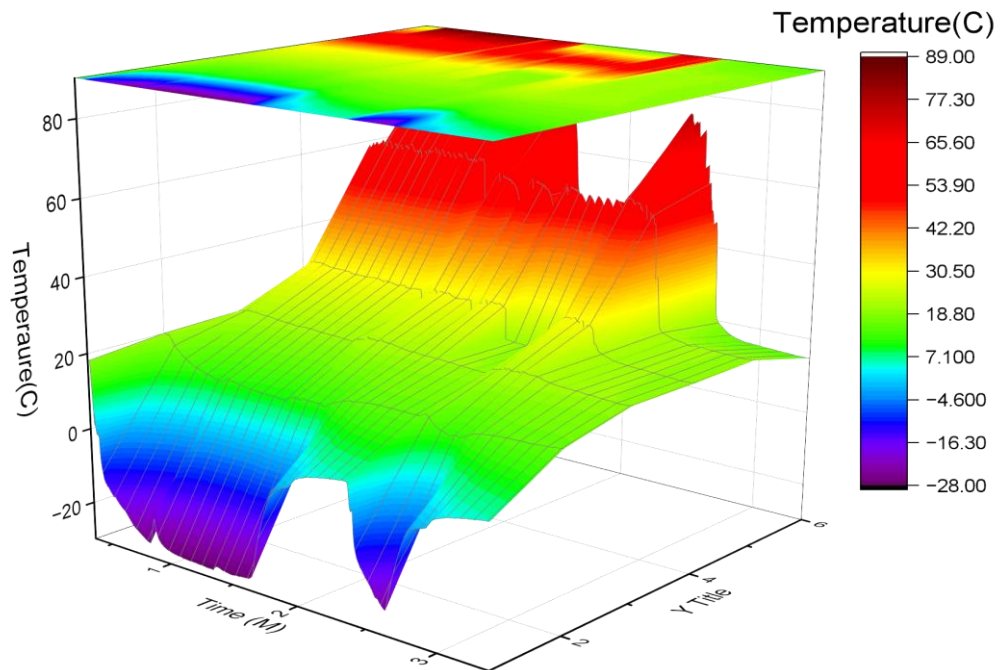


Figure 5.28. A three-dimensional model for the third experiment over three days.

Not much difference in the way both systems operate could be observed, and this allows the AC system to be interchangeable with the solar PV direct current (DC) system to drive the ARS absorption refrigeration system. This leads to a significant reduction in the costs of energy production, storage and maintenance, and also helps to reduce emissions, environmental pollution and global warming, unlike compression cooling systems. The temperatures obtained in both AC and DC

systems are sufficient for storing different types of food, in addition to storing vaccines and medicines that need to be stored at lower temperatures. Solar absorption cooling technology can be delivered to rural and remote areas which are difficult to supply with electric power grids. The use of DC electricity for heating is not restricted if the voltage fluctuates slightly due to winds or dust, unlike a compressor which needs a steady, stable electrical supply in compressive systems.

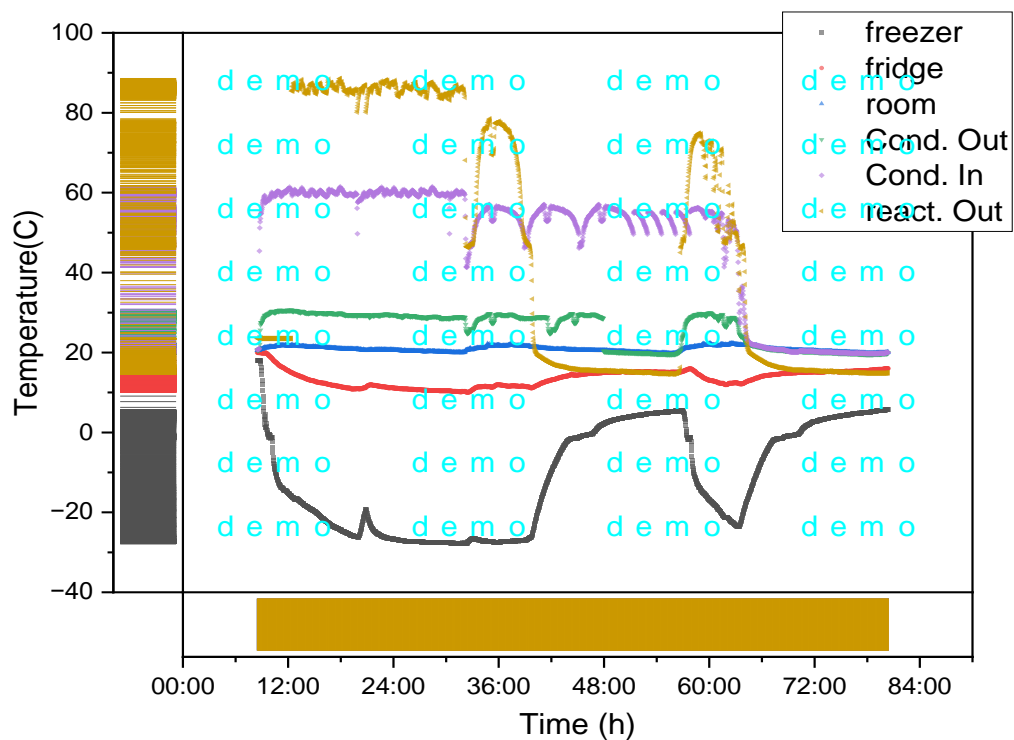


Figure 5.30. Temperature data are shown in the curves for three consecutive days of the third experiment, over a 72-hour period

#### 5.4. THE FOURTH EXPERIMENT

This experiment was conducted continuously on December 17, 2022 from 8.38 am to 10.00 pm the next day. The photovoltaic panel was adjusted at an angle of 30°C in terms of the intensity of solar radiation using an S 220-T 8 portable thermocouple temperature data recorder. Digital temperature sensors (TPM-10) were also used, and then the data were recorded every two minutes to ensure the accuracy of the recorded data shown in the curves of the experiment, which represent the parts of the

absorptive refrigeration system. The experiment was carried out for 2,246 minutes, which is equivalent to 37 hours, as shown in Figure 5.32.

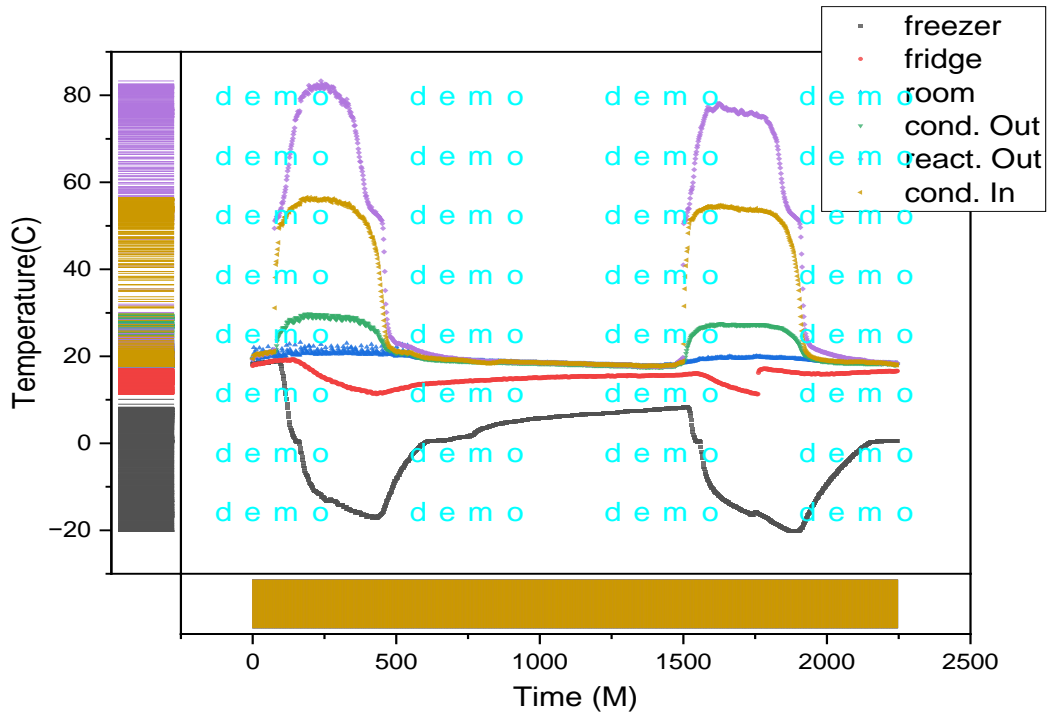


Figure 5.31. Temperature data for system components over a 2,246-minute period.

On the first day, after 7 hours of operating the refrigerator with photovoltaic solar energy, the experiment showed that the temperature decreased to below  $0^{\circ}\text{C}$  ( $-7.16^{\circ}\text{C}$ ) in the evaporator, after which the temperatures began to rise with the gradual decrease in the intensity of solar radiation. After 10 hours of operation,  $-4^{\circ}\text{C}$  was observed in the evaporator and temperatures continued to rise gradually, and after 12 hours,  $1.1^{\circ}\text{C}$  was recorded in the evaporator until  $8^{\circ}\text{C}$  was recorded in the evaporator after 1,400 minutes, equivalent to the first 24 hours at 8.30 am on September 18, 2022, as shown in Figure 5.33.



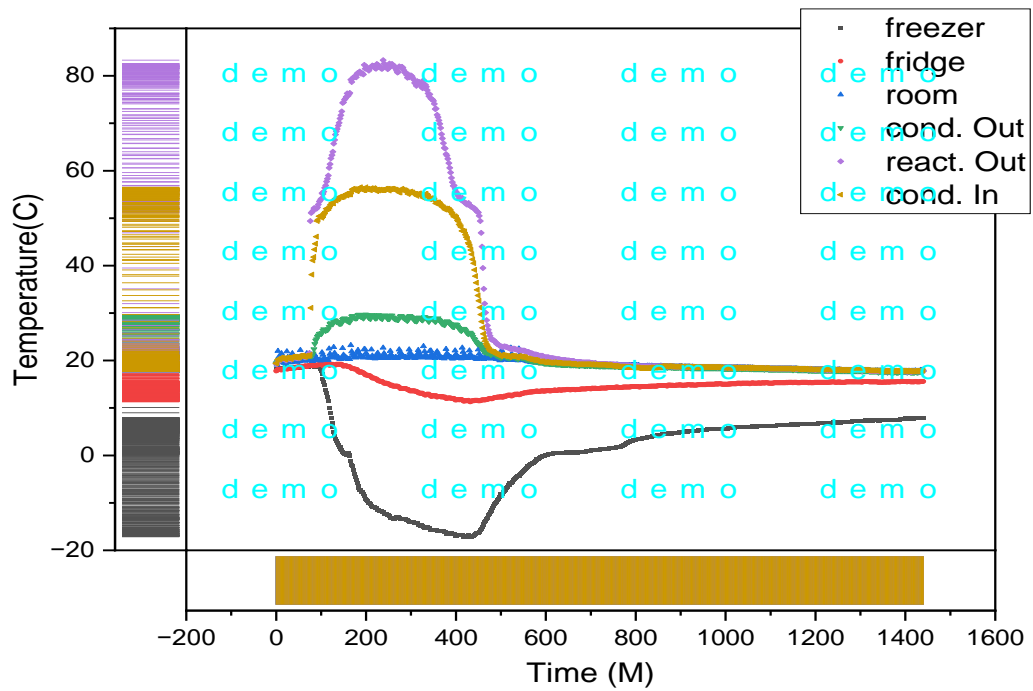


Figure 5.32. Comparison of the temperatures of the components of the system during 1,440 minutes

The next day at exactly 8.30 am, equivalent to 1,432 minutes from this experiment, we noticed 8°C. After 7 hours of operating the refrigerator on photovoltaic solar energy, the temperature decreased to below 0°C (-19.6°C) in the evaporator, after which the temperatures began to rise with the gradual decrease in the intensity of solar radiation. After 10 hours of operation, -7°C was observed in the evaporator, and the temperature continued to rise gradually, and after 12 hours, 0.3°C was recorded in the evaporator until 5°C was recorded in the evaporator after 800 minutes, equivalent to 13 hours, for the second day of this experiment on September 18, 2022. Figure 5.34 shows that the results for the first and second day are not much different in this experiment

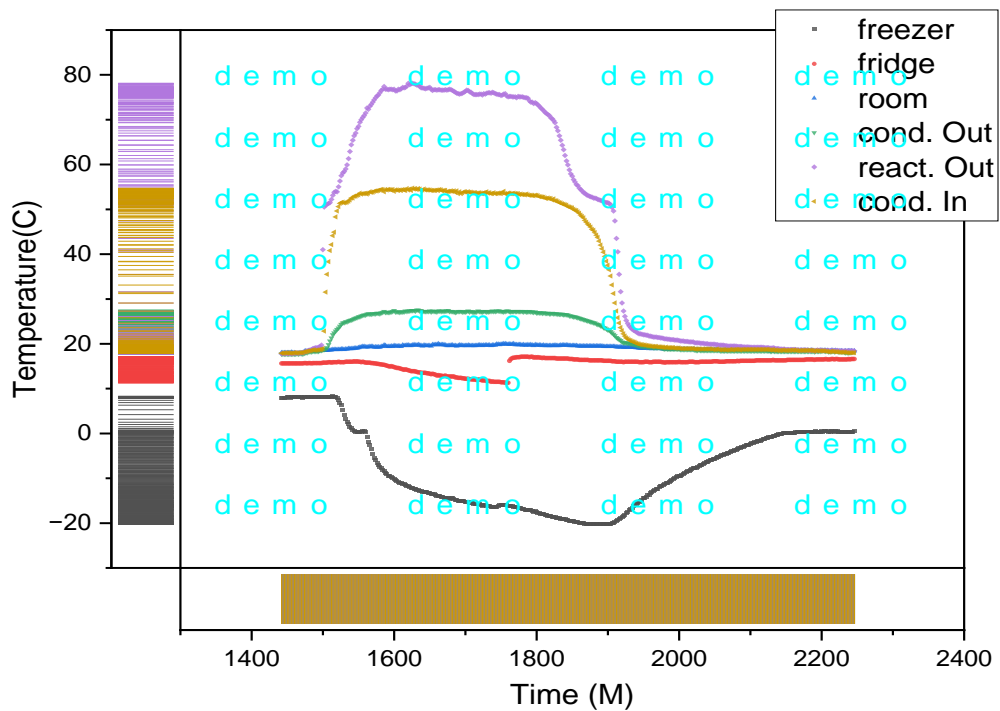


Figure 5.33. Temperature data over an 800-minute period for the second day within the last 13 hours.

In these temperatures, food, medicines, vaccines, etc. can be preserved. The experiment was repeated two days later, on December 20, 2022, but the angle was changed to  $20^\circ$ , and temperature measurements were taken every 2 minutes for most parts of the system. We noticed that after the passage of 7 hours in the evaporator ( $-24$ ) for the first day, as shown in Figure 47, we can conclude that adjusting the PV at an angle ( $20$ ) is better than adjusting it at an angle ( $30$ ), so through these experiments it is possible to reduce the percentage of consumption Electric energy (AC) by 50% during daylight hours, relying on photovoltaic energy to directly operate cooling and refrigeration systems, , which was shown through the four experiments. Photovoltaic energy can be used through photovoltaic systems to operate absorption ice systems directly and eliminate the costs of parts used in converting power from direct current to alternating current, as well as maintenance costs for 24 hours, thereby reducing harmful environmental effects and global warming. Moreover, the costs of producing electrical energy are to a large extent consumed in the operation of refrigeration systems and compressive refrigeration systems.

The experiment was repeated two days later, on December 20, 2022, but the angle was changed by 20°, using a portable thermocouple temperature data logger (S 220-T 8). Digital temperature sensors (TPM-10) were also used, and then the data was recorded with the temperature being recorded every two minutes to ensure the accuracy of the recorded data. After 7 hours of operating the ARS on a renewable energy source (photovoltaic solar energy), we noticed  $-24^{\circ}\text{C}$  in the evaporator on the first and second days of this experiment with the same efficiency, and we also noticed a rise in temperatures in the evaporator with a decrease in temperatures in the generator as a result, and a gradual decrease in the intensity of solar radiation (see Figure 5.35).

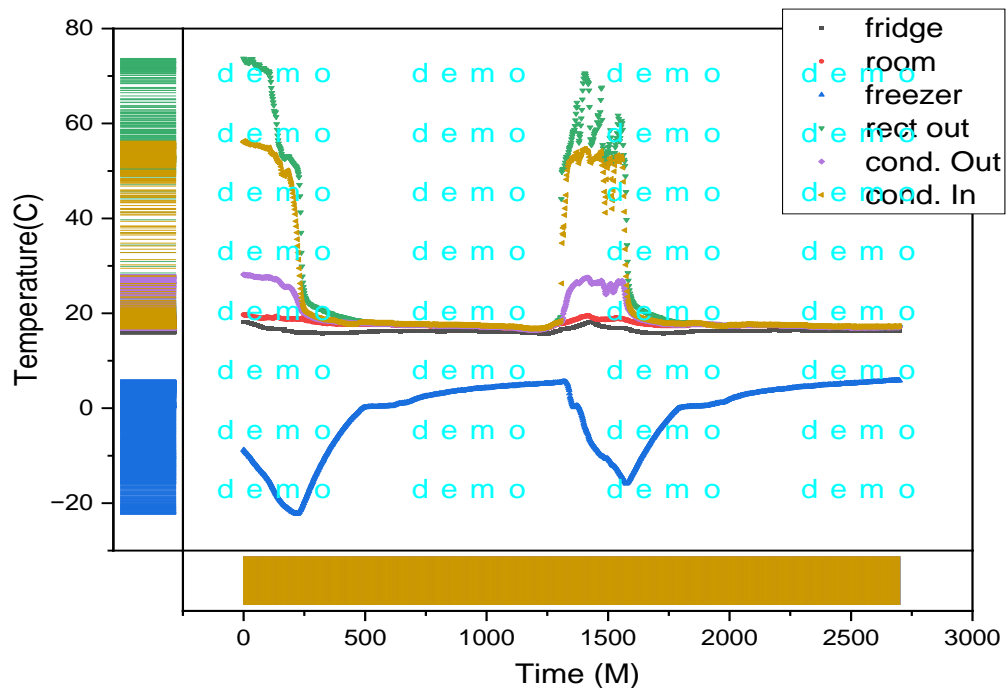


Figure 5.34. Temperature data for system components in curves over 2,700 minutes within 45 hours.

We can conclude that adjusting the PV panel to an angle of 20° is better than adjusting it at an angle of 30. It can also be understood through the experiments presented in this study that the percentage of electrical energy consumption (AC) can be reduced by 50% during daylight hours by relying on photovoltaic energy to operate directly in the cooling and refrigeration systems, as shown through the four

experiments. In addition to the costs of maintenance, photovoltaic energy can be used directly to operate absorptive refrigeration systems and eliminate the costs of the parts used in converting power from direct current to alternating current,. Thus, a percentage of the costs of producing electrical energy can be reduced, in addition to reducing any harmful environmental effects and phenomena of warming thermals. By means of the temperatures obtained in all the experiments mentioned in this study, it is possible to preserve food, foodstuffs, medicines and vaccines, especially in remote rural areas where it is difficult to deliver electricity and any medical supplies and materials that require low temperatures.

## **PART 6**

### **CONCLUSIONS AND RECOMMENDATIONS**

#### **6.1. CONCLUSIONS**

The results of this study are very interesting. Investing in the use of renewable energy resources is very important, especially in light of these fossil fuel resource crises. Moreover, the consequences of using fossil fuels include global warming and environmental pollution. Therefore, the results of this study can be summarised as follows.

- This system does not contain a compressor, so gases that pollute the environment and cause global warming are not used.
- The operation of this system is not greatly affected by voltage fluctuations due to weather fluctuations, unlike cooling systems that contain a compressor, as they need a constant current.
- It has been shown through experiments that adjusting the photovoltaic panel at an angle of 20° gives the best results in the operation of the system. In multiple tests, the refrigerator evaporator temperature reached  $-26^{\circ}\text{C}$  and the compartment temperature was approximately  $10^{\circ}\text{C}$ .
- The performance of this refrigerator using the photovoltaic panel was similar to its performance with the traditional electrical source (AC).

#### **6.2. RECOMMENDATIONS**

The following recommendations can be made in the wake of our study.

- Investigate the effect of different solar collectors on the performance of the absorption refrigerator. Different types of solar collectors can be used, such

as flat plate collectors, evacuated tube collectors, or concentrating collectors, and their performance can be analysed in terms of efficiency, cost, and suitability for the refrigeration system.

- Study the effect of different parameters such as ammonia concentration, water concentration, and hydrogen concentration on the performance of the absorption refrigerator. These parameters can be varied, and their effect on the system performance can be analysed in terms of coefficient of performance (COP) and cooling capacity.
- Investigate the effect of different operating conditions such as ambient temperature, solar radiation intensity, and flow rate on the performance of the absorption refrigerator. Experiments under different operating conditions can be performed, and the effect of these conditions on the system performance can be analysed.
- Study the feasibility of using the ammonia-water-hydrogen diffusion absorption refrigerator for cooling applications in remote areas or off-grid locations. The economic viability of the system can be analysed and compared with other cooling technologies.
- Investigate the stability and durability of the absorption refrigerator under different operating conditions. The long-term performance of the system can be studied and analyses can be performed on the degradation of the materials used in the system.
- Evaluate the performance of the ammonia-water-hydrogen diffusion absorption refrigerator in hybrid solar energy systems. Analyses can be made of the performance of the system when it is integrated with other renewable energy sources such as wind power, biomass, or geothermal energy.
- Investigate the feasibility of using the absorption refrigerator for air conditioning applications. The cooling capacity and efficiency of the system can be studied and compared with conventional air conditioning systems.
- Analyse the impact of different design parameters, such as the size and shape of the absorber and generator, on the performance of the absorption refrigerator. Experiments with different design parameters can be performed and their effect on the system performance can be analysed.

## REFERENCES

1. Gantz, C. (2015). Refrigeration. a history. McFarland.
2. Xia, X., D. Setlhaolo, and J. Zhang. Residential demand response strategies for South Africa. in IEEE Power and Energy Society Conference and Exposition in Africa. Intelligent Grid Integration of Renewable Energy Resources (PowerAfrica). 2012. IEEE.
3. Van den Berg, H., Risks Associated with South African Energy Pipelines. 2012. University of Johannesburg (South Africa).
4. Ristenpart, W., et al., non-coalescence of oppositely charged drops. *Nature*, 2009. 461(7262). p. 377-380. [https://www.researchgate.net/publication/338668623\\_Solar\\_Thermochemical\\_Fuel\\_Generation](https://www.researchgate.net/publication/338668623_Solar_Thermochemical_Fuel_Generation)
5. Babajide, O., et al., Use of coal fly ash as a catalyst in the production of biodiesel. 2010.
6. Fluri, T.P., The potential of concentrating solar power in South Africa. *Energy Policy*, 2009. 37(12). p. 5075-5080. [https://commons.wikimedia.org/wiki/File:Second\\_law\\_heat\\_engine.png](https://commons.wikimedia.org/wiki/File:Second_law_heat_engine.png)
7. Ellabban, O., H. Abu-Rub, and F. Blaabjerg, Renewable energy resources. Current status, future prospects and their enabling technology. *Renewable and sustainable energy reviews*, 2014. 39. p. 748-764.
8. et al., Study of a HVAC system for energy-efficient poultry houses in Arid Zone. 2022.
9. Harvey, C. and N. Heikkinen, Congress Says Biomass Is Carbon-Neutral, but Scientists Disagree. *Scientific American E&E News Environment*, 2018.
10. Alazraque-Cherni, J., Renewable energy for rural sustainability in developing countries. *Bulletin of Science, Technology & Society*, 2008. 28(2). p. 105-114.
11. Turkenburg, W.C. and A. Faaij, Renewable energy technologies. 2000, UNDP/UNDESA/WEC. *Energy and the Challenge of Sustainability*. World Energy ....
12. Armaroli, N. and V. Balzani, Towards an electricity-powered world. *Energy & Environmental Science*, 2011. 4(9). p. 3193-3222.

13. Armaroli, N. and V. Balzani, Solar electricity and solar fuels. status and perspectives in the context of the energy transition. *Chemistry–A European Journal*, 2016. 22(1). p. 32-57.
14. Quaschnig, V., Renewable energy systems. Technology-calculation-simulation. 8. upd. and enl. ed.; Regenerative Energiesysteme. Technologie-Berechnung-Simulation. 2013.
15. Bölük, G. and R. Kaplan, Effectiveness of renewable energy incentives on sustainability. evidence from dynamic panel data analysis for the EU countries and Turkey. *Environmental Science and Pollution Research*, 2022. p. 1-18.
16. Zhongming, Z., et al., Global energy review 2021. 2021. <https://renewablesnow.com/news/energy-crisis-prompts-sharp-increase-in-ieas-renewables-forecast-807346/>
17. Siler-Evans, K., et al., Regional variations in the health, environmental, and climate benefits of wind and solar generation. *Proceedings of the National Academy of Sciences*, 2013. 110(29). p. 11768-11773.
18. Energy, S.P., Technology roadmap. 2014, Technical Report, IEA, September 2014. Available online. <https://www.iea.org/> ....
19. Bansal, P. and A. Martin, Comparative study of vapour compression, thermoelectric and absorption refrigerators. *International Journal of Energy Research*, 2000. 24(2). p. 93-107.
20. Khudhur, J., Akroot, A., and Al-samari, A., "Experimental Investigation of Direct Solar Photovoltaics that Drives Absorption Refrigeration System", *Journal Of Advanced Research In Fluid Mechanics And Thermal Sciences*, 1 (1): 116–135 (2023).
21. Chakravarty, K.H., et al., A review on integration of renewable energy processes in vapor absorption chiller for sustainable cooling. *Sustainable Energy Technologies and Assessments*, 2022. 50. p. 101822.
22. Patel, B., N.B. Desai, and S.S. Kachhwaha, Optimization of waste heat based organic Rankine cycle powered cascaded vapor compression-absorption refrigeration system. *Energy conversion and management*, 2017. 154. p. 576-590.
23. Xu, Z. and R. Wang, Absorption refrigeration cycles. Categorized based on the cycle construction. *International Journal of Refrigeration*, 2016. 62. p. 114-136.
24. Kwak, D.-H., M. Binns, and J.-K. Kim, Integrated design and optimization of technologies for utilizing low grade heat in process industries. *Applied Energy*, 2014. 131. p. 307-322.
25. She, X., et al., Energy-efficient and-economic technologies for air conditioning with vapor compression refrigeration. A comprehensive review. *Applied Energy*,



2018. 232. p. 157-186. <https://marinerspointpro.com/vapour-absorption-refrigeration-system-working/>
26. Aphornratana, S., Theoretical and experimental investigation of a combined ejector-absorption refrigerator. 1995, University of Sheffield, Department of Mechanical and Process Engineering.
  27. Matsuda, A., et al., Effect of pressure and concentration on performance of a vertical falling-film type of absorber and generator using lithium bromide aqueous solutions. *International journal of refrigeration*, 1994. 17(8). p. 538-542.
  28. Cosenza, F. and G. Vliet, Absorption in falling water/LiBr films on horizontal tubes. *ASHRAE Transactions*, 1990. 96(1). p. 693-701.
  29. MORIOKA, I. and M. KIYOTA, Absorption of water vapor into a wavy film of an aqueous solution of LiBr. *JSME international journal. Ser. 2, Fluids engineering, heat transfer, power, combustion, thermophysical properties*, 1991. 34(2). p. 183-188.
  30. Kim, K., et al., Absorption of water vapour into falling films of aqueous lithium bromide. *International Journal of Refrigeration*, 1995. 18(7). p. 486-494.
  31. Benzeguir, B., F. Setterwall, and H. Uddholm, Use of a wave model to evaluate falling film absorber efficiency. *International journal of refrigeration*, 1991. 14(5). p. 292-296.
  32. Andberg, J. and G. Vliet, A simplified model for absorption of vapors into liquid films flowing over cooled horizontal tubes. *ASHRAE transactions*, 1987. 93. p. 2454-2466.
  33. Kang, Y.T. and R.N. Christensen, Transient analysis and design model of a LiBr-H<sub>2</sub>O absorber with rotating drums. *ASHRAE Transactions*, 1995(1). p. 1163-1174.
  34. Jeong, S., et al., Heat transfer performance of a coiled tube absorber with working fluid of ammonia/water/discussion. *ASHRAE Transactions*, 1998. 104. p. 1577.
  35. Ruiz, E., et al., Evaluation of ionic liquids as absorbents for ammonia absorption refrigeration cycles using COSMO-based process simulations. *Applied Energy*, 2014. 123. p. 281-291.
  36. Najjaran, A., et al., Experimental performance analysis of an ammonia-water diffusion absorption refrigeration cycle. 2017.
  37. Mazouz, S., R. Mansouri, and A. Bellagi, Experimental and thermodynamic investigation of an ammonia/water diffusion absorption machine. *International Journal of refrigeration*, 2014. 45. p. 83-91.
  38. Acuña, A., N. Velázquez, and J. Cerezo, Energy analysis of a diffusion absorption cooling system using lithium nitrate, sodium thiocyanate and water as

- absorbent substances and ammonia as the refrigerant. *Applied Thermal Engineering*, 2013. 51(1-2). p. 1273-1281.
39. Assilzadeh, F., et al., Simulation and optimization of a LiBr solar absorption cooling system with evacuated tube collectors. *Renewable energy*, 2005. 30(8). p. 1143-1159.
  40. Herrando, M., et al., Solar combined cooling, heating and power systems based on hybrid PVT, PV or solar-thermal collectors for building applications. *Renewable Energy*, 2019. 143. p. 637-647.
  41. Khan, M.M.A., et al., Performance assessment of a solar powered ammonia–water absorption refrigeration system with storage units. *Energy conversion and management*, 2016. 126. p. 316-328.
  42. Ramos, A., et al., Hybrid photovoltaic-thermal solar systems for combined heating, cooling and power provision in the urban environment. *Energy conversion and management*, 2017. 150. p. 838-850.
  43. Starace, G. and L. De Pascalis, An advanced analytical model of the diffusion absorption refrigerator cycle. *International Journal of Refrigeration*, 2012. 35(3). p. 605-612.
  44. Zohar, A., et al., The influence of the generator and bubble pump configuration on the performance of diffusion absorption refrigeration (DAR) system. *International Journal of Refrigeration*, 2008. 31(6). p. 962-969.
  45. Vicatos, G. and A. Bennett, Multiple lift tube pumps boost refrigeration capacity in absorption plants. *Journal of Energy in Southern Africa*, 2007. 18(4). p. 49-57.
  46. Jakob, U., et al., Simulation and experimental investigation into diffusion absorption cooling machines for air-conditioning applications. *Applied Thermal Engineering*, 2008. 28(10). p. 1138-1150.
  47. Kaynakli, O. and M. Kilic, Theoretical study on the effect of operating conditions on performance of absorption refrigeration system. *Energy conversion and management*, 2007. 48(2). p. 599-607.
  48. Arora, A. and S. Kaushik, Theoretical analysis of a vapour compression refrigeration system with R502, R404A and R507A. *International journal of refrigeration*, 2008. 31(6). p. 998-1005.
  49. Dalkilic, A. and S. Wongwises, A performance comparison of vapour-compression refrigeration system using various alternative refrigerants. *International communications in Heat and mass transfer*, 2010. 37(9). p. 1340-1349.
  50. Sun, Z., et al., Theoretical study on a novel CO<sub>2</sub> Two-stage compression refrigeration system with parallel compression and solar absorption partial

- cascade refrigeration system. *Energy Conversion and Management*, 2020. 204. p. 112278.
51. Wijaksana, H., et al. The investigation of influence ammonia concentration variations to the performance of a pump less ammonia-water absorption refrigeration system with water flooding evaporator. in *AIP Conference Proceedings*. 2019. AIP Publishing LLC.
  52. Karamangil, M., et al., A simulation study of performance evaluation of single-stage absorption refrigeration system using conventional working fluids and alternatives. *Renewable and Sustainable Energy Reviews*, 2010. 14(7). p. 1969-1978.
  53. Aman, J., P. Henshaw, and D.-K. Ting, Performance characterization of a bubble pump for vapor absorption refrigeration systems. *international journal of refrigeration*, 2018. 85. p. 58-69.
  54. Al-Tahaine, H., et al., Performance of a Hybrid TEG/Single Stage Ammonia-Water Absorption Refrigeration Cycle with a Combined Effect of Rectifier and Condensate Precooler. *Journal homepage*. <http://iicta.org/journals/ijht>, 2022. 40(1). p. 98-104.
  55. Gürbüz, E.Y., et al., Experimental and numerical investigation of diffusion absorption refrigeration system working with ZnO/Al<sub>2</sub>O<sub>3</sub> and TiO<sub>2</sub> nanoparticles added ammonia/water nanofluid. *Experimental Heat Transfer*, 2022. 35(3). p. 197-222.
  56. Martínez-Maradiaga, D., J.C. Bruno, and A. Coronas, Steady-state data reconciliation for absorption refrigeration systems. *Applied Thermal Engineering*, 2013. 51(1-2). p. 1170-1180.
  57. Sözen, A., T. Menlik, and E. Özbaş, The effect of ejector on the performance of diffusion absorption refrigeration systems. An experimental study. *Applied thermal engineering*, 2012. 33. p. 44-53.
  58. Najjaran, A., et al., Experimental investigation of an ammonia-water-hydrogen diffusion absorption refrigerator. *Applied energy*, 2019. 256. p. 113899.
  59. Farzadi, R. and M. Bazargan, Experimental study of a diffusion absorption refrigeration cycle supplied by the exhaust waste heat of a sedan car at low engine speeds. *Heat and Mass Transfer*, 2020. 56(4). p. 1353-1363.
  60. de Rezende, T.T.G., et al., A non-intrusive method for evaluation ammonia mass flow rate in the condenser for diffusion-absorption refrigerators. *Flow Measurement and Instrumentation*, 2020. 72. p. 101695.
  61. Bellos, E., I. Chatzovoulos, and C. Tzivanidis, Yearly investigation of a solar-driven absorption refrigeration system with ammonia-water absorption pair. *Thermal Science and Engineering Progress*, 2021. 23. p. 100885.

62. He, L., L. Tang, and G. Chen, Performance prediction of refrigerant-DMF solutions in a single-stage solar-powered absorption refrigeration system at low generating temperatures. *Solar Energy*, 2009. 83(11). p. 2029-2038.
63. Bermejo, P., F.J. Pino, and F. Rosa, Solar absorption cooling plant in Seville. *Solar energy*, 2010. 84(8). p. 1503-1512.
64. Fu, C., Q. Shen, and T. Wu, Exergo-economic comparisons of solar cooling systems coupled to series/parallel absorption chiller types considering the lowest heat transfer area. *Case Studies in Thermal Engineering*, 2022. 39. p. 102456.
65. Abed, A.M., et al., Techno-Economic Analysis of dual ejectors solar assisted combined absorption cooling cycle. *Case Studies in Thermal Engineering*, 2022. 39. p. 102423.
66. Wang, J. and Y. Yang, Energy, exergy and environmental analysis of a hybrid combined cooling heating and power system utilizing biomass and solar energy. *Energy Conversion and Management*, 2016. 124. p. 566-577.
67. Mehrpooya, M., B. Ghorbani, and S.S. Hosseini, Thermodynamic and economic evaluation of a novel concentrated solar power system integrated with absorption refrigeration and desalination cycles. *Energy Conversion and Management*, 2018. 175. p. 337-356.
68. Khan, M.S., et al., A new correlation for performance prediction of small and large capacity single-effect vapor absorption refrigeration systems. *Cleaner Energy Systems*, 2022. 1. p. 100002.
69. Monné, C., et al., Monitoring and simulation of an existing solar powered absorption cooling system in Zaragoza (Spain). *Applied Thermal Engineering*, 2011. 31(1). p. 28-35.
70. Al-Sulaiman, F.A., F. Hamdullahpur, and I. Dincer, Performance assessment of a novel system using parabolic trough solar collectors for combined cooling, heating, and power production. *Renewable Energy*, 2012. 48. p. 161-172.
71. Atmaca, I. and A. Yigit, Simulation of solar-powered absorption cooling system. *Renewable Energy*, 2003. 28(8). p. 1277-1293.
72. Elsafty, A. and A. Al-Daini, Economical comparison between a solar-powered vapour absorption air-conditioning system and a vapour compression system in the Middle East. *Renewable Energy*, 2002. 25(4). p. 569-583.
73. Wang, J., et al., Thermodynamic performance analysis and optimization of a solar-assisted combined cooling, heating and power system. *Energy*, 2016. 115. p. 49-59.
74. Wang, J., et al., Performance investigation of a solar-assisted hybrid combined cooling, heating and power system based on energy, exergy, exergo-economic and exergo-environmental analyses. *Energy conversion and management*, 2019. 196. p. 227-241.

75. Hau, O., Thermodynamic Analysis of Absorption Refrigeration System (Ars). Chemical Engineering. Malaysia. Bachelor of Science, 2010.
76. Haber-Schaim, U., The role of the second law of thermodynamics in energy education. *The Physics Teacher*, 1983. 21(1). p. 17-20.
77. Akroot, A., "Effect of Operating Temperatures on the Performance of a SOFCGT Hybrid System", *International Journal Of Trend In Scientific Research And Development*, Volume-3 (Issue-3): 1512–1515 (2019).
78. Kareem, A. F., Akroot, A., Wahhab, H. A. A., Talal, W., Ghazal, R. M., and Alfaris, A., "Exergo – Economic and Parametric Analysis of Waste Heat Recovery from Taji Gas Turbines Power Plant Using Rankine Cycle and Organic Rankine Cycle", (2023)..
79. Yi-Fang, C., Possible decrease of entropy due to internal interactions in isolated systems. *Apeiron*, 1997. 4(4). p. 97-99.
80. Joudi, K.A. and A.H. Lafta, Simulation of a simple absorption refrigeration system. *Energy conversion and Management*, 2001. 42(13). p. 1575-1605.
81. Ochoa, A., et al., The influence of the overall heat transfer coefficients in the dynamic behavior of a single effect absorption chiller using the pair LiBr/H<sub>2</sub>O. *Energy Conversion and Management*, 2017. 136. p. 270-282.
82. Zohar, A., et al., The influence of diffusion absorption refrigeration cycle configuration on the performance. *Applied thermal engineering*, 2007. 27(13). p. 2213-2219.
83. Bdaiwi, M., Akroot, A., Abdul Wahhab, H. A., Assaf, Y. H., Nawaf, M. Y., and Talal, W., "Enhancement Heat exchanger performance by insert dimple surface ball inside tubes: A review", *Results In Engineering*, 19 (July): 101323 (2023).
84. Assaf, Y. H., Akroot, A., Abdul Wahhab, H. A., Talal, W., Bdaiwi, M., and Nawaf, M. Y., "Impact of Nano Additives in Heat Exchangers with Twisted Tapes and Rings to Increase Efficiency: A Review", *Sustainability (Switzerland)*, 15 (10): (2023).
85. Talal, W. and Akroot, A., "An Exergoeconomic Evaluation of an Innovative Polygeneration System Using a Solar-Driven Rankine Cycle Integrated with the Al-Qayyara Gas Turbine Power Plant and the Absorption Refrigeration Cycle", *Machines*, 12 (2): 133 (2024).
86. DELIBAS, H. M. and ERHAN KAYABASI, "ENERGY, ENVIRONMENT AND ECONOMY ASSESSMENT OF WASTE HEAT RECOVERY TECHNOLOGIES IN MARINE INDUSTRY", *Materials And Engineering Technology*, 002 (2021): 39–45 (2019).
87. Akroot, A. and Nadeesh, A., "Performance Analysis of Hybrid Solid Oxide Fuel Cell-Gas Turbine Power System", (2021)..

88. Ozcan, H. and Kayabasi, E., "Thermodynamic and economic analysis of a synthetic fuel production plant via CO<sub>2</sub> hydrogenation using waste heat from an iron-steel facility", *Energy Conversion And Management*, 236 (February): 114074 (2021).
89. Chouder, A., et al., Etude comparative de simulation entre PVsyst3 et PSpice de la centrale photovoltaïque connectée au réseau du CDER. Revue des Energies Renouvelables CER, 2007. 7. p. 131-136.
90. Maammeur, H., Hamidat, A., & Loukarfi, L. (2013). A numerical resolution of the current-voltage equation for a real photovoltaic cell. Energy Procedia, 36, 1212-1221.

**APPENDIX A.**

**MEASUREMENT DEVICES**

## Measurement Instruments

### Digital Temperature Sensor (TPM-10)

The TPM-10 digital temperature sensor with a temperature range of  $-50^{\circ}\text{C}$  to  $+80^{\circ}\text{C}$  and an accuracy of  $1^{\circ}\text{C}$  was used to measure the temperature in the system (see Figure 4.1). Two LR44 batteries would provide the power. Boiling, clean water was used for the calibration of the digital temperature (TPM-10) sensors. The saturated water table states that  $99.6^{\circ}\text{C}$  is the boiling point at atmospheric pressure. The sensors reported temperatures between  $99^{\circ}\text{C}$  and  $99.5^{\circ}\text{C}$ . As a result, the allowable accuracy of these sensors was roughly  $-0.5^{\circ}\text{C}$ .



---

Digital temperature (TPM-10) sensor.

### The GM1312 Thermometer

As illustrated in Figure 4.2, this apparatus was used to measure the surface temperature of a solid object and the temperature of the liquid/vapours. The general parameters of the GM1312 thermometer have been compiled and are presented in Table 4.3. The characteristics of the thermometer are as follows.

- High precision
- User-friendly operation



- Units in Celsius and Fahrenheit
- MAXMINAVG and data hold
- A backlit double display showing T1, T2, and any combination of T1 and T2 as every possible option



Thermometer GM1312.

Specifications of thermometer GM1312.

<b>Range of Measurement</b>	<b>K-type. -200°C to 1,372°C (-328°F to 2,501°F)</b>
<b>Resolution</b>	0.1t < 1,000°; 1.0t ≥ 1,000°
<b>Accuracy</b>	±0.1% + 0.6°C
<b>Power Supply</b>	3 × 1.5 V AAA batteries
<b>Size</b>	72 mm × 29 mm × 145.5 mm
<b>Weight</b>	159.0 g
<b>Thermocouple of the K-type (two pieces attached)</b>	
<b>Scope of Measurement</b>	0~250°C (300°C in short time).
<b>Error Allowed</b>	2.5°C or 0.75% Class II
<b>Heat response time</b>	< 10 seconds

S220-T8 Data Logger

The S220-T8 thermocouple temperature data logger is a kind of high precision instrument, developed and manufactured by the HUATO company, which has passed all strict calibrations and professional testing via high precision instruments. It supports eight types of thermocouple (K, J, E, T, R, S, N, B), including a thermocouple temperature compensation function, and a wide variety of interchangeable thermocouple probes. Moreover, it can measure temperatures ranging from -200°C to 1,800°C. It features a sound and light alarm if user-defined max/min values are exceeded, in addition to a large LCD display with two or eight channels of data. It is switchable between °C and °F with an LCD display. Collected data can be downloaded through a USB interface. There is memory for 86,000 readings, with a freely selectable measurement cycle ranging from 2 seconds to 24 hours (see Figure 4.3).



S220-T8 Multi-Channel Handheld Thermocouple Temperature Data Logger.

## Experiment Preparation

### Thermal sensor panel connected to the refrigerator parts

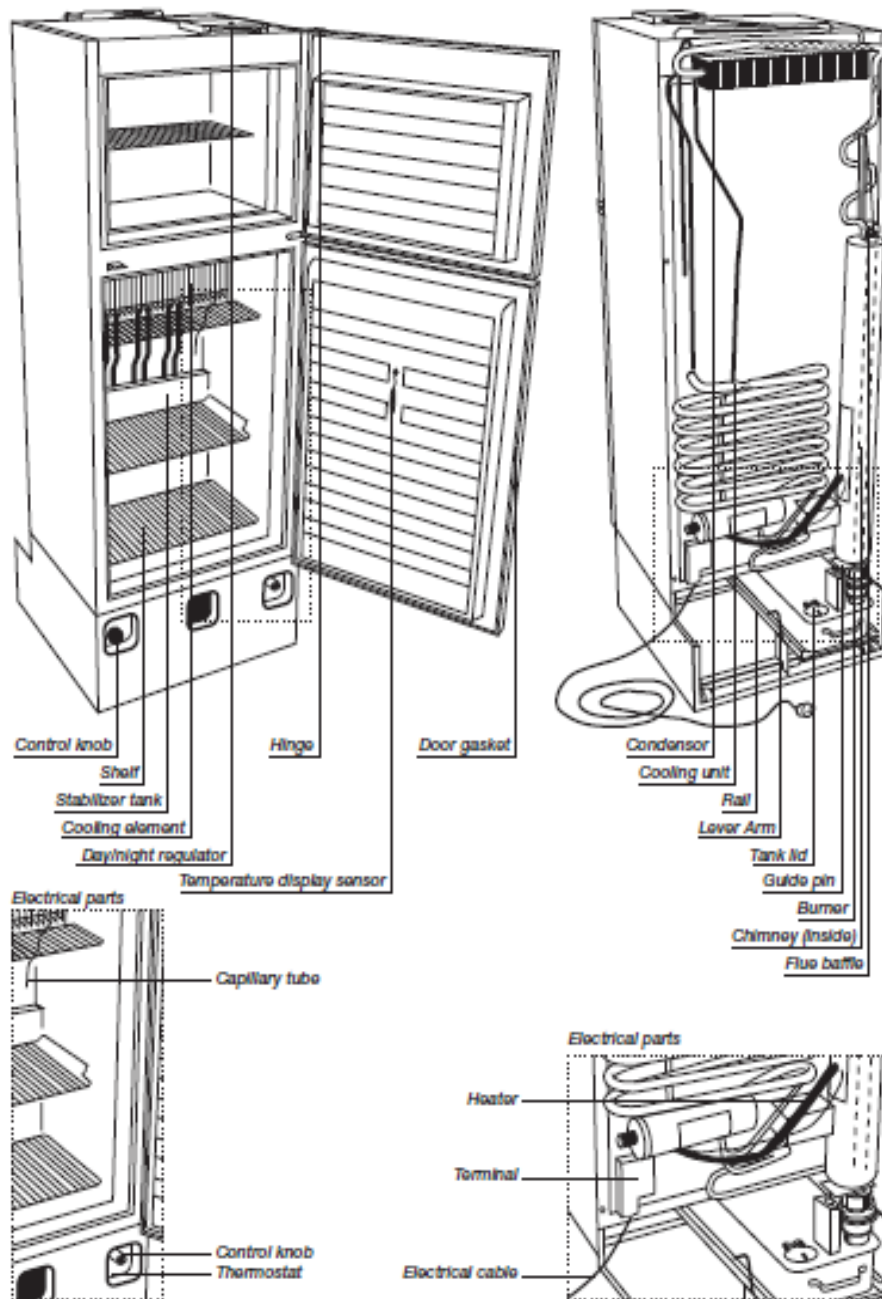
In order to ensure that the measurements acquired from the trials were correct, we prepared them by attaching eight TPM-10 temperature sensors to each component of the system. Parts of the freezer, refrigerator, inlet and outlet of the condenser and absorber, outlet of the mains, and inlet of the generator were the positions of the temperature sensors that were used to monitor the temperature in the room. In addition, a thermometer was installed at the exit of the generator so that the temperature could be observed. In addition to using a meter for the purpose of reading the voltage, one was used for the purpose of measuring the DC



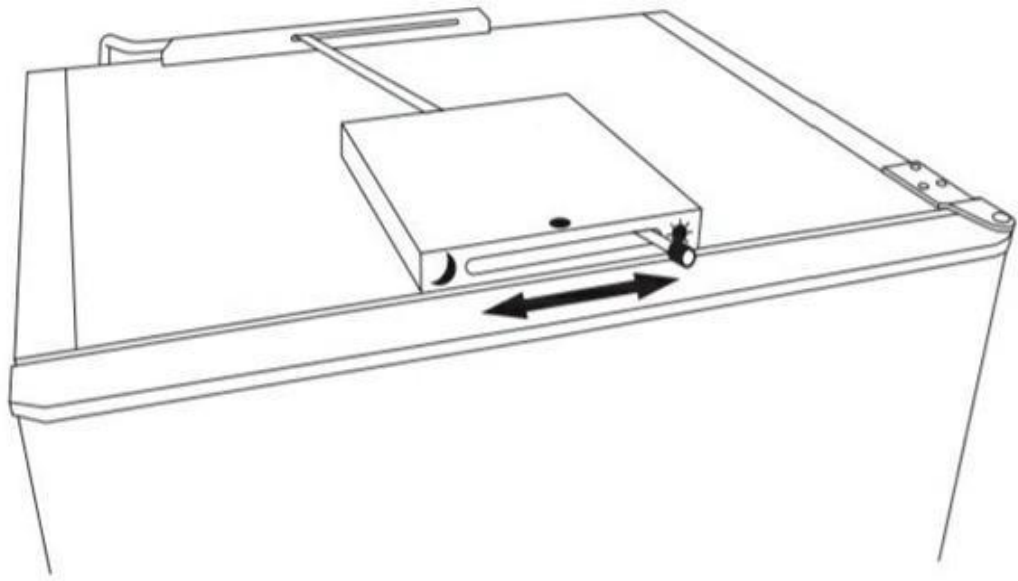
Thermal sensor panel linked to the various components of the refrigerator.

**APPENDIX B.**

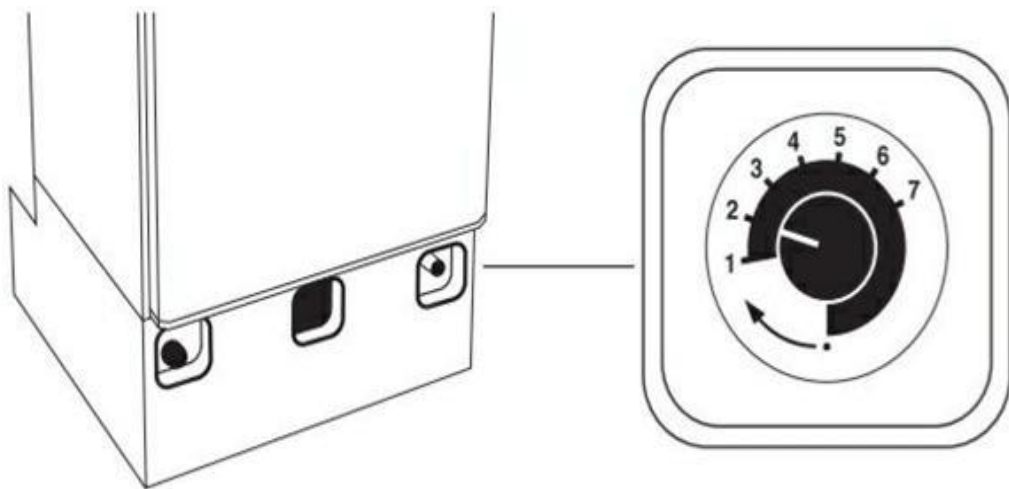
**ABSORPTION REFRIGERATION SYSTEM CATALOG**



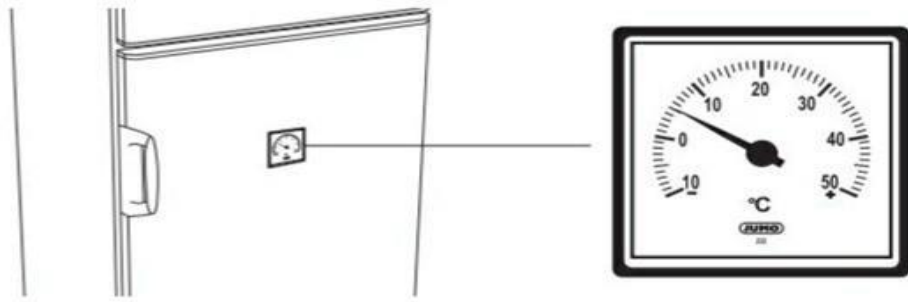
Schematic diagram shows the front and back of the refrigerator.



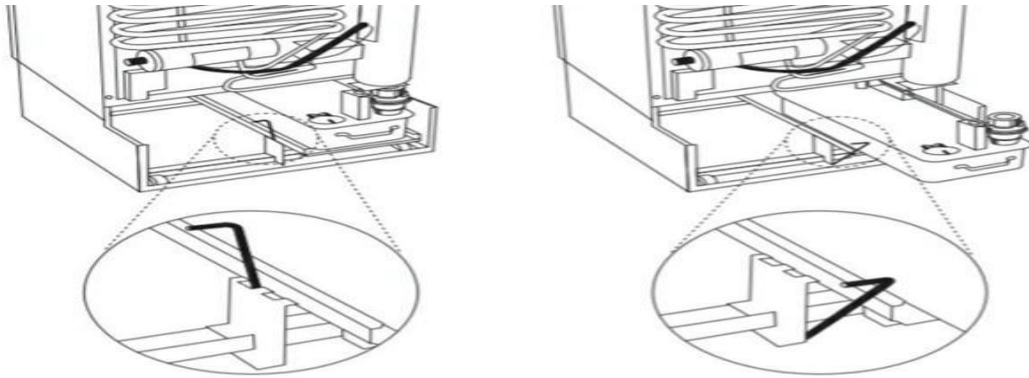
Day/night regulator



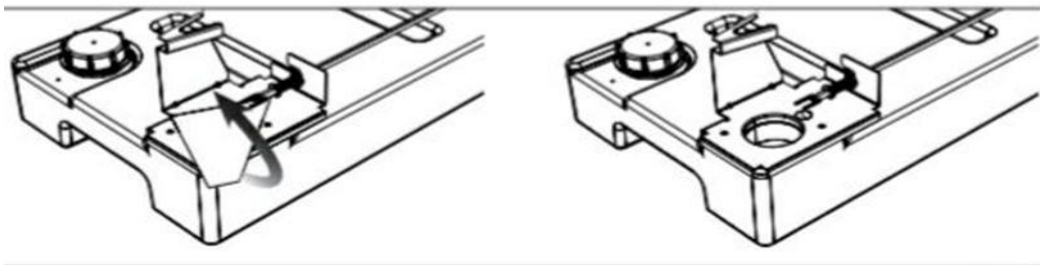
Control knob



Temperature display sensor



The process of withdrawing a kerosene tank




The protective label



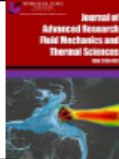
Jawad Khudhur<sup>1</sup>, Abdulrazzak Akroot<sup>1</sup>, Ahmed Al-Samari<sup>2</sup>, (2023). Experimental Investigation of Direct Solar Photovoltaics that Drive Absorption Refrigeration Systems. Journal of Advanced Research in Fluid Mechanics and Thermal Sciences, [https://semarakilmu.com.my/journals/index.php/fluid\\_mechanics\\_thermal\\_sciences/index](https://semarakilmu.com.my/journals/index.php/fluid_mechanics_thermal_sciences/index)  
[https://semarakilmu.com.my/journals/index.php/fluid\\_mechanics\\_thermal\\_sciences/article/view/2252](https://semarakilmu.com.my/journals/index.php/fluid_mechanics_thermal_sciences/article/view/2252)

*Journal of Advanced Research in Fluid Mechanics and Thermal Sciences* 106, Issue 1 (2023) 116-135



**Journal of Advanced Research in Fluid Mechanics and Thermal Sciences**

Journal homepage:  
[https://semarakilmu.com.my/journals/index.php/fluid\\_mechanics\\_thermal\\_sciences/index](https://semarakilmu.com.my/journals/index.php/fluid_mechanics_thermal_sciences/index)  
ISSN: 2289-7879



---

## Experimental Investigation of Direct Solar Photovoltaics that Drives Absorption Refrigeration System

Jawad Khudhur<sup>1</sup>, Abdulrazzak Akroot<sup>1</sup>, Ahmed Al-Samari<sup>2,\*</sup>

<sup>1</sup> Faculty of Engineering, Mechanical Engineering Department, Karabuk University, Turkey

<sup>2</sup> Faculty of Engineering, Mechanical Engineering Department, University of Diyala, Iraq

---

ARTICLE INFO	ABSTRACT
<p><b>Article history:</b> Received 25 January 2023 Received in revised form 24 April 2023 Accepted 2 May 2023 Available online 20 May 2023</p> <p><b>Keywords:</b> Diffusion absorption refrigeration; Ammonia-Water; renewable energy; technology PV system</p>	<p>Renewable energy used for refrigeration applications has become essential very recently due to the fossil fuel crisis and the global warming problem. Moreover, using photovoltaic PV to generate electricity than using inverters and energy storage represents a high-cost process. This study aims to investigate the opportunity of using PV output directly to operate a refrigeration system. The absorption refrigeration system uses heat as an energy source for the generator that drives the system. Moreover, the absorption refrigeration system doesn't have a compressor but a generator. As a result, the novel aspect of this study is the use of PV electricity's DC output to power the heater that provides the needed heat for the generator without the use of an inverter that provides AC electricity. The essential very difference here is that the compressor needs a consistent and steady electric supply. However, using DC electricity for heating is not very restricted if the voltage fluctuates a bit. A 580 W PV was used to power a refrigerator with a capacity of 70 liters. During several tests, the freezer of the fridge reached -26 C and the cabin temperature was around 10 C. This finding was similar to the performance of this fridge on a conventional heater.</p>

---

### 1. Introduction

Solar energy is the most sustainable and cost-free way to manage the world's energy [1]. Moreover, the need for energy and its usage for cooling is growing as technology advances. Since the world population grows rapidly, thermal load loads increase increases, and living standards rise. In a world of increasing scarcity of primary energy. Furthermore, air-conditioning systems may be responsible for 60% to 80% of the energy consumed in commercial and public buildings [2]. Meanwhile, according to the BP statistical analysis of world energy (2017), fossil-based fuels account for the vast bulk of global energy use (85.5%) [3]. It is critical to seek alternatives to traditional energy sources [4]. Energy usage is directly related to economic growth and population. HVAC consumes 10-20% of the total energy usage in wealthy nations [5], and Solar energy is one of the most essential renewable energy sources. More specifically, because it is more commonly available via photovoltaic

---

\* Corresponding author.

## **RESUME**

Engineer Jawad Yahya Khudhur KHUDHUR is now a master's student at Karabük University in Türkiye. He works as a supervisory engineer in the government sector, where he supervises engineering projects implemented by companies contracting with the government sector in Iraq in Diyala Governorate. In addition to being a representative of the government sector in supervising engineering projects, he has nearly 10 years of experience in supervising the implementation and follow-up of engineering projects, as well as experience in preparing the schedule of quantities and economic feasibility. He supervised many infrastructure projects for the Iraqi Ministry of Education within the ministry's projects and within the United Nations Development Program in Iraq in Diyala Governorate. He also completed tables of quantities and specific specifications and prepared statements for supplying schools in Diyala Governorate with solar energy systems.